GROWTH AND PHYSICAL PROPERTY STUDIES OF SOME BIOLOGICALLY IMPORTANT CRYSTALS

Thesis submitted to the University of Calicut
in partial fulfillment of the requirements for the award of the degree of

DOCTOR OF PHILOSOPHY IN PHYSICS
under the Faculty of Science

BY

JUMANATH E C

SUPERVISOR:
Prof.(Dr.) P.P.PRADYUMNAN
PROFESSOR

DEPARTMENT OF PHYSICS
UNIVERSITY OF CALICUT
KERALA 673635 - INDIA

AUGUST 2019

DEPARTMENT OF PHYSICS
UNIVERSITY OF CALICUT
KERALA 673635 - INDIA

Dr. P.P. PRADYUMNAN
Professor

Grams: UNICAL
91-0494-2401144,415,416
Fax- (0494) 2400 269
Residence: +09895961751
e-mail: drpradyumnan@gmail.com
Kerala, India. 673635.

CERTIFICATION OF SUPERVISOR

This is to certify that all the corrections/suggestions from the adjudicators have been incorporated in this thesis.

Calicut University

February 2020

Dr. P.P.Pradyumnan

DEPARTMENT OF PHYSICS
UNIVERSITY OF CALICUT
KERALA 673635 - INDIA

Dr. P.P. PRADYUMNAN
Professor

Grams: UNICAL
91-0494-2401144,415,416
Fax- (0494) 2400 269
Residence: +09895961751
e-mail: drpradyumnan@gmail.com
Kerala, India. 673635.

CERTIFICATE

Certified that the work presented in this thesis entitled '**GROWTH AND PHYSICAL PROPERTY STUDIES OF SOME BIOLOGICALLY IMPORTANT CRYSTALS**' is submitted to the University of Calicut in partial fulfillment of the requirements for the award of degree of Doctor of Philosophy in physics is a record of original research work done by **Ms. Jumanath E C** during the period 2014 - 2019 under my guidance in the Department of Physics, University of Calicut. The thesis has not formed the basis for the award of any Degree/Diploma and has undergone plagiarism check using URKUND software at CHMK Library, University of Calicut and the similarity index is found within the permissible limit.

Calicut University

August 2019

Dr. P.P.Pradyumnan

DECLARATION

I hereby declared that the work presented in this thesis entitled '**GROWTH AND PHYSICAL PROPERTY STUDIES OF SOME BIOLOGICALLY IMPORTANT CRYSTALS**' submitted to Calicut University in partial fulfillment of the requirement for the award of degree of Doctor of Philosophy in Physics is a record of original research work done by me during 2014 - 2019 under the supervision and guidance of Dr. P.P.Pradyumnan, Professor, Department of Physics, University of Calicut, Calicut University P.O, Kerala-673635 and it has not been included in any other thesis submitted previously for the award of any degree/Diploma of any institution. It is also declared that the thesis has undergone plagiarism check using URKUND software at CHMK Library, University of Calicut and the similarity index is found within the permissible limit.

Calicut University

August 2019 Jumanath E C

Acknowledgements

Foremost, I would like to express my sincere gratitude to my research guide Dr. P.P. Pradyumnan for the continuous support of my Ph.D study and related research, for his patience, motivation, immense knowledge and hard questions. His guidance helped me in all the time of research and writing of this thesis. I could not have imagined having a better adviser and mentor for my Ph.D study. I thankfully remember the way he ignited and triggered my research work, which has culminated in this thesis. He has performed a pivotal role in fostering my creativity. I recollect with overwhelming gratitude the consolation and affection he rendered me during moments of distress and tribulation in the course of my research.

I am extremely indebted to Prof. Vinodkumar, Head of the Department of Physics, University of Calicut for providing me valuable suggestions in various stages of the work. I also express my deepest sense of appreciation to former Head of the Department Prof. Antony Joseph and Prof. M.M Musthafa for their continuous encouragement. I am highly thankful to other faculties in the Department Dr. C D Ravikumar, Dr. Shahin Thayyil, Dr. Libu alexander and former faculties Dr. P A Subha and Dr. V M Bannur for their keen interest and sincere support to my research. All of them helped me to overcome many difficulties during the time of research.

My sincere appreciation towards the Head of the Department of Chemistry for analytical facilities provided for my research work and the Head of the Art and Photography unit in University of Calicut, for permitting me to use the photog-

raphy unit. My sincere gratitude also goes to Dr. C. Sudarsan Kumar and Monu Joy, MG University, Kottayam, Kerala, for providing single-crystal XRD facility. I also thank to the UGC–SAP, FIST 2 (Government of India) and DST - SERB for the research facilities in the Department of Physics, University of Calicut. I would like to thank the Central Sophiticated Instrumentation Facility, University of Calicut, provided characterization facilities for the research work. Also my sincere acknowledgment to UGC, Govt. of India for the award of UGC BSR fellowship.

I express my special thanks to my friends and fellow scholars in the Material Science lab, Department of Physics, University of Calicut, for their motivation and informative discussions. I really enjoyed the company of Mr. N.A.M Sabeer, Ms. Anju Paulson, Ms. Soumya P, Ms. Vineetha V, Ms. Shiny P, Ms. Nabeela KV, Mr. Midhun Shah, Dr. Jaya TP and Dr. Divya NK. Thanks are also due to Dr. Binitha M.P, Associate Professor, Department of Physics, Government Arts and Science College, Kozhikode, for her insightful comments and informative discussions. I appreciate other co-researchers and friends in the Department of Physics, Bintu, Vidya, Safna, Shabeeba, Jamshihas, Shan, Usha and Sruthi for their kind assistance. Besides them, I would like to thank the rest of the non-teaching staffs in the Department of Physics, University of Calicut.

I would like to pay high regards to my parents and relatives for their sincere support throughout my research and lifting me uphill this phase of life. My immense indebtedness goes to my husband Dr.P. Niyas for the incredible love, patience, endless encouragement and understanding he has shown, which helped me to achieve this goal. Beyond all, my love and gratitude to my dear daughter Isha, for her patience when I was occupied with my work and writing the thesis. I owe everything to her. Above all, I am thankful to Almighty for granting me the wisdom, health and strength to undertake this research task and enabling me to its completion.

Jumanath E C

Dedicated to

My
Family

Contents

List of Figures

List of Tables

Abbreviations

- AEMO - Alkaline Earth Metal Oxalate
- BCF - Burton, Carbrera and Frank
- CaAMH - Calcium Adipate Monohydrate
- CaCPH - Calcium Citrate Pentahydrate
- CADH - Copper Ascorbate Dihydrate
- CdCHH - Cadmium Citrate Hexahydrate
- CoATH - Cobalt Adipate Tetrahydrate
- CuAMH - Copper Adipate Monohydrate
- CuCDH - Copper Citrate Dihydrate
- DRS - Diffuse Reflectance Spectroscopy
- DSC - Differential Scanning Calorimetry
- DTA- Differential Thermal Analysis
- DTG - Differential Thermo Gravimetric
- FTIR - Fourier Transform Infrared
- ICDD - International Center for Diffraction Data
- KSV - Kossel, Strnski and Volmer

- NIR - Near Infrared
- ORTEP - Oak Ridge Thermal Ellipsoid Plot
- PVT - Physical Vapour Transport
- TCA - Tri Carboxylic Acid
- TG - Thermo Gravimetric
- TGA - Thermo Gravimetric Analysis
- UV-DRS - Ultra Violet Diffuse Reflectance Spectroscopy
- XRD - X-ray Diffraction
- ZnA - Zinc Adipate

List of Publications

International Journals / proceedings (Published):

1. 'Structural, spectroscopic and thermal property studies of cobalt adipate tetrahydrate single crystals', **E C Jumanath** and P.P.Pradyumnan, Journal of Crystal Growth, 479 (2017) 83-88. (IF - 1.573)

2. 'Growth and structural studies of hybrid single crystals of cadmium citrate hexahydrate', **E C Jumanath** and P.P.Pradyumnan, Journal of Molecular Structure, 1193 (2019) 231-238. (IF - 2.120)

3. 'Biomimetic growth, dielectric and magnetic features of copper ascorbate dihydrate crystals', **E C Jumanath** and P.P.Pradyumnan, Journal of Solid State Chemistry, 277 (2019) 538-547. (IF - 2.291)

4. 'Growth, characterization and dielectric property studies of zinc adipate dihydrate crystals', **E C Jumanath** and P.P.Pradyumnan, AIP Conference Proceedings, 2082 (2019) 070003.

5. 'Thermal degradation and spectroscopic studies of optically important single crystalline organo metallic calcium adipate monohydrate', **E C Jumanath** and P.P.Pradyumnan, Journal of Thermal Analysis and Calorimetry, (2019) doi: http://doi.org/10.1007/s10973-019-08916-z. (IF - 2.471)

List of Conference Presentations

1. 'Growth, characterization and dielectric property studies of zinc adipate dihydrate crystals', **E C Jumanath**, P P Pradyumnan, International Conference icONMAT 2019, CUSAT-Kerala, 2-5 January 2019

2. 'Structural and thermal characterization on gel grown iron (III) ascorbate crystals', **E C Jumanath**, P P Pradyumnan, Second International Conference ICMST 2016, ST. Thomas College Palai, 5-8 june 2016

3. 'Studies on growth and dielectric behaviour of zinc glutarate crystals by gel diffusion technique', **E C Jumanath**, P P Pradyumnan, National conference NCMOMS-2015, Farook College-Calicut, 17,18 December 2015

4. 'Growth of calcium tartrate crystals by gel diffusion technique', **E C Jumanath**, P P Pradyumnan, International Seminar on Recent trends in Physics, Govt. College Kodancheri - Calicut, 15-16 January 2015

Preface

Crystal growth is one of the fascinating fields, there always has been a need of good quality crystals for various applications. The demand of the modern technology has tempted researchers to synthesize and grow several new types of crystals. The requirement for better, less-expensive, and larger single crystals has driven large scale research and development in crystal growth. Biologically important crystals play an outstanding role in human body, plants, animals, and micro-organisms. Biomineral formation process under controlled conditions inspires researchers to develop designed single crystals. Crystals play major role in biology and most of the living beings are form crystals. The crystallization of metal carboxylate is important, not only of their biological relevance but due to their wide applications and variety of bonding modes in it; ionic , monodentate, chelating and bridging by dentate, which make their wide use in science and technology. The crystallization and properties of metal dicarboxylates were extensively studied by many investigators. Adipic acid is a dicarboxylic acid naturally found in beet juice and tobacco, study on the crystallization and properties of metal organic framework structures with adipate ligand has been fabricated by many investigators, where they were grown crystals by slow evaporation, precipitation method and hydrothermal method. However, there are a few studies on growth and properties of metal tricarboxylates. Citric acid is a very prevalent ligand in the physiological metal ion binders in tricarboxylic acids and it exists even in human plasma at a concentration of approximately 0.1 mM. Ascorbic acid is a form of vitamin C, mineral ascorbates are the salts of ascorbic acid, and they are formed by bonding of mineral cation to ascorbate anion. Ascorbate salts may better tolerated by the human body than the corresponding weak acidic

ascorbic acid. Among the various crystal growth methods, gel method provides an efficient and simple method for growing single crystals of biologically important materials.

In this thesis growth and characterization of twelve biologically important crystals are described. In which four crystals belonging to adipate (Ca, Co, Cu and Zn), three crystals belonging to citrate (Ca, Cu and Cd), other four crystals belonging to oxalate (Mg, Ca, Sr and Ba) and one in ascorbate (Cu). The thesis comprises of seven chapters; the division of a chapters with a brief outline of the contents is listed below.

The introductory chapter of this thesis accommodate a brief description of theory of crystal growth and different growth methods employed for growing single crystals. The chapter also includes both biological as well as industrial importance of adipic acid, citric acid, ascorbic acid and its derivatives. A brief literature survey, motivation to carry out this study and main objectives of the thesis work are also included in this chapter.

Chapter 2 deals with the mechanism and advantagous of gel growth technique. The chapter also discusses a detailed account of different characterization techniques used in this work. These include the basics of X-ray diffraction (XRD), Fourier Transform Infrared (FT-IR), micro Raman, UV/Vis Diffuse Reflectance Spectroscopy (DRS), thermal decomposition studies using Thermogravimetric (TG), Differential Thermal Analysis (DTA) and Differential Scanning Calorimetric (DSC) techniques and basic information on dielectric measurement are also accommodated in this chapter.

Chapter 3 constitutes the single crystal growth and fundamental characterization of four metal adipates; calcium, cobalt, copper and zinc. The influence of different growth parameters such as gel density, pH, gel ageing and concentration of the reactants on the growth of the crystal have been studied. Single crystals have been obtained for calcium and cobalt adipates, whereas crystallization of the copper and zinc adipates resulted in the growth of spherulitic crystals. The single crystal XRD and powder XRD were used for detailed structural studies. The FTIR and micro

Raman studies reported the modes of different functional group in adipate group as well as the presence of water of hydration. The DRS spectra of the adipate crystals were employed and the optical band gap were calculated based on the Kubelka Munk Function. To study the thermal decomposition behavior, TG, DTA and DSC studies were carried out and the stoichiometric composition of the grown crystals were deduced from TGA. Studies on dielectric properties of the grown crystals with respect to variation in the applied frequency have also been carried out. The ac conductivity of the crystals also calculated from the dielectric measurements.

Chapter 4 is devoted to describe the growth, characterization and dielectric property studies of three citrate crystals of cations: calcium, copper and cadmium. Single crystals have been obtained for cadmium citrate but calcium and copper citrates are spherulitic in morphology. The detailed structure of cadmium citrate were studied using single crystal XRD, and powder XRD were used for the structural studies of calcium and copper citrates. The citrate phase formation and presence of coordinated water molecule are confirmed by FTIR and micro Raman analysis, also the band assignments are interpreted and tabulated. The optical band gap of the crystals were determined by DRS studies. The thermal analysis results depicted that all the three citrate crystals show two stage decomposition and stoichiometry of the crystal have been obtained and discussed. The dielectric behavior of the grown crystals with respect to variation in the applied frequency have also been studied. It is observed that all metal citrate crystals exhibit a normal dielectric behavior as observed for adipate crystals.

The 5^{th} chapter describes the methodology employed to synthesize single crystals of copper ascorbate dihydrate. Very interesting result obtained in the case of these crystals and the results are comprised in this chapter. The crystal structure was initially studied by X-ray diffraction, the powder XRD confirm the new phase formation and crystallinity of the sample and the single crystal XRD reveals that the structure of the grown crystal as cubic copper. The X-rays may dissociates copper ascorbate dihydrate crystals into copper crystals, so the obtained data are resembled with that of metallic copper. Further characterizations, such as spectroscopic

studies (FTIR, Micro Raman, diffuce reflectance) and thermal analysis (Differential Scanning Calorimetry and Thermogravimetry) were also carried out. Spectroscopic studies confirm the ascorbate phase formation and the vibrations assigned to the different functional groups within the crystals are discussed and tabulated. The thermal decomposition of the material suggested a four-stage decomposition process and the end product is copper oxide. The stoichiometric composition of the grown crystals is confirmed to be $Cu(C_6H_6O_6)$ $2H_2O$. The optical band gap of the material was determined by based on the Kubelka Munk function. The polarization mechanism of the compound is explored using the dielectric measurements. Dielectric constant, a.c. conductivity and loss tangent were measured over a frequency range from 100 Hz to 5 MHz.

In chapter 6, reported the details of alkaline earth metal oxalate (AEMO) (magnesium, calcium, strontium and barium) single crystal growth by the decomposition of L-ascorbic acid in silica gel medium. We are conducted experiments to grow alkaline earth metal ascorbate crystals by using ascorbic acid as one of the reactants. Instead of ascorbates we have found the oxalate crystals of respective alkaline earth metals. During the growth of AEMO crystals it was found that experimental conditions, such as pH, density of gel, concentration of reactants and gel aging, have strong influence on the nucleation kinetics and the optimum conditions for the growth of good quality crystals are tabulated. The results obtained from powder XRD are also summarized and tabulated. The oxalate phase formation was identified using recorded FT-IR spectra and the band assignments were interpreted. The TG-DTA analysis depicted that the crystals are completely anhydrous below 300 ^{0}C and the stoichiometric composition of the crystals are also established. The optical band gap of the grown crystals were calculated using DRS results. The dielectric constant of metal oxalate crystals, decreases gradually with increasing frequency of the applied ac field.

The final chapter (chapter 7) comprises a general conclusion and scope for future research work on the present investigations.

Chapter 1

Crystal Growth and Biologically Important Crystals

1.1 Introduction

A crystal is a material in which constituent atoms, ions or molecules are 3-dimensionally arranged in a regular repeating pattern. Crystals are known to be the pillars of modern technology. Crystal growth is one of the important field in material science, which consists of controlled phase transformations. Crystal researchers have always been in quest of new compounds in their single crystalline phase. There are large number of methods for growing single crystals and are determined by size of the material and its characteristics [1]. The single crystal technology is the pivotal for all the current methods and prevalent in these fields. The development of the crystal growth research is highly interdisciplinary and the advances in the field of physics, material science, chemistry, metallurgy, chemical engineering, crystallography etc. have immensly contributed. Several kinds of single crystals and its applications are found in the evolution of technologies such as; semiconductor, laser, high and low energy particles in physics, medical diagnostics, nuclear fusion, display, thermal imaging etc. In addition to this, the technology have massive technological brilliance, crystals are used in many important areas of medicine, humanity,

technology, engineering and also strategic areas of defence and space science [2].

Crystallography is a scientific study of crystals regarding the process of crystallization, external morphology, properties, internal structure and classification of crystals. The process of crystal formation is known as crystallization. The crystal growth occurs either naturally or artificially. Untill the last century, the subject of crystal growth was treated as a part of crystallography. It is important to record that both the science of crystal growth and structural crystallography came out from curiosity about the large types of crystal forms existing in nature. Today, apart from naturally occurring crystals, there are well advanced laboratory techniques used for the production of crystals. It is interesting that the crystal growth can be regarded as an early subject, owing to the truth that the crystallization of sugar and salt was known to the ancient Indian and Chinese civilizations. The basic aspects of crystal growth had been obtained from early crystallization studies in the 18th and the 19th century [3, 4]. Theoretical understanding of crystal nucleation proceeds to growth developed on the basis of thermodynamics in the end of 19th century and in the beginning of 20th century.

Crystal growth can be considered as the process of the birth and growth of a solid phase with an ordered structure out of a irregular state. Thus it can be regarded as a first order phase transition. Crystal growth consists of addition of new atoms, ions or polymer strings into the characteristic arrangement of a crystalline Bravais lattice. The growth typically follows an initial stage of either homogeneous or heterogeneous nucleation process.

Biomineralisation involves the deposition and growth of materials in biological systems. It occurs by producing bioinorganic solids with fascinating outer and inner shapes well suited to their functions [5]. The key interest in medical field is to understand the biological crystal formation and their disolution. The formation of these crystals involve the combination of inorganic and organic components [6]. There is a significant demand to understand the beneficial growth of crystals in teeth and bones and also the reason for crystalline deposition in blood vessels, gallbladder, kidney, urinary tract, and many organs of living organisms [7]. The

type, form and function of biominerals are varied but all share a common theme in the control mechanism, which determines the crystal disposition, morphology and production of biomaterials [8]. Biominerals often have composite architecture and specific biological functions.

There has always been a need of good quality crystals for various applications. The demand of the modern technology has tempted researchers to synthesize and grow several new types of crystals. The requirement for better, less-expensive, and larger single crystals has driven advance research in crystal growth. Crystals are the back bone of today's technological development. Without crystals, there would be no mordern industrie including electronic industry and opto-electronic industries , which depends on materials/crystals such as semiconductors, transducers, superconductors, radiation detectors crystalline films for computer industries, microelectronics etc.

1.2 Crystal growth

Crystallization process consists of following steps.

1) Achievement of super saturation or super cooling.

2) Formation of crystal nuclei.

3) Successive growth of crystals to get distinct faces.

All the above steps may occur concurrently at different regions of crystallization units.

1.2.1 Super saturation

Super saturated solution is the solution in which the solute concentration exceeds that of the equilibrium condition at a given temperature. They are thermodynamically unstable. The supersaturation required for crystallization process will be achieved by (i) slow evaporation (ii) slow cooling and (iii) by the addition of external impurities. The slow cooling is the best method to grow bulk size crystals by solution technique. In this case, crystallization happens by lowering the temperature of

the solution under a controlled cooling rate. Another method for supersaturation is by slow evaporation of the solvent. This takes place in materials with very small temperature coefficient of solubility. Here crystallization takes place at a constant temperature. The supersaturation could also be attained by the addition of some impurities. The growth proceeds by the reduction of solubility of the solute due to the presence of impurity. The selection of suitable growth methods depend mainly on the shape of the solubility curve [9, 10]. The degree of supersaturation (S) of a solution could be expressed by the ratio:

$$S = C/C^* \tag{1.1}$$

where, C is the actual concentration of the solution and C* is the equilibrium saturation concentration of the solution at a given temperature. Thus, S = 1 represents saturated solution, S < 1 represent under saturation and S > 1 denotes supersaturation. The concentration driving force $\triangle C$ is given by

$$\triangle C = C\text{-}C^* \tag{1.2}$$

The relative supersaturation is defined as,

$$\delta = (C - C^*)/C^* \tag{1.3}$$

$$\delta = (C/C^*) - 1 \tag{1.4}$$

$$\delta = S - 1 \tag{1.5}$$

1.2.2 Nucleation

The process of nucleation is an important phenomenon in crystal growth. Being an heterogeneous chemical process, crystal growth involves conversion from one phase to another phase of compounds. Nucleation occurs by the formation of small embryos of the new phase inside the large volume of the old phase. Before the

crystal grows in the solution, there exist a number of minute solid bodies known as centre of crystallization. Nucleation occurs either spontaneously or artificially and are referred to as homogeneous and heterogeneous nucleation, respectively. Nucleation normally happens at nucleation sites on surfaces contacting the liquid or vapour. Minute bubbles or Suspended particles also provide nucleation sites this is called heterogeneous nucleation, whereas homogeneous nucleation is preferential nucleation sites. Homogeneous nucleation occurs randomly and spontaneously, but it requires super heating or super cooling of the medium. A theory for the formation of a nucleus was introduced by Volmer and Weber [11], in which the total free energy for a group of atoms was considered.

Embryos are the small cluster molecules, which formed by fluctuations within the supersaturated solution. The probability of growing an embryo to a stable nucleus depends on the change in free energy associated with its formation. If the free energy change between the solid and liquid is $\triangle$Gv, the free energy of the system decreases by $\triangle$Gv during the formation of a unit volume of the solid. However it increases by an amount equal to the interfacial energy σ, for each unit area of the solid-liquid interface formed. Hence the change in Gibbs free energy associated with the formation of a spherical embryo of radius 'r' is given by

$$\triangle G = 4\pi r^2\sigma - (4/3)\pi r^3 \triangle Gv \tag{1.6}$$

This equation is graphically represented in Figure 1.1, which exhibits the contribution due to both surface and volume to the free energy. The surface energy term increases with 'r^2' and the volume energy term decreases with 'r^3'. The net free energy change escalates with the increase in size, reaches a maximum and decreases for the further increase in the size of the nucleus. The size of the nucleus corresponding to the maximum free energy change is known as the "critical nucleus". It is the embryo with smallest size, which can grow further effecting the reduction in the free energy of the system. On the other hand, if the size of the nucleus formed is below the critical dimension, no further growth is possible and it will re-dissociate

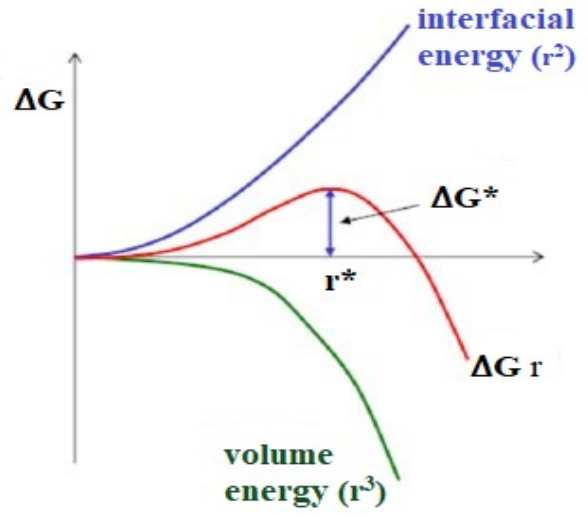

Figure 1.1: Free energy changes as a function of radius of the nucleus.

into the mother system.

The minimum size of a stable, critically sized nucleus is obtained by the maximization of Equation 1.6 for 'r', which leads to

$$\triangle \mathrm{G}/\triangle \mathrm{r} = 8\pi \mathrm{r}\sigma - 4\pi \mathrm{r}^2 \triangle \mathrm{Gv} = 0 \tag{1.7}$$

$$\mathrm{r}^* = 2\sigma/\triangle \mathrm{Gv} \tag{1.8}$$

It may be noted that the value of 'r*' decreases with G, i.e., with supersaturation or supercooling. The free energy change $\triangle$G* leading to the formation of the critical nucleus or, in other words, the activation energy necessary for nucleation, can be calculated by substituting 'r*' in Equation 1.6.

$$\triangle \mathrm{G}^* = 16\pi\sigma^3/3\triangle \mathrm{Gv}^2 \tag{1.9}$$

Equation 1.9 can be rearranged by introducing the Gibbs-Thomson relation and becomes

$$\triangle \mathrm{G}^* = 16\pi\sigma^3 V^2/3(KT\ln S)^2 \tag{1.10}$$

where V is the molecular volume. The rate of nucleation i.e., the number of nuclei formed per unit volume per unit time can be expressed as

$$\mathrm{J} = \mathrm{J}_0 \exp[-\triangle \mathrm{G}^*/\mathrm{KT}] \tag{1.11}$$

substituting for $\triangle$G*;

$$J = J_0 \exp[16\pi\sigma^3 V^2/3K^3T^3(\ln S)^2] \tag{1.12}$$

where J, is the pre-exponential factor. This equation shows that the nucleation rate is governed by the temperature, degree of supersaturation and the interfacial energy. Rearranging Equation 1.12 and arbitrarily choosing J = 1, so that *1n*.J =0, we get the expression for critical supersaturation as

$$Scri = exp[16\pi\sigma^3 V^2/3K^3T^3 \ln J_0] \tag{1.13}$$

1.3 Theories of crystal growth

The process of crystal growth involves the following steps: creation of reactants, carrying of reactants to the growth surface, adsorption at the growth surface, nucleation, growth, and removal of unwanted reaction products from the growth surface. When a crystal nucleus reaches the critical size, it grows into crystal of macroscopic dimension with fully developed faces. The kinetics and mechanism involved in the process of crystal growth, were explained by different theories such as surface energy theory, diffusion theory and surface adsorption theory.

Gibbs recommended a theory by considering the growth of a crystal similar to the growth of water droplet in mist. According to the theory, as the supersaturation increases, growth becomes quick in all directions and hence in the spherical shape of the crystal is attained. However, experimentally, it has been observed that well defined faces are developed when the supersaturation is high [12-16] . The diffusion theories were proposed by Noyes and Whitney [17] and by Nernst [18], based on

the following assumptions. (1) There is a concentration gradient in the vicinity of a growing surface. (2) The growth is a reverse process of dissolution. But this theory also fails due to the inconsistency with the experimental results. Later Kossel [19] and others analyzed the atomic inhomogeneity of a crystal surface and explained the role of step and kink sites on the growth process. However, this theory could not provide a complete explanation for the continuous growth of a crystal surface. A complete explanation for continuous growth at low supersaturation was given by Frank [3]. According to this, the crystal dislocations were capable of giving the sources of steps required for the continuous growth of a crystal. These theories have been extensively explained by many authors [21-23].

1.3.1 Adsorption layer theory by Kossel, Stranski and Volmer (KSV theory)

The role of surface discontinuities as nucleation sites was first identified by Kossel, Stranski and Volmer. According to this theory, the growth units advance towards a crystal surface do not incorporate immediately to the lattice, but become adsorbed and migrate over the surface. The absorbed atoms are possibly attached with adsorbed atoms on the crystal surface on ledge, terrace and kink site as shown in Figure 1.2. The binding energy between an atom and existing lattice increases from terrace to ledge to kink site.

Volmer first suggested the theory of crystal growth mechanism based on the existence of adsorbed layer of solute atoms or molecules on a crystal face. Volmer's theory (Gibbs-Volmer theory) is based on thermodynamic reasoning. When units of the crystallizing substance arrive at the crystal face, they are not immediately integrated into the lattice, but merely loss one degree of freedom and are free to migrate over the crystal face (surface diffusion). Hence there will be a loosely adsorbed layer of integrating units at the interface, and dynamic equilibrium is established between this layer and the bulk solution. The adsorption layer plays an important role in crystal growth, secondary nucleation and precipitation phenomena.

At the 'active centres', ions, atoms or molecules are linked into the lattice and

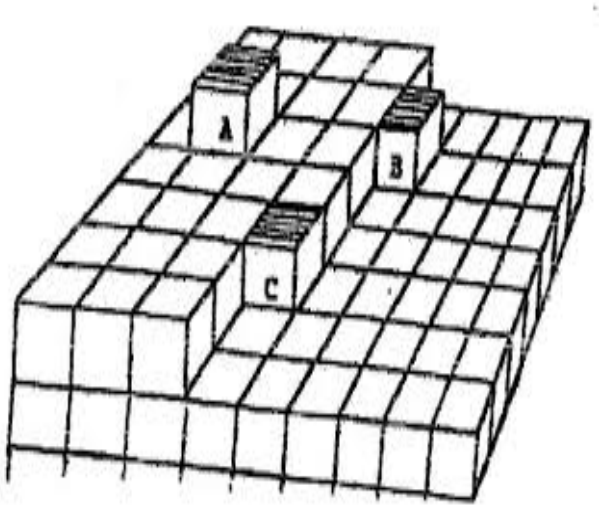

Figure 1.2: Possible lattice sites for the attachment of absorbed atoms.

under ideal condition this stepwise build-up will continue until the whole plane face is complete. Before the crystal face can continue to grow, a centre of crystallization must come into existence on the plane surface and Gibbs - Volmer theory suggests that a monolayer island nucleus, usually called a two - dimensional nucleus, is created [24-27].

1.3.2 Screw dislocation theory by Burton, Cabrera and Frank (BCF theory)

One major drawback of KSV theory is that once the kinked ledge has obtained sufficient atoms to move it to the edge of the crystal, it could not longer function as a low energy nucleation site. But if points of dislocations with screw components (screw dislocations) at crystal surface are present they can provide a continuous source of steps which can advance across the surface of the crystal. A theory of crystal growth including the mechanism of step generation and transport into the steps was given by Burton, Cabrera and Frank [27].

A screw dislocation emerging at a point on the crystal surface provides a step on the surface with a height equal to **'a'**, the projection of the Burgers vector of the dislocation. Since the step provided by the screw dislocation is anchored at

the emergence point of the dislocation, and since the inner parts of the step move radially at a faster rate than the outer parts, further growth takes place only by the rotation of step around the dislocation point. This mechanism is illustrated in Figure 1.3. Under a given condition of supersaturation these steps wind themselves up into a spiral, centred on the dislocation.

A relation between the rate of growth R and the relative super saturation was given by Burton, Cabrera and Frank. It is expressed as

$$R = C(\mathrm{S}^2/\ \mathrm{S}_1)\tanh(\mathrm{S}_1/S) \tag{1.14}$$

where

$$\mathrm{S}_1 = 19\ \gamma \mathrm{V}/2\ \mathrm{k}\ \mathrm{T}\ X_s \tag{1.15}$$

and

$$C = (D_s n_{se} \beta \mathrm{V}\ )\ /\ \mathrm{X}_s \tag{1.16}$$

where

γ - free energy

S - relative supersaturation

S_1 - a constant for B C F model

n_{se} - equilibrium concentration of growth units on surface

β - retardation factor

V - volume of the growth unit

D_s - Surface diffusion coefficient

k - Boltzmann constant.

The variation of the growth rate with supersaturation thus depends on two parameters:– C, which determines the absolute value of growth rate and S_1 which determines the actual growth rate.

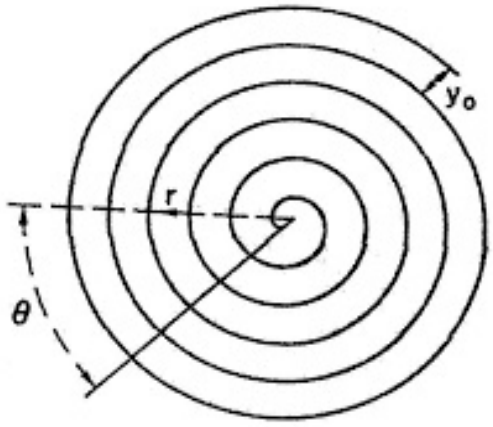

Figure 1.3: Development of spiral by screw dislocation in BCF.

The BCF theory predicts that the growth rate is proportional to the square of the supersaturation in the case of low supersaturation and changing to a linear dependence at higher supersaturation. The calculated growth rate for this mechanism is found in good agreement with observations. The spiral growth patterns have been observed on a large number of crystals grown by different methods.

1.4 Methods of crystal growth

Single crystals are produced by the transport and periodic segregation of crystal constituents in the solid, liquid or vapour phase. Based on the phase transformation process, crystal growth techniques are divided as

• Liquid-to-solid phase transformation - Solution growth

•Solid-to-solid phase transformation - Solid growth

•Vapour-to-solid phase transformation - Vapour growth

•Liquid to solid phase transformation happening at higher temperature (Melt of constituens) - Melt growth

Better choice of the growth method is essential because it determine the presence of possible impurity and other defect concentrations in the crystals for perticular applications. Choosing the best method to grow a given material depends on ma-

terial characteristics. Liquid growth includes both melt and solution growth. The growth methods suggest that almost 80% of the single crystals are grown from the melt compared with roughly 5% from vapour, 5% from low temperature solution, 5% from high temperature solution and 3% from the solid and only 2% by hydrothermal methods.

1.4.1 Growth from solution

Solution method is used for growing crystals from material of high solubility and have solubility variation with temperature also. The process will takes place only if the solution is supersaturated. Growth can be broadly classified into:

- High temperature solution growth
- Low temperature solution growth
- Hydrothermal growth
- Gel growth

High temperature solution growth

In this growth, the components of the material to be crystallized by dissolving in a suitable solvent and crystallization occurs when the solution becomes critically super saturated. The super saturation may be promoted by solvent evaporation, solution cooling or solute transportation from a hotter to a cooler region. This method is extensively used for the growth of oxide crystals. The procedure is to heat the container having flux and the solute to a temperature so that all solute materials dissolve. This temperature is maintained for a 'soak' period of several hours and then the temperature is lowered very slowly [28].

Low temperature solution growth

The method of crystal growth from low temperature aqueous solution is highly popular in the production of many technologically important single crystals. This method is used for crystal growth of materials having good solubility in water or any other solvents. Different inorganic and organic materials can be crystallized by

using this technique. Here also crystals can be grown from solution, if the solution is supersaturated. It can be achieved by slow cooling of the solution, slow evaporation of the solvent and the temperature gradient method [29, 30]. The crystal growth by low temperature solution growth requires time of either weeks, months or years.

Hydrothermal growth

Hydrothermal represents conditions of high pressure and high temperature. Substances like calcite and quartz are considered to be insoluble in water at normal condition of temperature and pressure but at high temperature and pressure, these substances are soluble. This method of crystal growth at high temperature and pressure is known as hydrothermal method. Temperatures are typically in the range of 400^0C to 600^0C and pressure in hundreds or thousands of atmosphere. The requirement of high pressure provides practical difficulties and hence there are only a few crystals of good quality were grown by this technique. Quartz is one of the example of industrial hydrothermal crystallization. One serious disadvantage of this technique is the frequent incorporation of OH_- ions into the crystal, which makes them unsuitable for many applications [31, 32].

Gel growth

Gel growth is an alternative technique to solution growth with controlled diffusion. The growth process is free from convection. Gel is a two component system of a semi solid, rich in liquid and inert in nature. The material, which decomposes before melting, can be grown in this medium by counter diffusing two suitable reactants. Crystals with dimensions of several mm can be grown in a period of 3 - 4 weeks. Since the growth takes place at room temperature, the crystals grown by this technique have high degree of perfection and fewer defects [33, 34]. The details of gel growth technique are given in the chapter 2.

1.4.2 Solid growth

In this method, single crystals are obtained by the preferential growth of a polycrystalline mass. This can be achieved by straining the material and subsequent annealing. Large crystals of several materials, especially metals, have been grown by this method [35]. Recently certain rare earth compounds are also grown using this method. Solid state growth is possible by atomic diffusion also and at normal temperature such diffusion is very slow except in the case of super ionic materials [36, 37].

1.4.3 Vapour growth

As per the reports on mordern technology, numerous methods of crystallization from the vapour phase have been developed. These methods are used for growing bulk crystals, epitaxial films, thin coatings and platelet crystals. Growth from vapour phase are broadly classified into physical vapour transport and chemical vapour transport.

Physical Vapour Transport (PVT) involves two techniques; sublimation – condensation and sputtering. The first method involves the sublimation of the charge at a high temperature end of the furnace followed by the condensation at the colder end [38] Sputtering techniques are mainly used to prepare thin films rather than discrete crystals. The advantage of this method is that film growth is possible at a temperature lower than in the sublimation-condensation growth. Various crystals and epitaxial films have been produced by PVT method [39-41].

Chemical vapour transport consists of a chemical reaction between the source material to be crystallized and the transporting agent. The material to be crystallized is converted into a gaseous product, which either diffuses to the colder end or gets transported by the transporting gas. At the colder end, the reaction is reversed so that the gaseous product decomposes to deposit the parent material, liberating the transporting agent which diffuses to the hotter end and again reacts with the charge. The temperature of the hot zone and the crystallization zone can be the-

oretically calculated [42, 43]. Different commercially important materials can be grown by this method [44-47].

1.4.4 Growth from melt

Single crystals of all materials can be grown from the melt provided they melt congruently without decomposition at the melting point. They do not undergo many phase transition between the room temperature and melting point. For fast growth, material should be melt congruently. To keep the technology simple, materials with high vapour pressure should be avoided. Depending on the thermal characteristics. The following techniques are employed from melt are Czochralski technique, Kyropoulos technique, Zone melting techniqu, Verneuil technique and Bridgeman technique.

1.5 Metal adipates

The rapid growth of solid state science and technology is attributed to the wide exploration of inorganic, organic and metal organic compounds possessing outstanding properties. Apart from the convenience in characterization, the synthesis of compounds in single crystal form has the additional benefit of direct application in devices and transducers. Metal carboxylates, which are formed by the coordination of metals with carboxylic acids, have emerged as a technologically important group with wide ranging applications. In the early stages, they were used as ingredients in lubricants, paints and waterproofing materials [48]. Extensive researches have brought out a wide variety of metal carboxylate crystals with interesting structures and promising applications. The use of these crystals for ferroelectric, piezoelectric, photoconductive, micro-electronic, opto-electronic, elasto optical and nonlinear optical devices is adding strong impetus to the research interest in these compounds [49-55] .

Based on the number of carboxyl groups involved, there occur mono, di and tri carboxylic acids. Formic and acetic acids come under monocarboxylic family

whereas oxalic, tartaric, malonic, malic, maleic, fumaric, adipic and succinic acids are in the dicarboxylic family. One among the commonly known tricarboxylic acids is citric acid. Adipic acid (hexadioic acid) is an organic dicarboxylic acid, with the chemical formula $C_6H_{10}O_4$ and naturally found in beet-root and tobacco. Adipic acid, despite its name (in Latin, adipis means fat), is not a normal constituent of natural lipids but is a product of oxidative rancidity. It was first obtained by oxidation of castor oil (ricinoleic acid) with nitric acid. It is now produced industrially by oxidation of cyclohexanol or cyclohexane, mainly for the production of Nylon 6-6. It is a naturally occurring ligand and formed via photo oxidation of olefins and hydrocarbons in the atmosphere [56-60]. Also, it is released into the environment by the burning of biomass as a motor exhaust and a chemical constituent of tobacco smoke. Adipic acid is identified as a biodegradation product of di-2-ethylhexyl adipate [61-64]. In the human being, the portion of absorbed adipic acid is metabolized by the process of beta-oxidation to succinic and acetic acids and subsequently to other normal intermediary metabolites. However, the remaining adipic acid is eliminated through urine [65, 66]. It's used in a variety of industrial and textile applications, such as to manufacture lubricants and nylon production. It can be found in carpet, automobile tires and clothing. The Chemical Company website explains that a majority of adipic acid production is used in these industrial applications. The other 10 percent is made specifically for use in foods and beverages.

A metal adipate is formed when the hydrogen atoms of adipic acid is replaced by metal ions. Adipates are salt of adipic acid with four methylene groups between the two carboxylic acid groups. They are used as a buffer and neutralizing agent in animal drugs, feeds and related products [67]. Significant amounts of adipates are used as a food ingredient, flavourant and gelling aid [68]. Each of the four terminal carboxyl oxygens in the adipate ligand can form coordinate bonds with central metal ions [62].

1.6 Metal citrates

Citric acid is a six-carbon tricarboxylic acid, which was first isolated from lemon juice. It is an organic acid and a natural component of many fruits and fruit juices and is used in the food and beverage industry for various purposes as pharmaceuticals and for other industrial uses. It is an organic carboxylic acid and can be extracted from the juice of citrus fruits by adding calcium oxide to form calcium citrate, which is an insoluble precipitate that can be collected by filtration; the citric acid can be recovered from its calcium salt by adding sulfuric acid. Citric acid is mainly produced by fungal fermentation, chemical synthesis of citric acid is possible, but it is expensive than fungal fermentation.

The crystallization and properties of metal dicarboxylates were extensively studied by many investigators [69-73]. However, there are a few studies on growth and properties of metal tricarboxylates. Citric acid is a very prevalent ligand in the physiological metal ion binders in tricarboxylic acids and it exists even in human plasma at a concentration of approximately 0.1 mM. It is also a part of the citric acid cycle (Krebs cycle) [74, 75]. Citric acid is considered as an excellent chelating agent. The most common uses of citric acid are, a preservative and flavouring agent in food and beverages such as soft drinks. It is also used as an emulsifying agent in ice-creams. It inhibits kidney stone formation and breaks up small stones that are beginning to form. Citric acid is protective; the more citric acid in urine, the more protected from forming new kidney stones. Citrate, used in calcium citrate supplements and in some medications (such as potassium citrate), is closely related to citric acid and also has stone prevention benefits.

Citric acid is used for softening water, which makes it useful in laundry detergents and soaps. It can also be used in shampoo for washing, colouring and wax from the hair. In industry, it is used to dissolve rust from steel and passivate stainless steels. Citric acid is used as an odorless alternative to white vinegar for home dyeing with acid dyes. It is an excellent soldering flux, either dry or as a concentrated solution in water [76].

A citrate is a derivative of citric acid; that is, the salts, esters, and the polyatomic

anion found in solution. When part of a salt, the formula of the citrate ion is written as $(C_6H_5O_7)^{3-}$ or $C_3H_5O(COO)_3^{3-}$. Citrate is an intermediate in the TCA cycle (TriCarboxylic Acid cycle or Krebs cycle), a central metabolic pathway for animals, plants and bacteria. Mineral citrates are formed by the bonding of a mineral cation to citrate anion, is a vital component of bone, helping to regulate the size of apatite crystals [77].

1.7 Copper ascorbate crystals

Ascorbic acid, a form of vitamin C, is an essential nutrient found in citrus fruits and vegetables [78]. The living body demands ascorbic acid in order to form and maintain blood vessels, bones, skin, etc. In addition to this, ascorbic acid also plays major roles in a plant's growth and hormone signalling. Most of the plants and animals are able to produce vitamin C from glucose. However, humans, other primates, guinea pigs and fruit bats require it to get from their nutrition [79, 80]. Vitamin C is a valuable food component because of its antioxidant and therapeutic properties [81, 82]. Vitamin C plays an important role in the human body. It is needed to maintain the health of skin, cartilage, teeth, bone and blood vessels [83]. It is also used to protect body's cells from damage [84]. It is a vital entity in cell cycle, cell expansion, as a part of the cellular redox system and as a cofactor for several important enzymes [85-87]. There are wide varieties of food which contains vitamin C. Fruits, vegetables, and organ meats are generally the best sources of ascorbic acid [88, 89]. The amount of ascorbic acid in plants varies greatly, depending on many factors such as the variety, weather and maturity [90]. In the case of fruits, its amount is influenced by various elements which include climatic/environmental conditions, maturity state, position on the tree, handling and storage, ripening stage, species, varieties of the fruits and temperature [91]. The outstanding chemical property of ascorbic acid is that it is a good reducing agent that may reduce ferric or cupric ions to ferrous or cuprous forms [92-94]. Mineral ascorbates are a group of salts of ascorbic acid. They are composed of a mineral cation and ascorbate

anion. These are highly reactive oxidants and used as dietary supplements and food additives [95].

Copper is a vital element to all living organisms as a trace dietary mineral because it is an important component of the respiratory enzyme complex cytochrome c oxidase [96]. The main organs where copper is found in human beings are liver, muscle and bone. The vitamin C reacts directly or indirectly with ceruloplasmin, a serum copper protein; specifically labilizing the bound copper atoms and facilitating their cross membrane transport [97]. Copper (II) ascorbate protect food against lipid peroxidation, discoloration and other oxidative damages. Furthermore, copper (II) ascorbate inhibit bacterial growth and thereby increased the microbiological stability of high-moisture food items [98]. Over consumption of ascorbic acid contained food or medicine may lead to the excess growth of crystalline metallic ascorbates in organs. The excess amount of cations like copper and ascorbate anion may lead to the formation of metallic ascorbate including copper (II) ascorbate in animal/human organisms. These may reduce the presence of copper like elements in the biological systems. Therefore the structure and property study of copper ascorbate crystal are very important. To study the behavior of crystallization and shape of this crystal we have been opted hydro silica gel as a medium for the growth. Since hydrosilica gel is a medium which mimics the secretions in the organs in animals and plants, we utilized this medium for the growth of ascorbate crystals.

1.8 Metal oxalate using ascorbic acid

Oxalic acid and its salts play an important role in human body, animals, plants and micro-organisms. Oxalic acid is produced naturally in body when ascorbic acid and glycine are metabolized. Ascorbic acid metabolism responsible for increased mean plasma oxalic acid level leading to renal failure is studied [99]. Vitamin C plays an important role in a number of metabolic functions including the activation of the folic acid, vitamin B, the conversion of cholesterol to bile acids and the conversion of the amino acid, tryptophan, to the neurotransmitter, serotonin[100-103]. During

the process of metabolism, it decomposes into oxalic acid. This compound is photosensitive and has least thermal stability. The decomposition of ascorbic acid has been studied in various conditions [104-108]. It is reported that decomposition of ascorbic acid in presence of Cd^{2+} ions leads to the formation of cadmium oxalate crystals [109].

1.9 Aim and Objectives of the study

The objectives of the present work are,

• Growth of single crystals in gel medium.

• Investigations of the effect of different growth parameters on the growth and morphology of these crystals.

• Structural characterization of gel grown single crystals using single crystal X-ray diffraction (XRD) and powder X-ray diffraction studies.

• Analysis of the bonding modes and functional groups of the grown crystals using spectroscopic techniques such as Fourier Transform Infrared (FTIR) and Micro Raman etc.

• Studies on thermal decomposition behaviour of the crystals by thermo-gravimetric (TG) analysis, differential thermal analysis (DTA) and differential scanning calorimetry and deduction of stoichiometric composition of the crystal.

• Evaluate the optical band gap of the material using UV-DRS

• Investigations on the dielectric property studies on these crystals as a function of frequency and temperature.

1.10 Motivation of the study

Biologically important crystals play an outstanding role in human body, plants, animals, and micro organisms. The human body, is an arrangement of liquid crystalline and mineral structure making up the crystal system. The crystal system forms the bones, tissues, cells and fluids of the body. When disease is present, these crystal

systems become unstructured, or distorted and will not be functioning in a normal pattern. The human body fluids contain minerals at various levels of saturation. When the body fluids get supersaturated with minerals, crystallization happens [110]. These crystals are highly beneficial and they produce pathological effects on humans. The major beneficial role of mineralization is formation of bones and teeth, which consists of oriented micro crystals of hydroxyapatite [111]. Biomineral formation process under controlled conditions inspires researchers to develop designed single crystals [112]. Crystals play major role in biology. Most of the living beings were form crystals. Our sense of balance and acceleration are depends upon small calcium carbonate (calcite) crystals present in the inner ear [113]. The pathological effects result in the crystal deposition diseases. The increasing incidence of crystal deposition diseases, such as heart disease, gout, gallstones, urinary stones etc., has demanded extensive research on these fields. Gallstones consist mainly of cholesterol with some quantities of calcium phosphates and calcium carbonates [114]. The clusters of small crystals formed in the urinary system give rise to urinary (renal) calculi, which consist primarily of different forms of calcium, such as calcium oxalates, calcium phosphates etc. [115].

The formation of stone in our body is identical to the crystal growth and can be grown synthetically. The gel method is most simple and versatile technique for growing urinary stones [116]. Gels promote the growth of high-quality crystals of small molecules. Crystallization of biological macromolecules was tested with different types of gels – agarose, silica or polyacrylamide in the last few decades. Although these gels possess many advantages in the crystal production over the other growth technique, but for the applications in technology, they are not much been used [117]. Crystal growth in the gel is a simple and inexpensive technique for growing single crystals of materials which show poor solubility in water and other organic solvents. It has obtained considerable importance due to its simplicity and effectiveness in growing single crystals of various biologically important compounds. When a gel is introduced in the crystallization medium, the convection is reduced and the molecule transport towards the crystal is more regular and

works in a diffusive mode. It is clear that the understanding and mimicking of the processes involved in biomineralization may provide new approaches to the growth of particular organic-inorganic hybrid materials [118].

Extensive study on the crystallization and properties of metal dicarboxilate such as oxalates, tartrates, and succinates are made by many investigators. However studies on systematic growth and properties of biologically important adipate and citrate crystals are very few in literatures. The growth of oxalate crystals using ascorbic acid is also minimal. Hence this thesis entitled ' Growth and physical property studies of some biologically important crystals' deals with the growth, characterization and property studies of four metal adipates (calcium, copper, cobalt and zinc), three metal citrates (calcium, copper and cadmium) and four metal oxalates (magnesium, calcium, strontium and barium) using ascorbic acid and one metal ascorbate (copper). The advantage of growing these crystals in silica gel is its insolubility in water. Gel method can be used to grow biologically important crystals at ambient temperature, since its viscous nature provides simulation of biological fluids.

References

[1] H. Brooks, The relationship between science and technology Research Policy **23** (1994) 477-486.

[2] Hans J. Scheel, The Development of Crystal Growth Technology Crystal Growth Technology, Edited by H. J. Scheel and T. Fukuda, John Wiley Sons (2003).

[3] D. Elwell, H. J. Scheel, "Crystal Growth from High-Temperature Solutions", Academic Press, London (1975).

[4] H. J. Scheel, "Historical Introduction", in "Handbook of Crystal Growth", Ed. D. T. J. Hurle, Vol. 1 Elsevier, Amsterdam (1993).

[5] Robert R. Crichton, Biomineralization, Biological inorganic chemistry, 2nd edition (2012).

[6] L. Mann, R. Harmoni, C. Power, Journal of Adolescence, **12** (1989) 265-278.

[7] Jiang Hu, Peter X. Ma, Biomineralization and bone regeneration, Principles of regenerative Medicine, 2nd edition (2011) .

[8] Jinhui Tao, Research methods in Biomineralization Science, Methods in Enzymology, (2013).

[9] Nývlt, Jaroslav, Journal of Crystal Growth, **3** (1968) 377-383.

[10] A. Mersmann, Chemical Engineering Research and Design, **74** (1996) 812-820.

[11] M. Volmer, A. Weber, Z. Phys. Chem., **119** (1925) 227.

[12] Curie P., Bull. Soc., Min. de France, **8** (1885) 145-156.

[13] Wulff G., Z. Krist., **34** (1901) 449-461.

[14] Marc R. and Ritzel A., Z. Physik Chem., **76** (1911) 584-597.

[15] Berthoud A., J. Chem. Phys., **10** (1912) 624-638.

[16] Valeton J., Sachs. Gus J.P.K., Wiss Match Physik, Leipzing, **67** (1951) 1-15.

[17] Noyes A.A. and Whitney W.R., Z. Physik Chem., **23** (1981) 689-704.

[18] Nernst W., Z. Physik Chem., **67** (1909) 470-487.

[19] Kossel W., 'Zur theorie des Kristallwachstums', Nachr. Ges. Wiss. Goettingen, **6**(1927).

[20] Frank F.C., Discussions Faraday Soc., **5** (1949) 48-55.

[21] Ueda R. and Mullin J.B., (Eds.), Crystal Growth and Characterisation, North Holland Publishing Company, Amsterdam, (1973).

[22] Vere A.W., Crystal Growth: Principles and Progress, Plenum Press, New York, **9**(1987).

[23] Goodman C.H.L., (Ed.), Crystal Growth: Theory and Techniques, Plenum Press, New York, **1**(1980).

[24] Kossel W., Nachr. Ges. Wiss. Goettingen Math. Phys., K1 11A **135** (1927) 18.

[25] Stranski I.N., Z. Phys. Chem., **136** (1928) 259.

[26] Volmer M., Die Kinetik der Phasenbildung, Steinkopff, Dresden, **20**(1939).

[27] Burton W.K., Cabrera N. and Frank F.C., Phil. Trans. Roy. Soc., A **243** (1951) 299.

[28] Shivaji Dagdale, Vikas Pahurkar and Gajanan Muley, Molecular Symposia,(2006) https://doi.org/10.1002/masy.201400254.

[29] J.Zaccaro1, B.Menaert, D.Balitsky and A.Ibanez, Crystal Growth - From Fundamentals to Technology, (2004) https://doi.org/10.1016/B978-044451386-1/50015-5.

[30] J.C. Brice Crystal Growth Processes [John Wiley and Sons, New York] (1986).

[31] R.A.Laudise and J.W.Nielsen, Solid State Physics, **12** (1961) 149-222.

[32] Colin D. McMillen and Joseph W. Kolis, **92** (2012) 2686–2711.

[33] H. K. Henisch Crystal Growth in gels (Pennsylvania State Univ. Press)1970.

[34] H. K. Henisch and J.M.García-Ruiz,Journal of Crystal Growth, **75** (1986). 195-202.

[35] Barrat C. S. and Massalski T.B., Structure of Metals, Mc Graw Hills, New York, 3rd edn., 1966-1993.

[36] Kentaro Ino, Makoto Wakeshima, Yukio Hinatsu, Mat. Res. Bull., **36** (2001) 207-235

[37] Keer H. V., Principles of the Solid State, Wiley Eastern Ltd., (1993).

[38] Faktor M.M. and Garret.I., Growth of Crystals from the Vapour, Chapman and Hall, London, **60** (1974).

[39] Bradley, The Art and Science of Growing Crystals, Gilman, J.J. Ed., Wiley, New York, **61** (1963).

[40] Reynolds, The Art and Science of Growing Crystals, Gilman, J.J. Ed., Wiley, New York, **62** (1963).

[41] Archibald P. and Parent E., Solid State Technology, **19** (1976) 32.

[42] K. Sunil and M.A. Ittyachen, Bull. Mater. Sci. **20** (1997) 231-295

[43] S. Kunjachan, I. Korah, and M.A. Ittyachen, Cryst. Res. Technol. **40** (2005) 871.

[44] Kaldis E., J. Crystal Growth, **17** (1972) 66.

[45] Kulkarni A.K., Bull. Mater. Sci., **17** (1994) 1379.

[46] Schafer H., Chemical Transport Reactions, Academic Press, New York, **68** (1964).

[47] Strobel P., Le Page Y. and Mc Alister S.P., J. Solid State Chem., **42** (1982) 242.

[48] R. C. Mehrotra, R. Bohra, Metal Carboxylates, Academic press, New York (1983).

[49] S. K. Arora, V. Patel, B. Chudasama, B. Amin, J. Cryst. Growth **275** (2005) 657.

[50] V. Thomas, A. Elizebeth, H. Thomas, G. Jose, N. V. Unnikrishnan, C. Joseph, M. A. Ittyachen, Optoel. Adv. Mater. **7** (2005) 2687.

[51] S. K. Arora, V. Patel, B. Amin, A. Kothari, Bull. Mater. Sci. **27** (2004) 141.

[52] S. K. Arora, V. Patel, R. G. Patel, B. Amin, A. Kothari, J. Phys. Chem. Sol. **65** (2004) 965.

[53] K. Suryanarayana, S. M. Dharmaprakash, K. Sooryanarayana, Bull. Mater. Sci. **21** (1998) 87.

[54] C. Medrano, P. Gunter, H. Arend, Phys. Stat. Sol. (b) **143** (1987) 749.

[55] K. D. Parikh, B. B. Parekh, D. Dave, M. J. Joshi, Indian J. Phys. **80** (2006) 719.

[56] C. Valcarce, A.Holmgren, J.Stenflo J. Biol. Chem. **269** (1994) 26011-26016.

[57] O'Neil MJ, Royal Society of Chemistry, **15** (2013) 30.

[58] Rodgman A, Perfetti TA The Chemical Components of Tobacco and Tobacco Smoke. **2** (2013) 2086.

[59] Yu J. et al, Environ Sci Technol. **32** (1998) 2357-70.

[60] Yu LE et al, Environ Sci Technol. **39** (2005) 707-15.

[61] Cronn DR et al, Atmos Environ. **11** (1997) 929-37.

[62] Stringfellow WT et a,l J Hazardous Materials **275** (2014) 37-54.

[63] Kawamura K., Kaplan IR. Environ Sci Technol. **21** (1987) 105-10.

[64] Hays MD et a,l Environ Sci Technol. **36** (2002) 2281-95.

[65] Darracq G et al, Water Sci Technol **59** (2009) 1315-22.

[66] Kennedy GL Jr Toxicity of adipic acid, Drug Chem Toxicol **25** (2002) 191-202.

[67] E. Bingham, B.Cohrssen, C. H. Powell, Patty's Toxicology Volumes 1-9 5th ed. John Wiley Sons. New York, N.Y. **5** (2001) 765.

[68] "Cherry Jell-O Nutrition Facts". Kraft Foods. (2012).

[69] A Lincy, V Mahalakshmi, J Thomas and KV Saban, IOSR Journal of Applied Physics (IOSR-JAP) **6** (2014) 56-61.

[70] V.Mathew, S.Jacob, C.K.Mahadevan, K.E.braham, Materials Letters, **65** (2011) 2142 - 2145.

[71] B B Parekh, P M Vyas, S. R Vasant and M J Joshi, Bull. Mater. Sci., 31 (2008) 143 -147.

[72] M. P Binitha and P. P. Pradyumnan, Phys. Scr. **87** (2013) 065603.

[73] B.Want, F. Ahamed, P. N. Kotru, Material Science and Engineering A, **431** (2006) 237 - 247.

[74] M. Matzapetakis, C. P. Raptopoulou, A. Tsohos, J. Am. Chem. Soc. **120** (1998) 13266-13267.

[75] D. Voet, J. G. Voet, C. W. Pratt. The structure of the citric acid cycle, John Wiley Sons, Inc., New York, NY (2002).

[76] Anchell, Steve. "The Darkroom Cookbook: 3rd Edition (Paperback)". Focal Press. Retrieved (2013).

[77] Y. Y. Hu, A. Rawal, K. Schmidt-Rohr, Proceedings of the National Academy of Sciences. **107** (2010) 22425–22429.

[78] Huma Tareen et al. Biological Forum – An International Journal; **7** (2015) 367-369.

[79] Ayson, J.Fac.Pharm, **38** (2009) 233-255.

[80] Guy Drouin, Jean-Rémi Godin, and Benoît Pagé, Curr Genomics. **12** (2011) 371–378.

[81] I. Muhammad, S. Ashiru, I. Ibrahim D., A. I. Kanoma, I. Sani, S. Garba. Open science. **2** (2014) 60-65.

[82] Joanne L. Slavin2, and Beate Lloyd3, Adv Nutr. Health benefits of fruits and vegetables **3** (2012) 506–516.

[83] Shailja Chambial, Shailendra Dwivedi, Kamla Kant Shukla, Placheril J. John, and Praveen Sharma, Indian J Clin Biochem. **28** (2013) 314–328.

[84] Sudha J. Devaki and Reshma Lali Raveendran, (2017), DOI: 10.5772/intechopen.70162.

[85] Nudrat A. Akram, Fahad Shafiq, and Muhammad Ashraf, Front Plant Sci.; **8**, (2017) 613.

[86] Ifigeneia Mellidou, Johan Keulemans, Angelos K Kanellis and Mark W Davey. BMC Plant Biology. **12** (2012) 239.

[87] J. Mandl, A. Szarka, and G. Bánhegyi, Br J. Pharmacol. **157**(2009) 1097–1110 .

[88] Food-based approaches to meeting vitamin and mineral needs. FAO/WHO expert consultation on human vitamin and mineral requirements.

[89] Linda B. Bobroff and Isabel Valentín-Oquendo, UF/IFAS Extension. Facts about Vitamin C, 2001.

[90] Saeed Nojavan, Faezeh Khalilian, Fatemeh Momen Kiaie and atiyeh Rehmi, Journal of Food Composition and Analysis, **21** (2008) 300-305 .

[91] Luisa J. B., Laura A. M. and Consuelo D. M. Rev.Fac.Nal.Agr.Medellín. **67** (2014) 7209-7218.

[92] Juan Du, Joseph J. Cullen, and Garry R. Buettner; Biochim Biophys Acta. **1826** (2012) 443–457.

[93] Edmnund M. Mystkowski, Clinical Laboratory, Royal Infirmary, Edinburgh, The Oxidation of Ascorbic Acid in the Presence of Copper (1942).

[94] Canan Unaleroglu , Yuksel Mert Birgul Zumreoglu-Karan, Synthesis and Reactivity in Inorganic and Metal-Organic Chemistry **1532** (2012) 0094-5714.

[95] EFSA ANS Panel (EFSA Panel on Food Additives and Nutrient Sources added to Food), EFSA Journal; **13** (2015) 4087.

[96] Balcke P, Oxalic acid metabolism in chronic renal failure; Wien Klin Wochenschr. Suppl. **160** (1985) 1-15.

[97] José Luis Silencio Barrita and María del Socorro Santiago Sánchez, Antioxidant Role of Ascorbic Acid and His Protective Effects on Chronic Diseases, http://dx.doi.org/10.5772/52181.

[98] K. O. Soetan, C. O. Olaiya and O. E. Oyewole; African Journal of Food Science **4**(5) (2010) 200-222.

[99] Luis Villacorta, Angelo Azzi, Jean-Marc Zingg; Molecular Aspects of Medicine, **28** (2007) 507-537.

[100] W.Eugene Knox, M.N.D. Goswami; Advances in Clinical Chemistry, **4** (1961) 121-205.

[101] Linda B. Bobroff and Isabel Valentín-Oquendo, UF/IFAS Extension. Facts about Vitamin C, (2001).

[102] X. Zhou, Z. Yan, X. Han, Mater. Lett. **118** (2014) 39–42.

[103] Gregory L. W. Simpson , B.J. Ortwerth; Biochimica et Biophysica Acta **1501** (2000) 12.

[104] I.T.A.P.F.H. Eilberg, N. Division, U.F. De Sa, **63** (2003) 1066–1071.

[105] John Knight1, Kumudu Madduma-Liyanage1, James A. Mobley2, Dean G. Assimos1, and Ross P. Holmes; Urolithiasis. **44** (2016) 289–297.

[106] P. Orioli, B. Bruni, M. Di Vaira, L. Messori, F. Piccioli, V. Uni, V. Lastruccia, , **41** (2002) 4312–4314.

[107] M. Araya, F. Pizarro, M. Olivares, M. Arredondo, M. Gonzalez et al. Biol Res **39** (2006) 183-187.

[108] Edward D. Harris and Susan S Percival, The American Journal of Chemical Nutrition, Copper transport: insight in to a ceruloplasmin-based system, (2015).

[109] Ernst Graf, J. Agric. Food Chem. **42** (1994), 161.

[110] H.C.W. Skinner, A.H. Jahren, Biochemistry; Treatise on Geochemistry, (2007).

[111] Liam C. Palmer, Christina J. Newcomb, Stuart R. Kaltz, Erik D. Spoerke,§ and Samuel I. Stupp, Chem Rev. **108** (2008) 4754–4783.

[112] Imai, H., Oaki, Y. Kotachi, Bulletin of the Chemical Society of Japan. **79** (2006) 1834-1851.

[113] Adele L. Boskey, M Elements , **3** 387–393.

[114] D. June Sutor and Susan E. Wooley; **14** (1973) 215-220.

[115] Vishal N Ratkalkar, MD and Jack G Kleinman; **9** (2011) 187–197.

[116] K. Suguna, M. Thenmozhi and C. Sekar; Bull. Mater. Sci., **35** (2012) 701–706.

[117] M. C. Robert, O. Vidal, J. M. Garcia-Ruiz F. Otalora, Crystallization in gels and related methods In Crystallization of Nucleic Acids and Proteins: A Practical Approach (second edition). A. Ducruix R. Giegé, eds., IRL Press (1999) 149- 175.

[118] S. I. Stupp, G. C. Mejicano, Hanson, Mater. Res., **27** (1993) 289.

Chapter 2

Crystal Growth in Hydrosilica Gel and Characterization Techniques

2.1 Introduction

The gel method is an elegant and simple technique for growing perfect and strain free crystals. This is a promising technique for growing single crystals of substances which are slightly soluble in water and which cannot be grown conveniently from melt or vapour. The gel method has also been applied to study the crystal formation in urinary calculi and rheumatic diseases [1, 2]. To date, crystal growth in gel has got great popularity because of its suitability to grow crystals of biological macromolecules and in studies including biomineralization. The growth of variety of crystals having immense importance for their practical consideration and theoretical interest has been achieved by gel technique (Henisch 1988) [3, 4]. The importance of the gel growth is attributed to its simplicity in technique, effectiveness in growing single crystals of compounds that cannot easily be grown by other methods. Though the origin of the method dates back to 1899 – the famous work of Liesegang who discovered the periodic crystallization in gels, interest in gel technique received attention only after the work of Henisch and his co-workers [5-7]. A review of the literature reveals many reports describing the growth of crystals by this method.

Though it is not possible to grow big crystals, this technique has become popular because of its simplicity in developing perfect crystals. Using gel method ionic, organic and metallic crystals are grown at ambient temperatures. Also crystals of water-soluble salts are grown by reducing their solubility [8, 9]. A large variety of oxalate, tartrate, malonate and succinate crystals and mixed crystals of oxalates, tartarates of many elements have been reported to be grown by this method [10-20].

Gel growth is a particular case of solution growth where the solution is trapped in a polymeric structure. Gel is a two component system formed by linking of three dimensional system of cross-linkages between molecules of one of the components.

2.1.1 Principle of gel growth

The single crystals are growing due to the controlled chemical reaction. Solutions of two suitable compounds which give rise to the required insoluble crystalline substance by mere chemical reaction between them are allowed to diffuse into the gel medium and chemically react as follows.

A X + B Y $\rightarrow$ A Y + B X

Where

AX and BY are solutions of two compounds

AY is the sparingly soluble or insoluble substance formed.

BX is the substance formed which is highly soluble in water.

2.1.2 Types of gel

The gel can be regarded as a loosely interlinked polymer. When the dispersion medium is water, the material should be called 'hydrogel' to distinguish it from the brittle solids, which are often obtained by subsequent drying. The mechanical properties of fully developed gels can vary widely depending on the density and other precise conditions such as pH of gel, gel ageing etc. Gels can be prepared from organic as well as inorganic materials. Among these gels, silica gel is a versatile medium for growing crystals. Depending on the method of preparation, gels are classified into two, chemical and physical gels.

(1) Chemical gel: Gel formed by chemical reaction such as hydrolysis or polymerization. E.g.:- Silica, Polyacylamide, etc.
(2) Physical gel: Gel which is obtained by physical process such as cooling. E.g.:- Gelatin, Agar, Clay, etc.

2.1.3 Silica hydrogel: Preparation and structure

The most commonly used gel for crystal growth is the silica hydrogel due to its better suitability compared with organic gels [21, 22]. Silica gel is prepared from an aqueous solution of sodium metasilicate powder and a mineral or organic acid. The acid component helps to vary the pH of the system. In many cases these acid components serve as one of the reactants. Gelling process depends on the silicate concentration and on the degree of acidity. The gelation time varies from a few minutes to several days. The mechanical properties of the gel vary widely with the density of sodium metasilicate solution [23]. Greater gel density implies smaller pore size, which in turn decreases the diffusion rate of ions through it [24]. Very dense gels generally produce poor crystals, whereas gels of insufficient density take a long time to form and are mechanically unstable. In many systems, sodium metasilicate solution having density in the range of 1.03 - 1.06 g/cc yield better experimental results.

Extensive studies have been conducted on the mechanism of gel formation [25]. Silica gel is the polymerized form of silicic acid. When sodium metasilicate is dissolved in water, monosilicic acid is produced in accordance with the dynamic equilibrium.

$Na_2SiO_3 + 3\ H_2O \longleftrightarrow H_4SiO_4 + 2\ NaOH$

The process occurs continuously until a three-dimensional network of Si-O links is established as shown in Figure 2.1. The water molecules liberated during polymerization accumulate on the top of the gel surface. This phenomenon is known as 'syneresis'.

The pH of the gelling solution increases during syneresis due to the progressive and stabilizing hydroxyl substitution for oxygen in the polymerized structure. Since

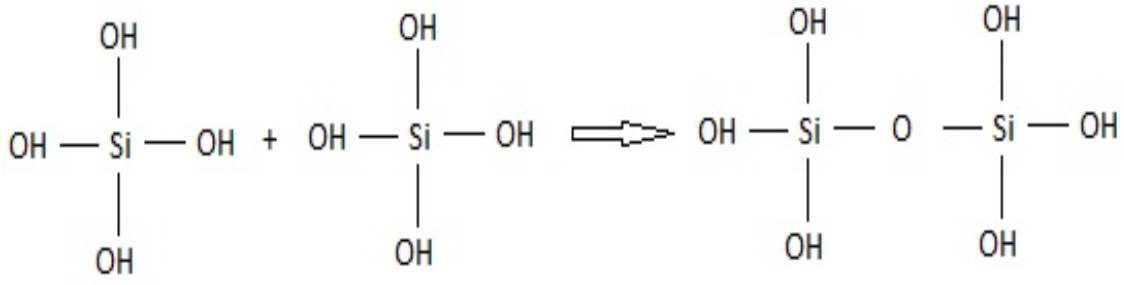

Figure 2.1: Polymerization of monosilicic acid.

these variations in the pH of the gel are difficult to control, the initially measured value of pH is taken as the pH of the gel. Before selecting the pH of the gel for the growth of a specific material, it has to be optimized through a series of trials, since slight changes in the growth environment affects the quality of the crystals.

The dependence of the gelling rate (measured in terms of turbidity) on temperature is found to be linear [26, 27]. Most systems become semitransparant or opaque in the course of gelling. The structural network in silica hydrogel are characterized by two types of pores [28], 'primary' pores of nearly molecular dimensions and 'secondary' pores which behave as normal capillaries [29].

2.1.4 Methods of gel growth

There are two types for gel growth.

(1) Single diffusion methods

(2) Double diffusion method

Single diffusion method

In this method one of the component, either AX or BY which is highly soluble in water and chemically inactive with the gel, is impregnated in acidified gel medium, considered as inner reactant. After gelation other component (outer reactant) is taken over the set gel. Diffusion of this solution through the gel and the reaction with the inner reactant produce crystals (AY). Some other component BY is also produced which is highly soluble in water and dissolve in water present in the hydro

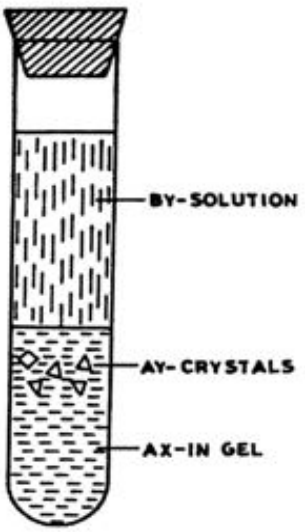

Figure 2.2: Schematic diagram of single tube method of crystal growth in gel medium.

gel medium (Figure 2.2).

Double diffusion method

Both the reactants are found to be chemically reactive with the hydro gel or soluble in water double diffusion method is used. By diffusion, the two components meet at a common region of the gel medium, normally the bend portion of the U tube and they react chemically thus crystals are formed. The experimental set up is shown in Figure 2.3.

2.1.5 Advantages of gel method:

1. Crystal growth takes place at ambient temperatures and hence crystal defects are reduced.

2. The crystals can be observed practically in all stages of their growth.

3. This method enables the control on the rate of reaction required for crystallization of a particular material.

4. All crystals are held in the position of their formation and this limits the container impact on the growth of crystals.

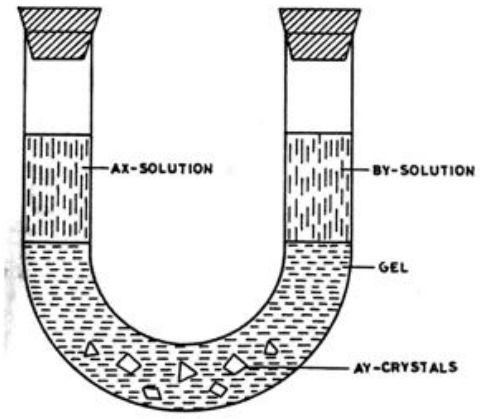

Figure 2.3: Double diffusion; 'U' tube method for crystal growth in gel.

5. The gel medium prevents convection currents and turbulence.

6. The number of nucleation sites and the size and morphology of the crystals can be controlled by changing the growth conditions.

7. Since all nuclei are spatially separated, the interaction between them is considerably diminished.

8. The growth procedure is simple and economical.

9. Gel mimics biological systems, the media can be used for growing crystals commonly observed in biological systems like oxalates, phosphates, cholesterole etc.

A few disadvantages of this method are the smaller size of the crystal and longer growth period. [30].

In the present work, grown crystals were characterized by various methods like XRD, FTIR, Micro Raman, TGA, DTG, DSC, UV-VIS Spectrophotometers, Dielectric properties. This chapter deals with the description of the characterization techniques.

2.2 X-ray diffraction studies:

X-ray diffraction (XRD) is one of the most important and considered to be non-destructive method for structural materials characterization, phase identification and crystalline size analysis. Max von Laue, in 1912, discovered that crystalline

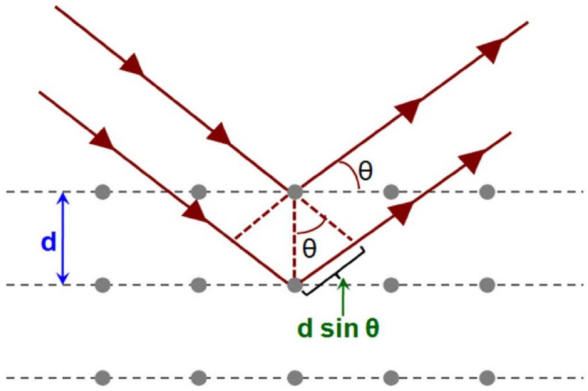

Figure 2.4: Interaction of X-rays with crystal planes.

substances act as three-dimensional diffraction gratings for X-ray wavelengths similar to the spacing of planes in a crystal lattice, which enabled the use of X-rays in the study of crystalline materials to determine the crystal structure and other relevant parameters. The crystal diffracts the X-ray; the basic law associated with it is the Bragg's law.

Bragg's law states that essential condition which must be met if diffraction occurs. When, X-ray radiation falls on a series of parallel planes equally spaced at a distance d (Figure 2.4) . Then the path difference is 2dsinθ for the reflected rays where is measured from the plane. For constructive interference, the path difference is nλ, where λ is the wavelength and 'n' is an integer. Condition for constructive interference is

$$n\lambda = 2d\sin\Theta \tag{2.1}$$

Where d the inter-planer spacing, Θ is the Bragg angle and λ is the wavelength of diffracted ray.

In this work the structure determination include single crystal X-ray diffraction technique and powder X-ray diffraction technique.

2.2.1 Single crystal X-ray diffraction studies:

Single crystal X-ray diffraction provides detailed information about the internal lattice of crystalline substances, including unit cell dimensions, bond-lengths, bond-angles, and details of site-ordering. Directly related is single-crystal refinement, where the data generated from the X-ray analysis is interpreted and refined to obtain the crystal structure [31].

X-ray diffractometers consist of three basic elements, an X-ray tube, a sample holder, and an X-ray detector. X-rays are generated in a cathode ray tube by heating a filament to produce electrons, accelerating the electrons towards a target by applying a voltage, and impact of the electrons with the target material. When electrons have sufficient energy to dislodge inner shell electrons of the target material, characteristic X-ray spectra are produced. These X-rays are filtered to produce monochromatic radiation, collimated and directed onto the sample. When the geometry of the incident X-rays impinging the sample satisfies the Bragg Equation, constructive interference occurs. A detector records and processes this X-ray signal and converts the signal to a count rate which is then output to a device such as a printer or computer monitor [32].

The single crystal X-ray diffraction study was carried out by Bruker AXS Kappa Apex II CCD diffractometer, with graphite monochromatic Mo-Kα radiation with λ = 0.71073 Å. The structure were solved by direct methods using programme SIR-92 and refined using a full matrix least square procedure on F^2 using SHELXL 97. Anisotropic displacement parameters were applied to non-hydrogen atoms in full matrix least square refinement based on F^2. Hydrogen atoms were refined isotropically in positions previously determined in the corresponding Fourier map. The IUCR software MECURY 3.1 is used for molecular graphics.

2.2.2 Powder X-ray diffraction studies:

In powder XRD, X-rays are generated by a cathode ray tube, filtered to produce monochromatic radiation, collimated to concentrate, and directed towards the sam-

ple. The interaction of the incident rays with the sample produces constructive interference (and a diffracted ray) and satisfy Bragg's Law ($n\lambda$=2d sin Θ). This law relates the wavelength of electromagnetic radiation to the diffraction angle and the lattice spacing in a crystalline sample. These diffracted X-rays are then detected, processed and counted. By scanning the sample through a range of 2Θ angles, all possible diffraction directions of the lattice should be attained due to the random orientation of the powdered material. Conversion of the diffraction peaks to d-spacings allows identification of the mineral because each mineral has a set of unique d-spacings [34, 35]. Powder patterns are like fingerprints: the resulting pattern of a compound is dependent on how the atoms are arranged within the material. Therefore, an experimentally-determined powder data can be compared to a collection of known diffraction patterns of materials in the International Centre for Diffraction Data. These not only provide information about the identity of the product isolated, but also allows scientists to comment on the number of compounds present in the sample. While a majority of the diffraction patterns listed in the database are in the family of extended solids such as minerals and zeolites, examples of inorganic molecules can be found [33].

We have employed a Rigaku Miniflex 600 X-ray diffractometer with Cu-Kα monochromator of wavelength 1.541 Å, operating at 45 kV and 15mA, using Cu target and graphite monochromator. The intensity data is recorded by continuous scan from 10 to 90^0 with a step size of 0.02^0 and scan speed of 10^0/minute. The analysis of the XRD pattern was carried out by PDXL software. Experimentally obtained diffraction pattern of the samples were compared with the standard powder diffraction data file published by International Centre for Diffraction Data (ICDD) database.

2.3 Fourier transform infrared spectroscopy

FTIR Spectroscopy is used to identify functional groups that are present in a molecule. It is a tool for qualitative analysis of every kind of material. IR can be

categorized into three wavelength regions: near IR (400 - 10 cm^{-1}), mid IR (4000 - 400 cm^{-1}) and far IR (14000 - 4000 cm^{-1}). This is important because knowing the functional groups present in the material help us to identifying an unknown substance and molecule in it. Infrared spectroscopy is the study of interactions between matter and electromagnetic fields in the IR region. In which, IR radiation is passed through a sample. Part of the IR radiation is absorbed by the sample and part of it is passed through (transmitted)it. The probability of a particular IR frequency being absorbed depends on the actual interaction between this frequency of radiation and the molecule. In general, a frequency will be strongly absorbed if its photon energy coincides with the vibrational energy levels of the molecule. The resulting spectrum represents the molecular absorption and transmission, creating a molecular fingerprint of the sample. Like a fingerprint no two unique molecular structures produce the same infrared spectrum [36]. The spectrum with IR absorption versus frequency is useful to identify the functional groups and bonds in the material. The characteristic band produced by impurities helps to quantify the impurity concentration within the material. The analysis of the obtained interferrogram is not an easy process, thus it is achieved through a mathematical tool, Fourier transformation. In general this transformation is carried out within the computer and we get a final desired spectrum, which can be easily analysed [37].

IR spectroscopy involves two kinds of fundamental vibration for molecules, stretching and bending.

Stretching: In which the distances between the two atoms increases or decreases, but the atoms remain in the same bond axis. Stretching vibration is found to occur in the order of bond strength.

Bending: In which the position of the atoms changes relative to the original bond axis. Bending vibrations generally requires less energy and occur at longer wavelength.

In this thesis work we have used Jasco model No.4100 fourier transform infrared spectrophotometer (FTIR). The KBr pellet method was used to carry out the measurement in the wavenumber range (400 - 4000 cm^{-1}) at room temperature.

2.4 Raman spectroscopy

Raman spectroscopy is a form of molecular spectroscopy that involves the scattering of electromagnetic radiation with atoms or molecules. It probes the vibrational, rotational and other low frequency modes of molecules; the Raman signal is observed as inelastically scattered light. Every molecule or chemical species has its own unique Raman spectrum; this allows us to develop database of known standards that can later be used for the identification, or verification of unknowns. Raman can also provide structure information and to track changes in frequency shift as well as differences in peak bandwidth [38].

In Raman spectroscopy, a sample is irradiated with a laser, most of the radiation will scatter "off" the sample at the same wavelength as that of the incoming laser radiation, a process known as Rayleigh scattering. However, a small amount will scatter from that sample at a wavelength shifted from the original laser wavelength. A molecule at rest resides in the ground vibrational and electronic states, the electric field of the laser light raises the energy of the system for an instant by inducing a polarization in the chemical species. The polarized condition is not a true energy state and is widely referred to as a "virtual state". Relaxation from the virtual state occurs almost instantaneously and predominately returns to the initial ground state. This process results in Rayleigh scatter. Relaxation to the first excited vibrational level results in a Stokes-Raman shift. Stokes-Raman shift scatter is of lower energy (longer wavelength) than that of the laser light. Most systems have at least a small population initially in an excited vibrational state. When the Raman process initiates from the exited vibrational level, relaxation to the ground state is possible, producing scatter of higher energy (shorter wavelength) than that of the laser light. This type of scatter is called anti-Stokes- Raman scatter [39].

The vibrational states probed by Raman spectroscopy are the same as those involved in infrared spectroscopy. As such, Raman spectroscopy is very similar to the more frequently used fourier transform infrared (FT-IR) spectroscopic technique. This two vibrational spectroscopic techniques are, in fact, complementary. Vibrations that are strong in an infrared spectrum (those involving strong dipole

moments) are usually weak in a Raman spectrum. Likewise, non-polar functional group vibrations that give very strong Raman bands usually result in weak infrared signals [40]. Micro Raman spectra of the samples under study were collected at room temperature using JASCO 4200 spectrophotometer, with laser wavelength 532 nm.

2.5 Thermal analysis techniques

A group of techniques in which a property of the sample is monitored against time or temperature while the temperature of the sample, in a specified atmosphere, is programmed. The term "Thermal Analysis" incorporates those techniques in which some physical parameter of the system is determined and or recorded as a function of temperature. Thermal behaviour is one of the physical properties of any material. It gives fair estimation, of constituents and nature of material. The traditionally adopted procedures for Thermo gravimetry and calorimetry are tedious, time consuming and involve human intervention. Modern thermal analysis systems overcome all the problems associated with the traditional techniques as the versatile computers for setting up of experiment, its control, data acquisition/storage and analysis. Use of electronic sensors for physical measurements increases sensitivity, accuracy and case of operation.

There are various techniques of thermal analysis; some of them are discussed here:

- Thermo gravimetric analysis [TGA]
- Differential thermal analysis [DTA]
- Differential Scanning Calorimetry [DSC]

2.5.1 Thermo gravimetric analysis (TGA)

Thermo gravimetric (TGA) analysis provides a quantitative study of any weight change associated with time or temperature due to dehydration or decomposition of a material. Thermo gravimetric curves are characteristics for a given compound or systems because of the unique sequence of physical or chemical reactions, which

occur over definite temperature ranges and at rates that are a function of the molecular structure. TGA is useful for investigating the thermal stability of solids and liquids. A sensitive microbalance measures the change in mass of the sample as it is heated or held isothermally in a furnace. The purge gas surrounding the sample can be either chemically inert or reactive. TGA instruments can be programmed to switch gases during the test to provide a wide range of information in a single experiment. TG can be utilized for the analysis of thermal decomposition, oxidization, dehydration, heat resistance, and kinetics analysis. By combining with the other measurement techniques, variety of information can be achieved from one sample [41].

Changes in weight are a result of the rupture and/or formation of various physical and chemical bonds at elevated temperature that lead to the evolution of volatile product or the formation of heavier reaction products. From such curves, data are obtained concerning the thermodynamics and kinetics of the various chemical reactions, reaction mechanism, and the intermediate and final reaction products. The usual temperature range is from ambient to 1200^0C with inter or reactive atmospheres. The derivative in TG is often used to pinpoint completion of weight – loss steps or to increase regulation of overlapping weight – loss occurrences.

2.5.2 Differential thermal analysis (DTA)

Differential thermal analysis is a technique which records the temperature difference between sample and a reference material, against time or temperature, as the two samples are subjected to identical temperature regimes in an environment heated or cooled at a controlled rate. The DTA plot shows sharp increase or decrease in the temperature difference, depending on whether a change in the sample causes absorption or liberation of heat. The method records all changes in enthalpy, whether accompanied by a change in weight or not, or chemical reactions.

2.5.3 Differential scanning calorimetry (DSC)

A technique in which the temperature of the sample unit, formed by a sample and reference material, is varied in a specified program, and the temperature difference between the sample and the reference material is measured as a function of temperature. DSC enables the measurements of the transition such as the glass transition, melting, and crystallization. Furthermore, the chemical reaction such as thermal curing, heat history, specific heat capacity, and purity analysis are also measurable. Recently, with the development of the highly-functional polymeric material, analysis of these thermal properties are increasing dramatically. DTA and DSC detect the temperature differences between the sample and the reference; however, DSC can perform the quantitative measurement of the amount of heat on top [42].

In the study the thermogravimetric analysis, differential thermal analysis and differential scanning calorimetric analysis of the samples were carried out by Perkin Elmer STA 6000 simultaneous TG-DTA-DSC analyser. The purge gas used is nitrogen at a flow rate of 200 ml/minute. The measurements were carried out by heating a known weight of the sample at a heating rate of 10 ^{0}C/minute.

2.6 UV-visible spectroscopy

UV-visible spectrophotometry is used to determine the absorption or transmission of UV-visible light (200 to 700 nm) by a sample. It can also used to measure concentrations of absorbing materials based on developed calibration curves of the material. A spectrometer is employed to measure the amount of light that a sample absorbs. The instrument operates by passing a beam of light through a sample and measuring the intensity of light reaching a detector. The beam of light consists of a stream of photons. When a photon encounters an analytic molecule (molecule being studied), there is a chance the analytic will absorb the photon. This absorption reduces the number of photon in the beam of light, thereby reducing the intensity of the transmitted light beam.

The optical phenomenon known as diffuse reflectance is commonly used in the

UV-visible, near-infrared (NIR), and mid-infrared (sometimes called DRIFT or DRIFTS) regions to obtain molecular spectroscopic information. It is usually used to obtain spectra of powders with minimum sample preparation. A reflectance spectrum is obtained by the collection and analysis of surface-reflected electromagnetic radiation as a function of frequency (usually in wavenumbers (cm^{-1})) or wavelength (usually in nanometers) [43].

In the case of powder sample, the powder is dispersed in water, ethanol, etc. to carry out the UV-Visible absorption spectroscopy analysis. As the size of the particles reduces, the chance for precipitation increases and thus limits the application of UV-visible absorption spectroscopy in the band gap estimation of powder samples. This can be solved by the use of diffuse reflectance spectroscopy (DRS).

Diffuse reflectance spectroscopy (DRS)

The band gap estimation of the prepared sample was done using diffuse reflectance spectroscopy. Kubelka - Munk (KM) theory proposes the study of diffuse reflectance spectra of samples. When light falls on the material, some part of the light gets reflected at the powder surface and some part enters to the powder sample and diffuses. The measured diffuse reflected light at different wavelengths will provide a diffused reflectance spectrum. The intensity of this output at the limit of infinitely thick sample is given by,

$$k/s = (1\text{-}R)^2/2R = F(R) \tag{2.2}$$

Where, R is the absolute diffuse reflectance, F(R) is the Kubelka-Munk function, k is the absorption coefficient and s is the scattering coefficient which varies with particle size and packing. This equation is known as Kubelka –Munk equation. The acquired diffuse reflectance data is used to find Kubelka-Munk function F(R). Since Kubelka-Munk function is proportional to the absorption coefficient, the expression (2.1) becomes,

$$(h\nu F(R))^2 = A^1(h\nu - Eg) \tag{2.3}$$

where A^1 is the proportionality constant and $\nu = 1/2$ for the current samples. Using this relation, the band gap energy can be obtained by extrapolating the linear part of $(h\nu F(R))^2$ to the $h\nu$ axis.

In the present work, band gap of grown single crystals has been estimated by recording diffuse reflectance spectrum of the powdered crystals in the wavelength range of 200-900 nm using JASCO V-550 UV/VIS spectrophotometer.

2.7 Dielectric properties

Dielectric materials are essentially insulators, which means that no current will flow through the material when a voltage is applied. However, certain changes do happen at the atomic scale. When a voltage is applied across a dielectric object, it becomes polarized. Since atoms are made of a positively charged nucleus and negatively charged electrons, polarization is an effect which slightly shifts electrons towards the positive voltage. Once the voltage source is removed from the material, it either returns to its original non-polarized state, or stays polarized if the molecular bonds in the material are weak. The difference between the terms dielectric and insulator is not very well defined. All dielectric materials are insulators, but a good dielectric is one which is easily polarized. A dielectric material possesses one or more of the basic types of electric polarization. There are three major mechanisms of electric polarization which are electronic, ionic and orientational polarization. At moderate electric field (low frequency) and for materials with a very low conductivity, these mechanisms of polarization contribute to the dielectric constant. The further increase in the frequency of the applied field, the contributions from different polarization starts reducing. In electronic and atomic polarization electric field causes deformation or translation of the electron clouds of atoms or molecules from their symmetrical distribution. This is essentially the displacement of the outer electron clouds with respect to inner positive atomic cores. Orientational polarization occurs only in a material consisting of molecules or particles with a permanent dipole moment. The electric field causes the orientation of the dipoles towards the direction of

the field. In a dielectric material, polarization due to migration of charge carriers to form space charges at interfaces or grain boundaries, it becomes important at high concentration of charge carriers. This type of polarization is called space charge polarization. The contribution towards polarization from space charge effects depends on the purity and perfection of crystals, because the impurities or other forms of imperfection create potential barriers, limiting the transport of charge carriers and hence increasing the value of dielectric constant [45, 46].

Dielectric constant:

The dielectric constant of a material, also called the permittivity of a material, represents the capacity of a material to accumulate charges, under applied electric feild. All materials, including vacuum, store energy when placed in an electric field. The permittivity of vacuum is defined as the physical constant ϵ_0, which is approximately $\epsilon_0 = 8.854$ x 10^{-12} F/m (farads per meter). Other properties such as dielectric strength and dielectric loss are equally important in the choice of materials for a capacitor in a given application. [47].

Since most capacitors are not made of vacuum, it makes sense to define permittivity for every material. The permittivity of a material is defined as $\varepsilon = \varepsilon_0 \varepsilon_r$, where ε_0 is the absolute permittivity and ε_r is the relative permittivity. ε_r is a number which is always greater than 1, meaning that all materials store more energy than free space when subjected to an electric field. The dielectric material increases the storage capacity of the capacitor by neutralizing charges at the electrodes, which ordinarily would contribute to the external field. The capacitance with the dielectric material is related to dielectric constant. This property is quite useful in capacitor applications. It should be noted that the relative permittivity depends on many factors, such as temperature, pressure and even frequency, which is why materials with more stable dielectric constant are favoured in some applications [48, 49].

$$\mathrm{C} = \epsilon_r \epsilon_0 \ \mathrm{A/d} \tag{2.4}$$

where C is the capacitance, ε_r is the relative permittivity of the material, ε_0 is the permittivity of vacuum, A is the area of the plates and d is the distance

between the plates. The capacitance of the dielectric material is related to the dielectric constant as indicated in the above equations. It becomes clear that the larger ε_r is, the larger the resulting capacitance becomes.

Dielectric loss:

When an a.c. field is applied to a dielectric material, some amount of electrical energy is absorbed by the dielectric material and is dissipated in the form of heat. This loss of energy is known as dielectric loss. These losses happen because as the material changes polarization, the tiny electron shifts can be regarded as a tiny alternating current flow. Different materials have different losses at different frequencies, and this characteristic must be accounted for in some high frequency applications [50].

Dielectric studies were carried out by LCR Hi TESTER 3532-50. LCR Hitester is an impedance meter which has a computer interface that enables extremely easy operation. The test frequency can be set from 100 Hz to 5 MHz at high resolution. The instrument is able to measure maximum of four parameters like impedance, phase angle, inductance L, capacitance C, resistance R, dielectric loss (D), etc. out of the fourteen parameters within the scope of the machine at a time [51]. The sample were finely ground and made in the form of pellets using a hydraulic press and are placed in a conductivity cell, made up of copper. For temperature variations the cell containing the sample were placed inside a microprocessor controlled furnace with an accuracy of $\pm 1^0$C.

References

[1] Janeth B. Presores, Katherine E. Cromer, Christina Capacci-Daniel, and Jennifer A. Swift; Cryst. Growth Des., **13** (2013) 5162–5164.

[2] Antonio J. Reginato and Brenda Kurnik, Seminars in Arthritis and Rheumatism, **18** (1989) 198-224.

[3] Henisch H.K., Dennis J. and Hanoka J.I., J. Electrochem., **112** (1965) 627.

[4] Henisch H.K., Dennis J. and Hanoka J.I., J. Phys. Chem. Solids **26** (1965) 493.

[5] H. K. Henisch; Crystals in Gels and Liesegang Rings. . Cambridge University Press, Cambridge (1988) 197 -ISBN 0-521-34503-0.

[6] H. K. Henisch; Crystal Growth in gels (Pennsylvania State Univ. Press) (1970).

[7] H.K.Henisch and J.M.García-Ruiz, Journal of Crystal Growth, **75** (1986) 195-202.

[8] Glocker D. A and Soest I.F., J. Chem. Phys., **51** (1969) 3143.

[9] Brezina B. and Haveankova, Mater. Res. Bull., **87** (1971) 537.

[10] B. B. Parekh, P. M. Vyas, Sonal R. Vasant and M. J. Joshi, Bull. Mater. Sci., **31** (2008) 143–147.

[11] D. Valarmathi1, Leela Abraham S. Gunasekaran, Indian Journal of Pure Applied Physics **48** (2010) 36-38.

[12] P. V. Dalal and K. B. Saraf, Bull. Mater. Sci., **34** (2011) 377–381.

[13] B. Donkova, D. Mehandjiev, Thermochimica Acta **421** (2004) 141–149.

[14] K. V. Bangera and P. Mohan Rao, Bull. Mater. Sci.,**15** (1992) 339-347.

[15] M. P. Binitha, P. P. Pradyumnan, J Therm Anal Calorim; **114** (2013) 665–669. DOI. 10.1007/s10973-013-2998-2.

[16] S. K. Arora, Vipul Patel, Anjana Kothari, and Brijesh Amin Crystal Growth Design **4** (2004) 343-349.

[17] V.Mathew, S.Jacob, C.K.Mahadevan and K.E.Abraham; Material Letters, **65** (2011) 2142-2145.

[18] P. A. Varughese, K. V.Saban, J. George, I. Paul, G. Varghese; Journal of Materials Science **39** (2004) 6325– 6331.

[19] M.P. Binitha, P.P. Pradyumnan Journal of Crystal Growth. **396** (2014) 38–44.

[20] M. P. Binitha and P. P. Pradyumnan, Phys. Scr. **87** (2013) 065603.

[21] Eitel W., The Physical Chemistry of Silicates, The University of Chicago, Chicago, 1954.

[22] Plank C.J and Drake L.C, J. Colloid Sci., **2** (1974) 413.

[23] Lefaucheux L., Robert M.C., Gils S., Bernard Y. and Gauthier B., Rev. Int.Hauter Temp. Refract., **23** (1986) 57.

[24] Greenberg S. A. and Sinclair D., J.Phys. Chem., **59** (1955) 435.

[25] Audsley A. and Aueston J., J. Amer. Chem. Soc., **84** (1962) 2320.

[26] Blitz M., Z. Phys. Chem., **126** (1927) 356.

[27] A. R. PATEL and A VENKATESWARA RAO, Crystal growth in gel media, Bull. Mater. Sci, 4. No. **5** (1982) 527 - 548.

[28] M. C. Robert and F. Lefaucheux, Journal of Crystal Growth **90** (1988) 358—367

[29] Enas M. Ahmed, Journal of Advanced Research; **6** (2015) 105–121.

[30] U. Vijayalakshmi, A. Balamurugan and S. Rajeswari , Trends Biomater. Artif. Organs, **18** (2005).

[31] K. Hasegava, The Rigaku Journal, **28** (2012).

[32] A. E. Goeta and J A K Howard, Chem. Soc. Rev., **33** (2004) 490.

[33] F. Smith, Industrial Applications of X-ray Diffraction,CRC Press (1999).

[34] Thermo ARL Basics of X-ray Diffraction: Chapter 7 (1999).

[35] B. D. Cullity, Elements of X-Ray Diffraction, Addison-Wesley Publishing Company, Inc. (1956).

[36] B. Stuart , Infrared Spectroscopy: Fundamentals and Applications; John Wiley Sons, Ltd(2004).

[37] John Coates, Interpretation of Infrared Spectra, A Practical Approach, Encyclopedia of Analytical Chemistry R. A. Meyers (Ed.) 10815–10837, John Wiley Sons Ltd, Chichester, 2000.

[38] R. H. ATALLA, U. P. AGARWAL, and J.S. BOND, Raman Spectroscopy, Springer Series in Wood Science Methods in Lignin Chemistry (Edited by S.Y. Lin and C.W. Dence) Springer-Verlag Berlin Heidelberg 1992.

[39] E N Kauffmann Characterization of Materials, John Wiley Sons (2003).

[40] John R. Ferraro, Kazuo Nakamoto and Chris W. Brown , Introductory Raman Spectroscopy, (Second edition) Elsevier, (2003).

[41] D.B.Sirdheshmukh, L. Sirdheshmukh and K.G.Subhadra, Spriner Series in material science (2006).

[42] H. K. D. H. Bhadeshia, Differential Scanning Calorimetry, University of Cambridge, Materials Science Metallurgy.

[43] Sabiu Said Abdullahi1, Sadik Güner2, Yuksel Koseoglu3 Ibrahim Murtala Musa4, Bala Ismail Adamu5, and Mahmud I Abdulhamid, Journal of the Nigerian Association of Mathematical Physics **35** (2016) 241-246.

[44] G. A. V. Sowter, J.audio Eng, Soc. **35** (1987) 10.

[45] Liu Hongbo, Dielectrics under Electric Field (2018), doi.org/10.5772/intechopen.72231.

[46] M. S. Venkatesh1 and G. S. V. Raghavan, Canadian Biosystems Engineering **47** (2005).

[47] T. T. Grove, M. F. Masters, and R. E. Miers, Am. J. Phys. **73** (2005).

[48] Reza Zamiri, Ajay Kaushal, Auto Rebelo, J.M.F.Ferreira, Ceram. Int. **40** (2014) 1635.

[49] Xihong Hao, Journal of Advanced Dielectrics **3** (2013) 1330001.

[50] Gary L. Johnson, Solid State Tesla Coil, chapter 3 : Lossy Capacitors (2001).

[51] H.M. El-Mallah, Acta Physica Polonica A **122** (2012) 174-179.

Chapter 3

Growth and Characterization of Metal Adipate Crystals

3.1 Introduction

Metal organic frameworks are one of the most attractive fields of materials for application in catalysis, gas adsorption, sensing, luminescence, drug delivery, etc. [1]. The study of organo-metallic hybrid materials focused on the following points: (1) exploration of new preparative methodology for hybrid materials, (2) new combinations between different materials, (3) functionalization of hybrid materials, (4) modification of hybrids for industrial applications and (5)the study crystallization of materials in biological and organic systems [2]. A metal organic framework consists of metal ion and an organic ligand. In most cases, the inorganic metal part acts major role on the overall structure and physical behavior including mechanical strength. Various crystallographic studies in this field have been reported with diverse crystal structures, resulted in different optical, electronic and magnetic properties [3]. The gel diffusion method is one of the most promising technique for growing organo-metallic single crystals. Gels promote the growth of high-quality crystals of various molecules. This method possess many advantages for growing high quality biologically important crystals at ambient condition [4].

This research work reports the single crystal growth, characterization and property studies of crystalline adipates of calcium, cobalt, copper and zinc. Adipic acid with relatively smaller central moiety is act as a ligand for the growth of adipate single crystal. The crystals were grown by single diffusion gel technique. Adipic acid impregnated silica gel provides a controlled medium for the diffusion of supernatant cations into it, which leads to the controlled reaction and thus to form respective crystals. Structural, spectroscopic, thermal and dielectric properties of grown crystals also were described.

3.2 Growth of crystals

The single crystals of metal adipates were grown by single diffusion gel technique. Sodium meta silicate powder was dissolved in double distilled water and the solution was filtered out. The density of prepared stock solution is determined using specific gravity bottle. After making this solution at a particular specific gravity, the gel was set by incorporating the cation component (adipic acid) with sodium meta silicate solution so that the pH of the solution was brought to the desired value. This mixture was taken in test tubes and kept for gelation. After setting the gel, chloride solutions of Ca, Co, Cu and Zn were poured over the gel along the sides of the test tube separately, without breaking the gel. The crystals of calcium adipate monohydrate (CaAMH), cobalt adipate tetrahydrate (CoATH), copper adipate monohydrate (CuAMH) and zinc adipate (ZnA) appeared inside and interface of the gel. The following chemical reactions were expected to take place for the formation of the title compounds.

$CaCl_2 + (C_6H_{10}O_4) + H_2O \rightarrow Ca(C_6H_8O_4)\ H_2O + 2HCl$

$CoCl_2 + C_6H_{10}O_4) + 4H_2O \rightarrow Co\ (C_6H_8O_4\ 4H_2O) + 2HCl$

$CuCl_2 + (C_6H_{10}O_4) + H_2O \rightarrow Cu(C_6H_8O_4)\ H_2O + 2HCl$

$ZnCl_2 + (C_6H_{10}O_4) \rightarrow Zn(C_6H_8O_4) + 2HCl$

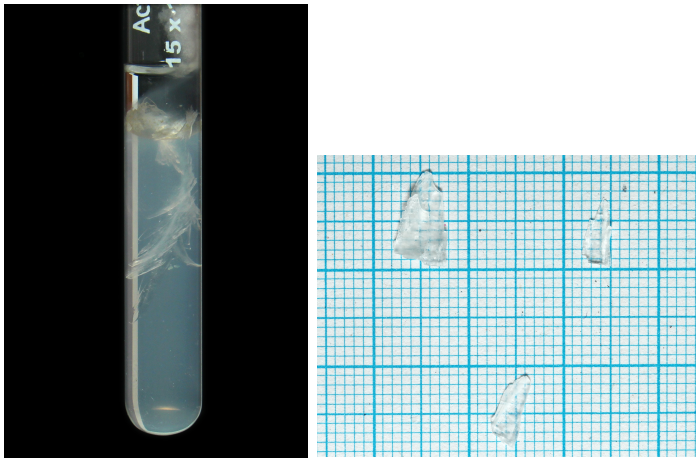

Figure 3.1: CaAMH crystals during growth and grown crystals.

3.2.1 CaAMH crystals

During the growth of CaAMH crystals, the concentration of the diffusant is optimum, a few critical-sized nuclei are produced. Due to the subsequent diffusion of Ca^{2+} ions, $Ca(C_6H_8O_4)$ H_2O crystals with definite faces and good sizes are formed . The habits of the crystals formed within the gel were leaf-like and transparent. The grown CaAMH crystal in growth apparatus is shown in Figure 3.1.

3.2.2 CoATH crystals

The supernatant solution of $CoCl_2$ diffuses into the gel column and reacts with adipic acid in the gel to produce necessary supersaturation for the slow precipitation of Co $(C_6H_8O_4)$ $4H_2O$. When the concentration of the added $CoCl_2$ solution, and the gel density and the adipic acid concentration are optimum, few critical-sized nuclei were produced and due to the subsequent diffusion of this diffusant, crystals with definite faces and good sizes were formed. The crystals formed in the gel were rectangular, whereas at the gel solution interface small plates-like single crystals of good transparency were formed. The crystals formed in and above the gel showed a change in their morphology only, with no change in the molecular formula and structure, as observed from XRD and thermal studies. Good quality CoATH crystals having dimension $3\times1\times0.5$ mm^3 were obtained from the gel. An example of

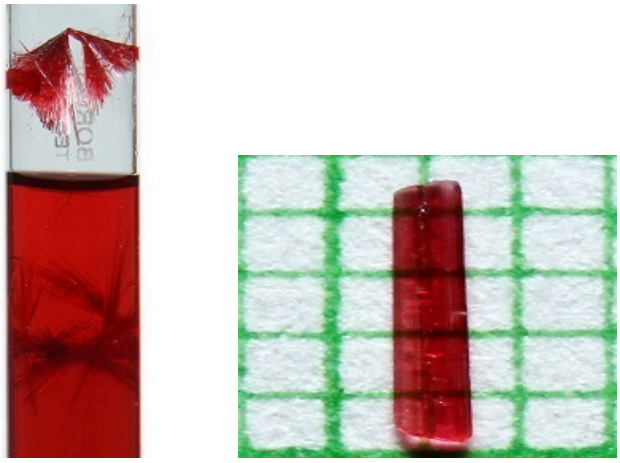

Figure 3.2: CoATH crystals during growth and grown single crystal.

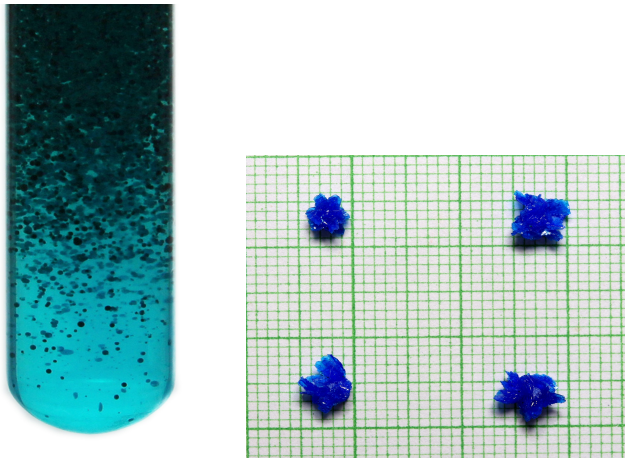

Figure 3.3: Growth of CuAMH crystals in testube and grown crystals.

growth test-tube and grown crystals is shown in Figure 3.2.

3.2.3 CuAMH crystals

It was noted that when the concentration of the diffusant is optimum, a few critical-sized nuclei were produced and due to the subsequent diffusion of Cu^{2+} ions crystals are formed. The habits of the crystals formed within the gel were spherulitic and blue in color. The experiment resulted in the formation of crystals of maximum size $5\times5\times5$ mm^3. The crystals of CuAMH are shown in Figure 3.3.

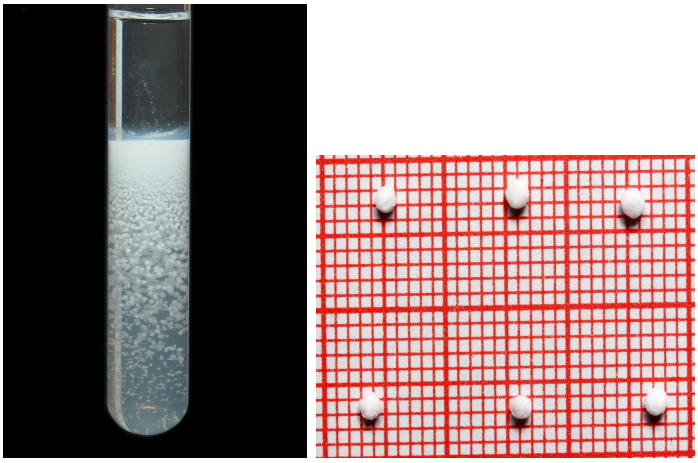

Figure 3.4: Growth of ZnA crystals in testube and grown crystals.

Table 3.1: Optimum conditions for the growth of adipate crystals

Paramaeters	CaAMH	CoATH	CuAMH	ZnA
Gel density	1.05	1.06	1.05	1.05
pH	6	6	6	6
Gel set time	1 day	1 day	1 day	1 day
Growth period	35 days	28 days	35 days	35 days
Concentration of adipic acid	1M	1M	1M	1M
C oncentration of upper reactant	1M	1M	1M	1M

3.2.4 ZnA crystals

It was noted that when the concentration of the diffusant is optimum, a few critical-sized nuclei are produced and due to the subsequent diffusion of Zn^{2+} ions crystals are formed. The habits of the crystals formed within the gel were spherulitic. The experiment resulted in the formation of crystals of maximum size $2\times2\times2$ mm^3. The crystals of ZnA are shown in Figure 3.4.

The effect of various growth parameters such as gel pH, gel density, gel age and concentration of reagents on the growth of CaAMH, CoATH, CuAMH and ZnA crystals were investigated. The optimum growth conditions for obtaining good-quality crystals are summarized in Table 3.1.

Well grown good quality crystals were separated from the gel medium and structural, spectroscopic and thermal characterizations were performed.

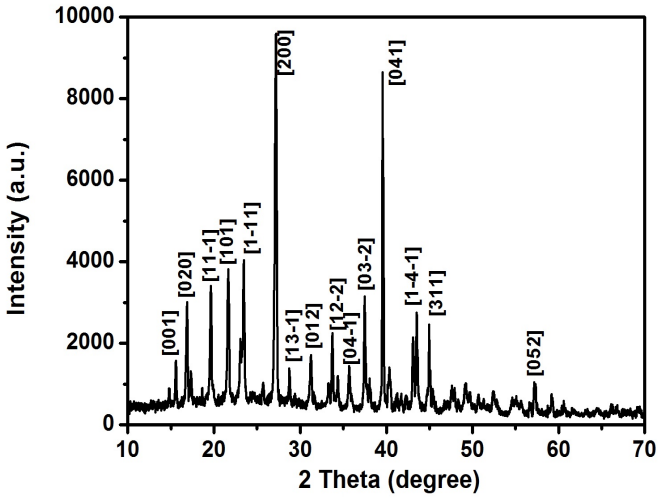

Figure 3.5: Powder XRD pattern of CaAMH crystal.

3.3 Structural studies

3.3.1 CaAMH crystals

Figure 3.5 shows the powder XRD pattern of the CaAMH crystal. The crystallinity of the material is quite clear from this diffraction pattern. The powder XRD spectrum matches well with the ICDD Card number 00-061-1260. The calculated cell parameters reveal that the crystal belongs to the triclinic system having space group P-1(2). The unit cell parameters of the crystal calculated by PDXL software by matching with the above ICDD card are a = 6.807 Å, b= 10.838 Å, c = 5.04 Å, $\alpha = 98.24^o$, $\beta = 96.99^o$, $\gamma = 79.08^o$ and unit cell volume = 421.253 $(Å)^3$, and are in agreement with the literature [5]. The experimental d-values are in conformity with the calculated ones obtained by using the above cell parameters for crystals.

3.3.2 CoATH crystals

Single crystal XRD studies showed that the structure of CoATH crystal is monoclinic, with the following measured cell parameters: a = 7.9805 Å, b = 14.9720 Å, c = 9.5815 Å, $\alpha = 90^o$, $\beta = 90.689\ ^o$, $\gamma = 90\ ^o$. Figure 3.6 shows the ORTEP (Oak Ridge Thermal Ellipsoid Plot) of CoATH.

In this structure, Co^{2+} ion is in a six coordinate environment (Figure 3.7), defined by six O atoms from six different adipate groups. The Co–O bond distances vary between 2.027 and 2.210 Å and O–Co–O bond angles vary in a very wide range from 85.140 to 180.0 Å. The crystal data and structure refinement parameters are presented in Table 3.2. The atomic coordinates and equivalent thermal parameters for all the non-hydrogen atoms are given in Table 3.3. Tables 3.4 and 3.5 give the selected bond lengths and bond angles. The four water molecules present in the crystal involve the extensive network of hydrogen bond amongst themselves and are responsible for the stability of the structure. The oxygens O7 and O6 of water molecules serve as receptors or donors of O-H...O hydrogen bond and are hydrogen-bonded to carboxylate oxygens of adipate group (O1 and O4). Table 3.6 gives the parameters of hydrogen bonding.

The powder XRD pattern of the grown crystal is presented in Figure 3.8 and the 'd' values of the Braggs peaks in the XRD pattern of the crystal were compared with the corresponding ICDD values and were found to match well with the standard card (No: 00-051- 2302). The Miller indices of the faces appearing in the growth morphology of the crystal is marked in Figure 3.8. The sharp peaks at specific Braggs angles confirm the crystallinity of the entire sample.

3.3.3 CuAMH crystals

Figure 3.9 shows the powder XRD pattern of the CuAMH crystal. The crystallinity of compound is quite clear from this diffraction pattern. The powder XRD spectrum matches well with the ICDD Card number 00-055-1541. The calculated cell parameters reveal that the crystal belongs to the monoclinic system having space group P21/c(14). The unit cell parameters of the crystal calculated by PDXL software by matching with the above ICDD card are a = 18.31 Å, b= 11.23 Å, c = 9.76 Å, $\alpha = \gamma = 90.00^{o}$, $\beta = 109.35^{o}$ and unit cell volume = 1893.5 $(Å)^3$, and are in agreement with the literature [6].

Table 3.2: Crystal data and structure refinement for CoATH crystal

Parameter	CoATH crystal
Identification code	Shelxl
Emperical formula	$C_6H_{10}CoO_9$
Formula weight	285.07
Temperature	273(2) K
Wavelength	0.71073 Å
Crystal system, Space group	Monoclinic, P21/n
Unitcell dimensions	a = 7.9805 Å, b=14.972 Å, c = 9.5815 Å, $\alpha = \gamma = 90^0$, $\beta = 90.689^0$
Volume	1144.75 (12) $Å^3$
Z, Calculated density	4, 1.654 Mg/m^3
Absorption coefficient	3672 mm^{-1}
F(000)	580
Theta range for data collection	2.893 to 24.999 deg
Limiting indices	-9$\leq h \leq 9, -17 \leq h \leq 17, -11 \leq h \leq 11$,

Table 3.3: Atomic coordinates (Å$\times 10^{-4}$) and equivalent isotropic displacement parameters ($Å^2 \times 10^3$) for grown crystals

Atoms	X	Y	Z	U(eq)
Co1	0.5	0.5	0	0.0183(3)
Co2	0	0.5	0	0.0201(3)
O1	0.5741(4)	0.3834(2)	0.9108(4)	0.0304(8)
O2	0.3289(4)	0.3239(2)	0.8622(4)	0.0341(9)
O3	0.3469(4)	0.4191(2)	0.2903(4)	0.0345(9)
O4	0.5824(4)	0.4530(2)	0.1870(3)	0.0306(8)
O5	0.2458(3)	0.4463(2)	0.0338(3)	0.0214(7)
O6	-0.0877(4)	0.4623(3)	0.1899(4)	0.0409(9)
O7	-0.0876(4)	0.3825(2)	-0.0853(4)	0.0353(9)
O8	0.0668(6)	0.2985(3)	0.6815(6)	0.0684(15)
O9	0.0665(5)	0.4220(3)	0.4482(4)	0.0425(10)
C1	0.4825(6)	0.3271(3)	0.8485(5)	0.0225(10)
C2	0.5659(6)	0.2636(3)	0.7527(5)	0.0270(11)
C3	0.6435(6)	0.3108(3)	0.6295(5)	0.0268(10)
C4	0.5164(6)	0.3489(3)	0.5278(5)	0.0267(11)
C5	0.6062(6)	0.3941(3)	0.4107(5)	0.0284(11)
C6	0.5019(6)	0.4235(3)	0.2895(5)	0.0235(10)

Table 3.4: Selected bond lengths of CoATH crystal [Å]

Co1-O4	2.027(3)	O2-C1	1.235(6)
Co1-O1	2.034(3)	O3-C6	1.238(6)
Co1-O5	2.210(3)	O4-C6	1.261(6)
Co1-O6	2.037(4)	C1-C2	1.484(7)
Co1-O7	2.058(3)	C2-C3	1.515(7)
Co1-O5	2.141(3)	C3-C4	1.510(6)
O1-C1	1.261(5)	C4-C5	1.500(7)
O1-Co1	2.034(3)	C5-C6	1.487(6)

Table 3.5: Selected bond angles [^{0}] for CoATH crystal

O4- Co1-O4	180	O7- Co2-O5	92.60(12)
O4- Co1-O1	91.14(14)	O6- Co2-O5	94.86(13)
O4- Co1-O1	88.86(14)	O6- Co2-O5	85.14(13)
O1- Co1-O1	180	O7- Co2-O5	92.60(12)
O4- Co1-O5	88.12(12)	O7- Co2-O5	87.40(12)
O1- Co1- O5	91.21(12)	O5- Co2-O5	180
O1- Co1- O5	88.79(12)	C1-O1- Co1	127.1(3)
O4- Co1- O5	91.88(12)	C6-O4- Co1	130.4(3)
O4- Co1- O5	88.12(12)	Co2-O5-Co1	133.01(14)
O1- Co1- O5	88.79(12)	O2-C1-O1	123.1(5)
O1- Co1- O5	91.21(12)	O2-C1-C2	119.6(4)
O5- Co1- O5	180.00(6)	O1-C1-C2	117.3(4)
O6- Co2-O6	180.0(2)	C1-C2-C3	112.0(4)
O6- Co2-O7	89.95(17)	C4-C3-C2	113.6(4)
O6- Co2-O7	90.05(17)	C5-C4-C3	109.2(4)
O6- Co2-O7	89.95(17)	C6-C6-C4	116.7(4)
O7- Co2-O7	180	O3-C6-O4	122.8(4)
O6- Co2-O5	85.14(13)	O3-C6-C5	122.0(4)
O7- Co2-O5	92.60(12)	O4-C6-C5	115.2(4)

Table 3.6: Geometries of H-bonds in CoATH crystal; D = donor, A = acceptor

D-H...A	d(D-H) [Å]	d(H...A)[Å]	D(D...A) [Å]	DHA [^{0}]
O7-H7...O1	0.82	1.88	2.700	178.0
O6-H6...O4	0.82	1.88	2.636	152.1

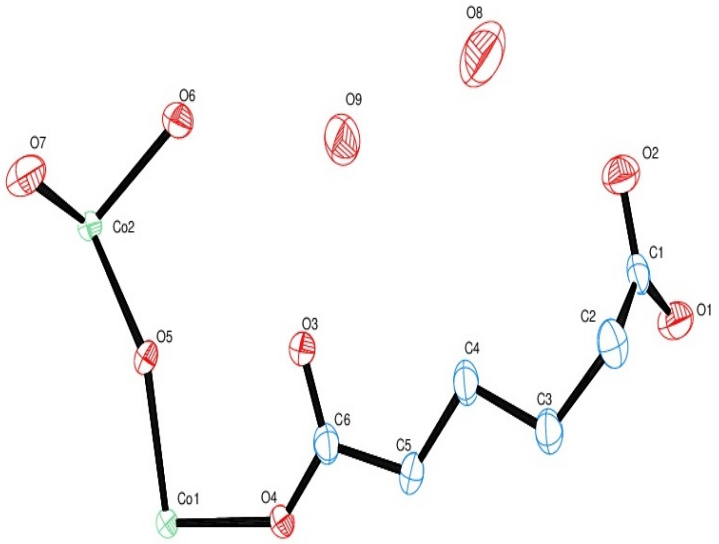

Figure 3.6: ORTEP image of CoATH single crystal.

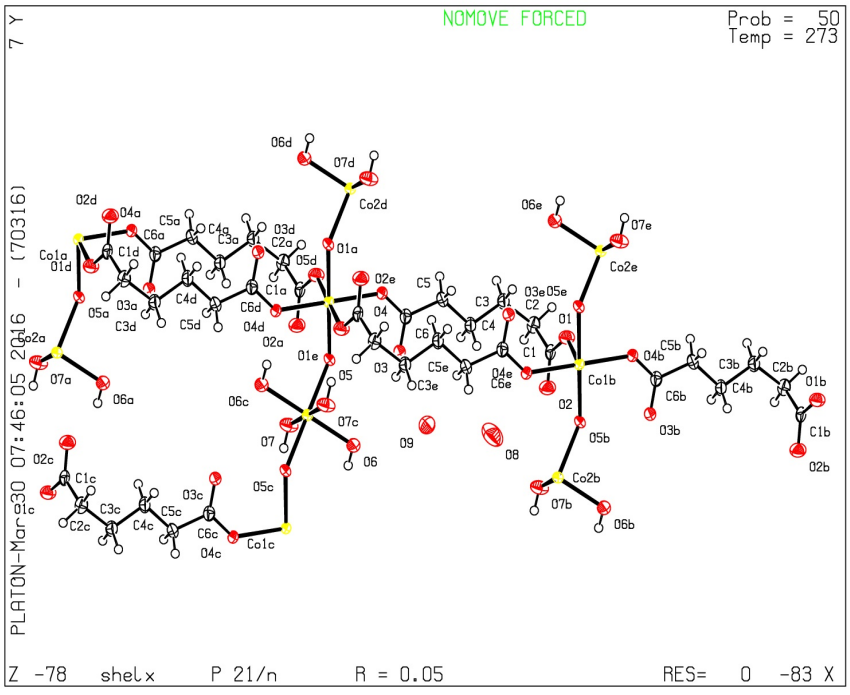

Figure 3.7: Three dimensional polymeric structure of CoATH single crystal.

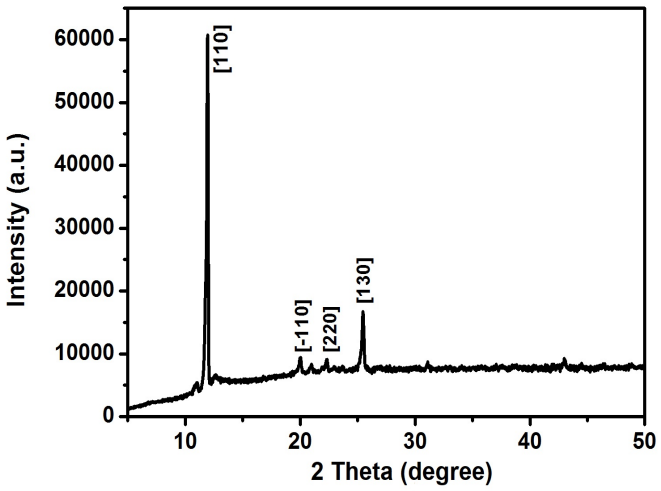

Figure 3.8: Powder XRD pattern of CoATH crystal.

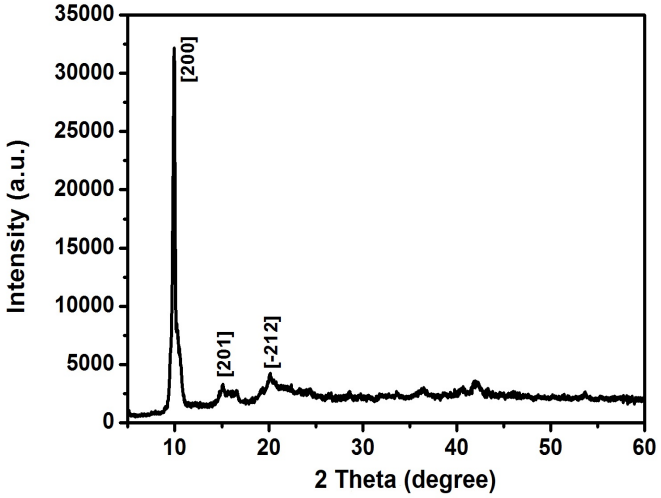

Figure 3.9: Powder XRD pattern of CuAMH crystal.

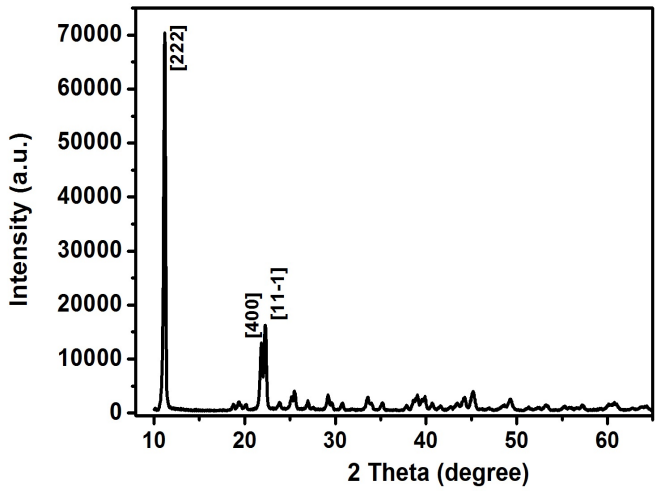

Figure 3.10: Powder XRD pattern of ZnA crystal.

3.3.4 ZnA crystals

Figure 3.10 shows the powder XRD pattern of the ZnA crystal. The calculated cell parameters obtained from powder XRD reveal that the crystal belongs to the monoclinic system having space group C2/c(15). The unit cell parameters of the crystal calculated by PDXL software by matching with the ICDD card 00-031-1995 are a = 19.144 Å, b= 4.794 Å, c = 9.286 Å, $\alpha = \gamma = 90.00^{o}$, $\beta = 91.80^{o}$ and unit cell volume = 851.815 $(Å)^3$, and are in agreement with the literature [7].

3.4 FTIR and micro Raman studies

3.4.1 CaAMH crystals

The FTIR and micro Raman spectra of the prepared sample are given in Figure 3.11 (a) and (b) respectively. The spectra are analyzed by comparing with those of related compounds available in literature [8-11]. The assignments of some selected wave numbers are given in Table 3.7. The internal vibrations are due to the carboxylate group, methylene group and internal water.

The band observed at 3425 cm^{-1} in FTIR spectrum assigned to the asymmetric

stretching mode associated with the water molecules. The weak band observed at 2358 cm^{-1} is assigned to the bonded hydroxyl stretching due to carboxyl chromosphere. The higher harmonic of this frequency is observed in 2358 cm^{-1}.

The CH stretching region 3050 - 2850 cm^{-1} exhibits two distinct bands at 2934 cm^{-1} and 2861 cm^{-1} supporting structured C-H stretch. The band observed at 1246 cm^{-1} is ascribed to deformation mode $\delta(CH_2)$ of the methylene group. The absorption band observed at 1330 cm^{-1} and 781 cm^{-1} result from the rocking of CH_2 groups. The band observed at 928 cm^{-1} is assigned to stretching mode of ν(C-O-C) of the adipate group.

Raman spectrum is quite useful in searching the Metal-Metal (M-M) stretching modes in binuclear carboxylates in which very short M-M separation is present. The weak Raman line observed at 1572 cm^{-1} is assigned to asymmetric stretching vibration ν_{as}(OCO). The broad band centered around 1581 cm^{-1} in IR spectrum is also assigned to ν_{as}(OCO).

The strong lines observed at 2900 cm^{-1} and 2853 cm^{-1} are assigned to hydroxyl stretching vibration ν(OH). Two bands are observed in the range 1650 - 1400 cm^{-1} in FTIR and the corresponding Raman region consists of five Raman lines. Contributions from R-C-O-O, ν_{as}(OCO) and ν_s(OCO) are expected in this region. Two ν_s(OCO) are clearly observed at 1474 cm^{-1} and 1448 cm^{-1}. A medium line in the Raman spectrum at 1572 cm^{-1} assigned to asymmetric ring breathing vibrations of (OCO) group. Raman spectrum is evidenced as a weak line at 1297 cm^{-1} is assigned to the stretching mode of C-O group. The remarkable intensity of Raman line in the region below 500 cm^{-1} coupled with OCO stretching frequencies in FTIR is to be taken into account for arriving at the nature of carboxylate bonding configuration.

To conclude, the results of this spectroscopic study confirm the strong structural analogies between calcium adipate monohydrate and adipic acid, which are strictly isostructural. The presence of adipic acid or the biadipate ion is discarded due to the absence of IR carbonyl ν(C=O) [1735 - 1705 cm^{-1}] in the title material as recorded in FTIR spectra.

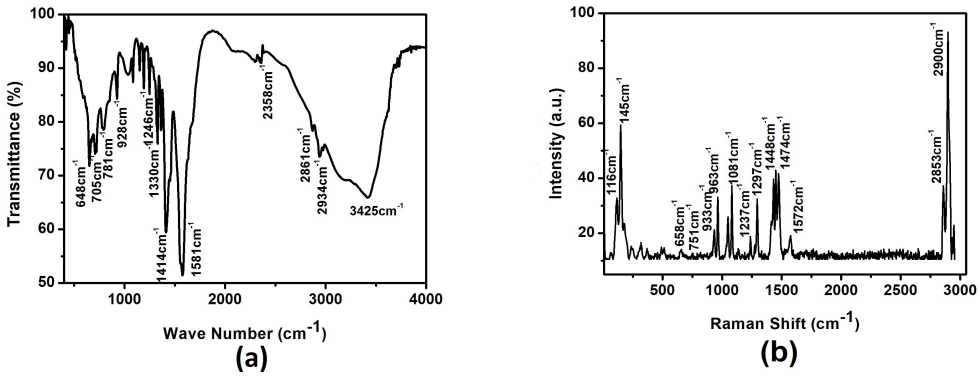

Figure 3.11: (a) FTIR spectrum of CaAMH (b) Micro Raman spectrum of CaAMH.

Table 3.7: Assignment of some selected FTIR and Raman wave numbers of CaAMH crystal

FTIR band (cm^{-1})	Raman band (cm^{-1})	Assignment of peaks per band
3425	-	ν(OH)
2934	2900	ν_{as}(C-H)
2861	2853	ν_{as}(C-H)
1581	1572	ν_s(COO-)
1414	1474	$\nu_{as}(CH_2)$
1330	1448	$\nu_s(CH_2)$
1246	1297	ν_{as}(C-O)
924	963	$\rho_t(CH_2$
705	751	O-H Deformation
648	658	δ(OCO)
498	145	ν(Ca-O)
-	116	ν(Ca-O)

3.4.2 CoATH crystals

The FTIR spectra obtained for the grown crystals of cobalt adipate is shown in Figure 3.12 (a). The infrared spectrum was recorded in the wave number range 4000 – 400 cm^{-1} using a KBr pellet technique. The characteristics infrared spectrum recorded here shows all the bands expected from metal adipate crystals with water of crystallization.

The characteristic absorption band at 1720 cm^{-1} corresponding to C=O vibration is absent in the spectrum which assures that all the four oxygen atoms of adipic acid coordinates to cobalt atoms. A free adipate ion has no hydroxyl groups, so no bands can be expected for the stretching vibration of the hydroxyl group. But a broad band centered at 3420 cm^{-1} has been observed. Thus, this broad and strong peak is due to the OH stretching mode of vibration of water present in the crystal [12]. The absorption bands at 2937 and 2864 cm^{-1} can be assigned to asymmetric and symmetric C–H stretching vibrations of $–CH_2$ groups. The absorption band at 1571 cm^{-1} is due to asymmetric stretching vibrations due to COO– group. The absorption band at 1410 cm^{-1} is due to deformation of $–CH_3$ group. The absorption bands at 1321 and 1190 cm^{-1} are due to asymmetric and symmetric C–C stretching, respectively. The bending and rocking vibration of COO– are observed in 647 cm^{-1}. It is thus clear that the FTIR spectroscopic results of cobalt adipate hydrate crystals confirm the presence of water of crystallization, adipate ligands and establishes that adipate ions are doubly ionized.

The micro-Raman spectrum of the crystal was recorded in the range 130 - 4000 cm^{-1} and is depicted in the Figure 3.12 (b). The spectrum exhibit broad peak at 3414 cm^{-1} shows the presence of water of crystallization in the crystal. The absorption bands at 2920 cm^{-1} and 2871 cm^{-1} can be assigned to asymmetric and symmetric C-H stretching vibrations of $–CH_2$ group. The absorption band at 1560 cm^{-1} is due to the symmetric stretching vibrations of COO- group. The strong band at 1417 cm^{-1} corresponds to symmetric stretching vibrations of the carboxylate group. The strong bands at 1195 cm^{-1} and 926 cm^{-1} are due to asymmetric and symmetric C-C stretching vibrations respectively. The peak at 850 cm^{-1} is assigned

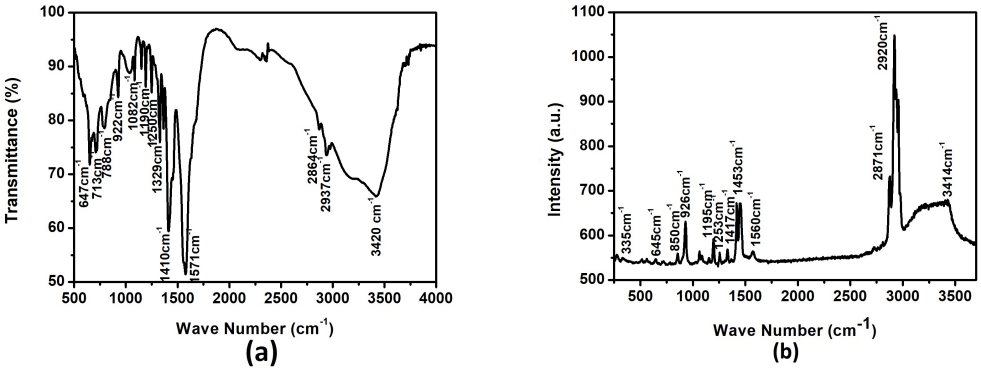

Figure 3.12: (a) FTIR spectrum CoATH (b) Micro Raman spectrum of CoATH.

Table 3.8: FTIR and micro Raman band assignment of CoATH crystal

FTIR band (cm^{-1})	Raman band (cm^{-1})	Assignment of peaks per band
3420	3414	ν(OH)
2937	2920	ν_{as}(C-H)
2864	2871	ν_{s}(C-H)
1571	1560	ν_{as}(OCO)
1410	1417	$\nu_{as}(CH_2)$
1250	1295	ν_{as}(C-O)
922	926	$\rho_t(CH_2$
788	850	O-H Deformation
647	645	δ(OCO)
-	335	ν(Co-O)

to the wagging vibrations of the methylene group. The assignments of some selected wave numbers are given in Table 3.8.

3.4.3 CuAMH crystals

The FTIR and micro Raman spectra of powdered sample of CuAMH is given in figure 3.13 (a) and (b). The O-H stretching vibration is observed at 3445 cm^{-1} in FTIR spectrum. The absorption bands at 2947, 2863 cm^{-1} can be assigned to asymmetric and symmetric C-H stretching vibrations of -CH_2 groups. The corresponding Raman line is observed at 2921 cm^{-1}. The absorption bands of asymmetric stretching vibrations of COO- group are observed at 1585 cm^{-1} and Raman lines observed at 1438 cm^{-1}. The absorption bands at 1153 and 877 cm^{-1} are due to asymmetric

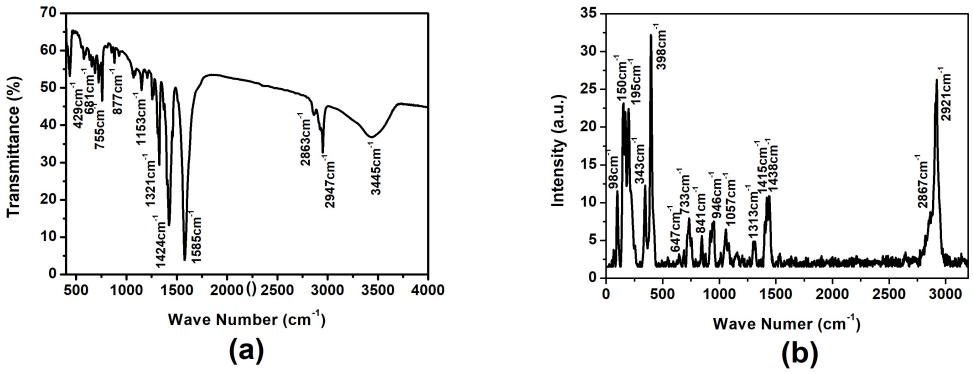

Figure 3.13: (a) FTIR spectrum of CuAMH (b) Micro Raman spectrum of CuAMH.

and symmetric C-C stretching, respectively. The bending and rocking vibration of COO- are observed in 755 and 429 cm^{-1}. The intense bands in Raman spectrum at 1057 and 946 cm^{-1} are due to asymmetric and symmetric C-C stretching vibrations, respectively. It is noted that the four Raman lines at 343, 195, 150 and 98 cm^{-1} are representation of copper - Oxygen bonding in the crystal [13]. From the spectroscopic studies, it may be concluded that the functional groups present in the crystal are exactly same as in the adipate ligand, and also confirm the presence of water of crystallization. The assignments of some selected wave numbers are given in Table 3.9.

3.4.4 ZnA crystals

The infra-red spectroscopy combined with micro Raman is a significant tool that provides information regarding the structural details of a material. The FTIR and micro Raman spectra of the grown crystals are shown in Figure 3.14 (a) and (b). The spectral bands are interpreted and proposed assignments of some selected wave numbers are given in Table 3.10.

The internal vibrations of the title material are mainly due to carboxylate group and methylene group. Generally the bands in the region 3460 - 3150 cm^{-1} is due to lattice water. In the spectra there is no band observed at this region, so water of hydration is absent in the crystal. The absorption bands at 2954, 2870 cm^{-1} can be

Table 3.9: Assignment of some selected FTIR and Raman wave numbers of CuAMH crystal

FTIR band (cm^{-1})	Raman band (cm^{-1})	Assignment of peaks per band
3445	-	ν(OH)
2947	2921	ν_{as}(C-H)
2863	2863	ν_s(C-H)
1585	1438	ν_s(COO-)
1424	1415	$\nu_{as}(CH_2)$
1321	1313	$\nu_s(CH_2)$
1153	946	$\rho_t(CH_2$
877	841	$\rho_r(CH_2)$
755	733	$\rho_r(H_2O)$
681	647	δ(OCO)
429	398	ν(Cu-O)
-	343	ν(Cu-O)
-	195	ν(Cu-O)
-	150	ν(Cu-O)
-	98	ν(Cu-O)

assigned to asymmetric and symmetric C-H stretching vibrations of -CH2 groups in the FTIR spectrum, are evidenced at 2915 cm^{-1} and 2868 cm^{-1} as strong lines in the Raman spectrum. The medium band at 1452 cm^{-1} in the IR spectrum is evidenced as a weak Raman line at 1451 cm^{-1} , are ascribed to the symmetric stretching vibrations of COO- group. The band observed at 1043 cm^{-1} in FTIR spectrum is evidenced by the intense bands at 1041 and 957 cm^{-1} are due to asymmetric and symmetric C-C stretching vibrations. The bending and rocking vibration of COO- are observed in 745 and 576 cm^{-1} in FTIR spectrum. The peak at 446 cm^{-1} is evidenced at 316 cm^{-1} and 117 cm^{-1} in Raman spectrum are assigned to stretching vibrations (Zn-O) vibrations of the zinc adipate.

3.5 Thermal decomposition studies

3.5.1 CaAMH crystals

TG-DTA and DSC curves of CaAMH crystals are depicted in Figures. 3.15 (a) and (b) respectively. The TGA was carried out from room temperature to a maximum

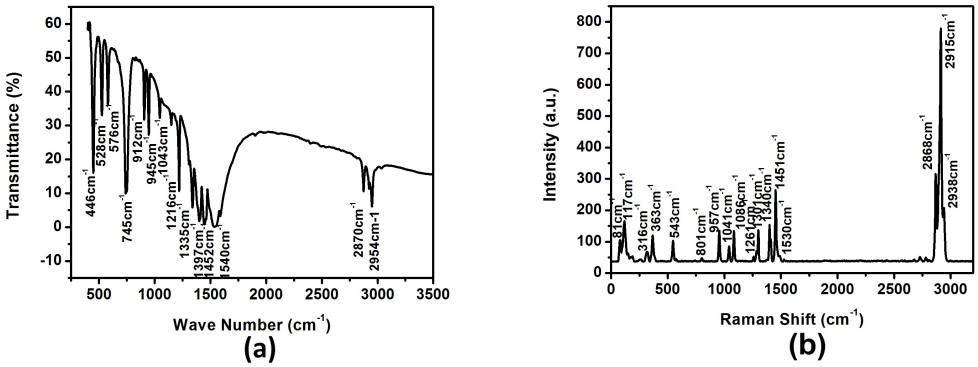

Figure 3.14: (a) FTIR spectrum of ZnA (b) Micro Raman spectrum of ZnA.

Table 3.10: Assignment of some selected FTIR and Raman wave numbers of ZnA crystal

FTIR band (cm^{-1})	Raman band (cm^{-1})	Assignment of peaks per band
2954	2938	ν_{as}(C-H)
2870	2915, 2868	ν_s(C-H)
1540	-	ν_{as}(COO-)
1452	1451	ν_s(COO-)
1397	1340	(CH_3) deformation
1335	1301	ν_{as}(C-O)
1216	1261	ν_s(C-O)
1043	1086, 1041	ν_{in}(C-CO2)
945, 912	957	$\rho_t(CH_2)$
745	801	$\rho_r(H_2O)$
576, 528	543	δ(OCO)
446	316	ν(Zn-O)
-	117	ν(Zn-O)

of 700 °C at a heating rate of 10 °C/min in an atmosphere of nitrogen.

The material remains stable up to a temperature 103 °C and starts decomposing at about 103 °C, after which it reduces to its carbonaceous compound at 571 °C and process, continue. Some of the decomposing steps in the TG show considerable overlapping but are very much distinct in the DTA curve. A combined study of TG and DTA indicates a decomposition pattern as shown in Table 3.11. The first stage of decomposition (103 - 174 °C) results in the elimination of one water molecule and the formation of anhydrous CaAMH. The calculated and observed mass loss corresponding to this is 11.22 and 8.95% of the total mass taken. This dehydration occurring at low temperature (103 - 174 °C) range suggests the presence of water of crystallization, this is matched by the observations made by B.Want et. al.[15]. Corresponding to this dehydration, there is an endothermic peak in the DTA curve at about 153.91 °C.

The second stage of decomposition between 371 and 450 °C, there occurs a loss of 8H and 4C, thereby reducing the anhydrous calcium adipate to calcium oxalate. The measured and theoretical values of mass losses at this stage are 34.635 and 36.633% of the total mass taken. Corresponding to these losses there is an exothermic peak in DTA at about 402 °C and endothermic peak at 428 °C. This suggests that the loss of four hydrogen molecules takes place about 402 °C and results an exothermic reaction, while loss of carbon takes place about temperature 428 °C and shows endothermic type of reaction. Simultaneous loss of 8H and 4C can be confirmed from the peak observed in DTA curve.

In the third stage of decomposition in the temperature range from 450 to 571 °C, the loss of one CO molecule, leading to the formation of calcium carbonate. The measured and theoretical values of mass loss at this stage are 51.402 and 50.495% of the total mass taken. Corresponding to this mass loss there is an endothermic peak in DTA at about 504 °C, suggesting a further crystallographic phase transition in the material (Table 3.11). In the fourth step, we are expecting that the material may continue to decompose and reduces to calcium oxide. The thermal decomposition reactions are usually endothermic. However, some of the DTA peaks

Table 3.11: The results of the decomposition process of $Ca(C_6H_8O_4)$ H_2O

Steps	Temperature range/^0C	Observed mass loss/%	Calculated mass loss /%	Loss of molecules in the step	Corresponding DTA peak/^{0}C
I	103-174	8.95	11.222	H_2O	154
II	371-450	34.63	36.633	8H+4C	429
III	450-571	51.40	50.495	CO	551

are exothermic, this is due to the concomitant oxidation reactions taking place along with decomposition reactions. These types of investigations are also found in literature [16].

The figure 3.15 (b) shows the DSC profile of CaAMH crystal in nitrogen at 10 °C min^{-1}. The profile displayed one endothermic peak at 152 °C, is accounted for the dehydration step. The DTA portion of the thermal curve is consistent with the description of DSC results. Critical examination of the TG and DSC curves indicates that the decomposition pattern is typical of a hydrated CaAMH and transformations are associated with mass changes and there are no physical (crystallographic) transformations independent of mass change or decomposition of the material.

Following is the stoichiometry of the different intermediates involved in the decomposition process of CaAMH.

1. $Ca(C_6H_8O_4).H_2O$ - $H_2O \rightarrow Ca(C_6H_8O_4)$
2. $Ca(C_6H_8O_4)$ - (8H+4C) $\rightarrow Ca(C_2O_4)$
3. $Ca(C_2O_4)$ - CO $\rightarrow Ca(CO_3)$

3.5.2 CoATH crystals

TG/DTA and DSC curves of the sample are depicted in Figure 3.16 (a)and (b) respectively. TG curve shows that the mass loss occurring in the first stage (75 – 142^{0}C) corresponds to a dehydration process. In the DSC curve, an endothermic peak is seen at 107 ^{0}C. This makes it evident that the dehydration proceeds via one step and the corresponding energy is involved. The peak corresponds to the

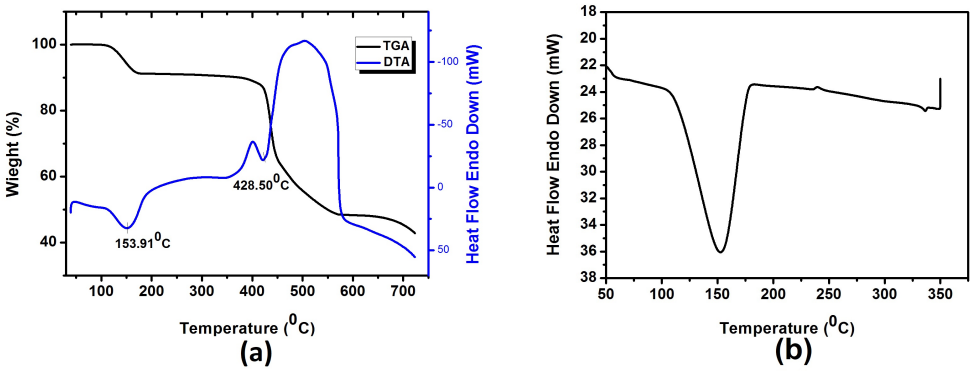

Figure 3.15: (a) TG-DTA curves of grown crystals (b) DSC thermogram of CaAMH crystal.

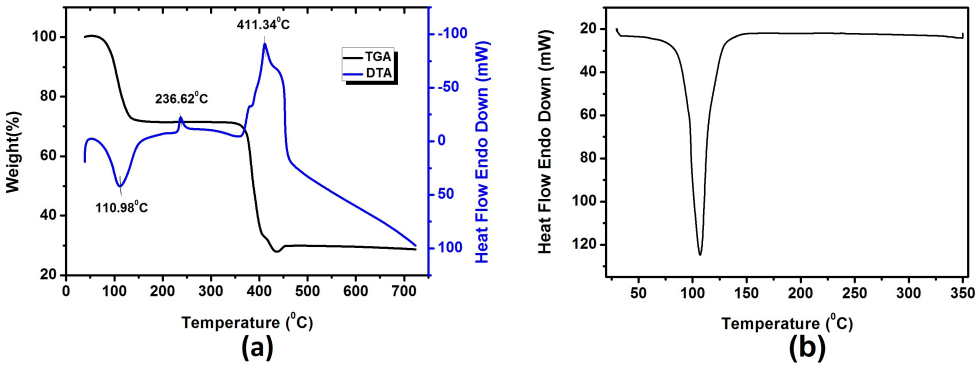

Figure 3.16: (a) TG-DTA curves of grown crystals (b) DSC thermogram of CoATH crystal.

loss of four molecules of water of crystallization. The observed mass loss of 27% in the dehydration process is in close match with the calculated value of 26.18%. The anhydrous cobalt adipate so obtained remains stable up to 336 ^{0}C and there is an exotherm at 110.98 ^{0}C in DTA curve (107 ^{0}C in DSC) in this region which corresponds to the phase transition. The second stage is associated with the decomposition of the anhydrous cobalt adipate by decarboxylation with the formation of cobalt carbonate accompanied by carbonaceous residue. This happens in the temperature range 336 – 411 ^{0}C and the endothermic DTA peak corresponding to this degradation is at 411 ^{0}C. The observed mass loss of 38.5 in this process is in agreement with the calculated value of 41.38% [17, 18].

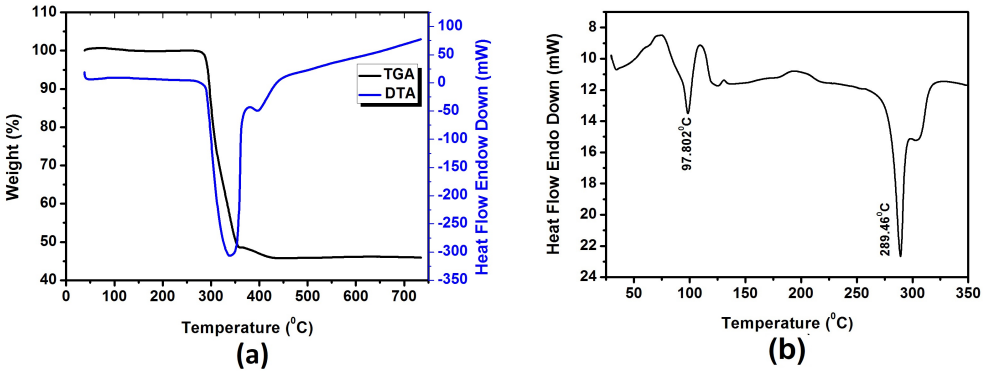

Figure 3.17: (a) TG-DTA curves of grown crystals (b) DSC thermogram of CuAMH crystal.

3.5.3 CuAMH crystals

Figure 3.17 (a) shows the observed thermal degradation curve. The compound displays mainly one thermal process in the temperature range of 50 - 700 ^{0}C. The compound losses one water molecule, four carbons and eight hydrogen molecules in the temperature range 278 - 358 ^{0}C corresponding to an exothermic DTA peak at 304 ^{0}C with a weight loss of 51.26% (calculated weight loss 48.83%). Thus the remaining weight of 51.26% indicates that the final product may be copper oxalate (CuC_2O_4). The formation of oxalates of other adipate compounds is also reported in the literature [19]. From the TG/DTA plot, only one chemical reaction has been proposed to take place during the thermal decomposition of the compound. Figure 3.17 (b) shows the thermogram obtained from DSC, two endothermic peaks at 98 °C and 289 °C corresponding to dehydration and it is also supported the TG/DTA results.

3.5.4 ZnA crystals

The thermo gravimetric analysis of ZnA was carried out in the temperature range of 50 - 700 ^{0}C under nitrogen atmosphere at a heating rate of 10 °C/min. Figure **??** depicts the thermal properties of the ZnA crystal. The material remains stable up to a temperature 387 °C, after which it reduces to zinc oxide at 473 °C. The compound displays only one thermal process in the temperature range of 50 - 700

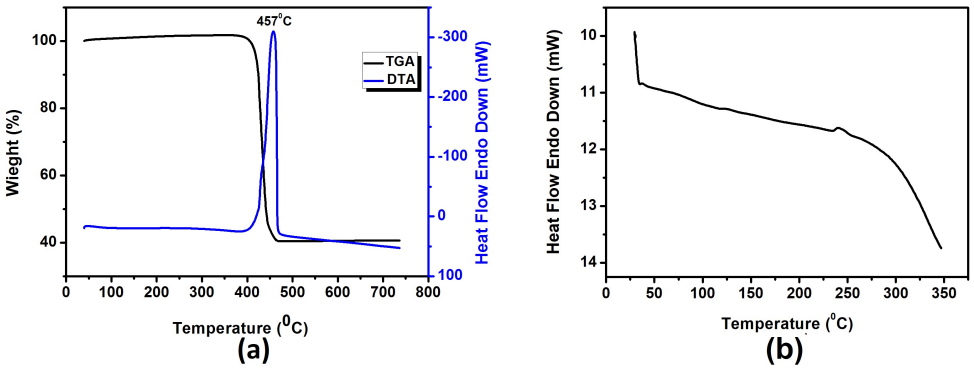

Figure 3.18: (a) TG-DTA curves of grown crystals (b) DSC thermogram of ZnA crystal.

^{0}C. The compound losses six carbon atoms, eight hydrogen and three oxygens in the temperature range 387 - 473 ^{0}C corresponding to an endothermic DTA peak at 457 ^{0}C with a weight loss of 59.54% (calculated weight loss 64.41%).

3.6 Optical property studies

3.6.1 CaAMH crystals

Optical absorption measurement of the powdered sample of CaAMH crystal was carried out in the range 200 – 900 nm at room temperature and is shown in Figure 3.19 (a). The spectrum shows maximum absorption in the near UV range (200 - 350 nm) at 216 nm for which percentage of reflectance is 66.83. This crystal is used for suitable optical applications due to its wide transparency window in the part of visible region above 216 nm. From Kubelka-Munk function [4]

$$F(R) = (1\text{-}R)^2/2R = k/s \tag{3.1}$$

where R is reflectance, k is absorption coefficient and s is scattering coefficient. The optical band gap of the material was determined by extrapolating the linear portion of the plot of $[(k/s)h\nu]^2$ versus $h\nu$ (Figure 3.19 (b)). The calculated band gap is 5.3 eV.

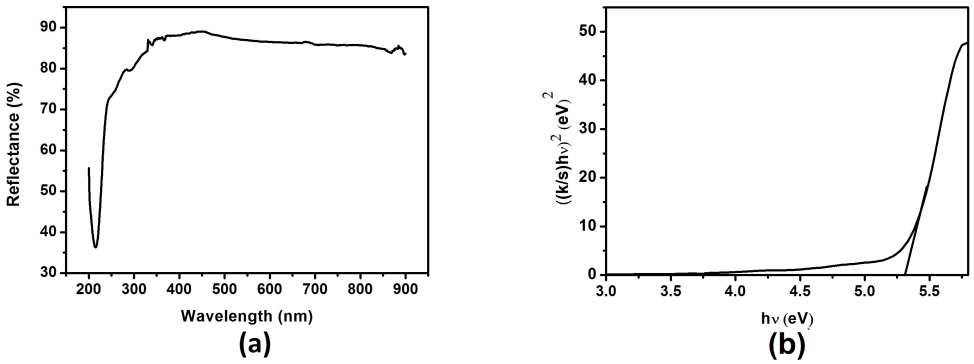

Figure 3.19: (a) Diffuse reflectance spectrum of CaAMH (b) Plot of $[(k/s)h\nu]^2$ versus $h\nu$ for CaAMH.

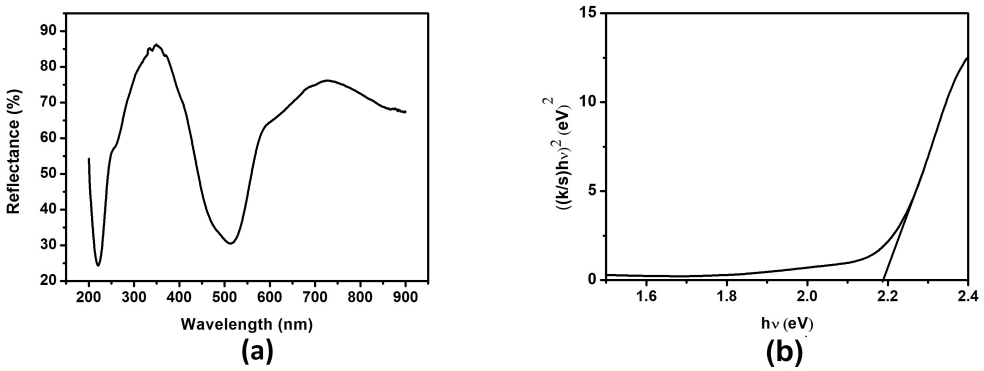

Figure 3.20: (a) Diffuse reflectance spectrum of CoATH (b) Plot of $[(k/s)h\nu]^2$ versus $h\nu$ for CoATH.

3.6.2 CoATH crystals

The absorption spectrum of cobalt adipate tetrahydrate crystal is derived from the diffuse reflectance spectrum shown in Figure 3.20 (a). The absorption bands at 631nm and 514nm in the spectrum are due to the ${}^4T_1(g)(F) \rightarrow^4 T_2(g)(F)$ and ${}^4T_1(g)(F) \rightarrow^4 A_2(g)(F)$ respectively. The energy of the other transition is 474.8 nm, which is due to ${}^4T_1(g)(F) \rightarrow^4 T_2(g)(P)$ [22]. The absorption peak below 400 nm is ascribed to the intra-ligand electronic transition. The optical band gap of the material was determined by extrapolating the linear portion of the plot of $[(k/s)h\nu]^2$ versus $h\nu$ (Figure 3.21 (b)). The calculated band gap is 2.18 eV.

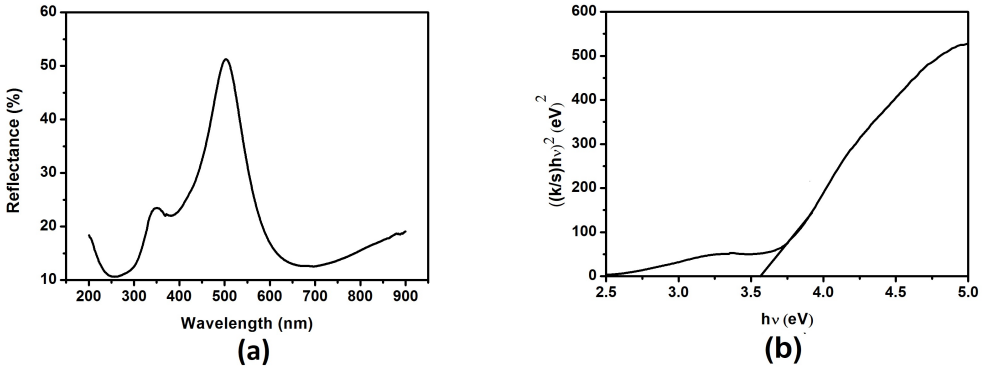

Figure 3.21: (a) Diffuse reflectance spectrum of CuAMH (b) Plot of $[(k/s)h\nu]^2$ versus $h\nu$ for CuAMH.

3.6.3 CuAMH crystals

Optical absorption measurement of the powdered sample of CuAMH crystal was carried out in the range 200 – 900 nm at room temperature and is shown in Figure. 3.21 (a). The optical band gap of the material was determined by extrapolating the linear portion of the plot of $[(k/s)h\nu]^2$ versus $h\nu$ (Figure 3.21 (b)). The calculated band gap is 3.45 eV. The absorption spectrum of copper adipate dihydrate , constructed from DRS spectrum shows a broad absorption peak at 699 nm. It is attributable to the d-d transition of the distorted square pyramidal geometry around the Cu(II) ion , which is consistent with the literature report [23-25]. The other two absorption peaks below 400 nm are assigned to the intra – ligand electronic transitions.

3.6.4 ZnA crystals

Optical absorption measurement of the powdered sample of ZnA crystal was carried out in the range 200 – 900 nm at room temperature and is shown in Figure 3.22 (a). The crystal shows the absence of absorption in the entire visible range and that is an essential parameter to an NLO crystal. This crystal is used for suitable optical applications due to its wide transparency window in the part of visible region above 216 nm. The optical band gap of the material was determined by extrapolating the linear portion of the plot of $[(k/s)h\nu]^2$ versus $h\nu$ (Figure 3.22 (b)). The calculated

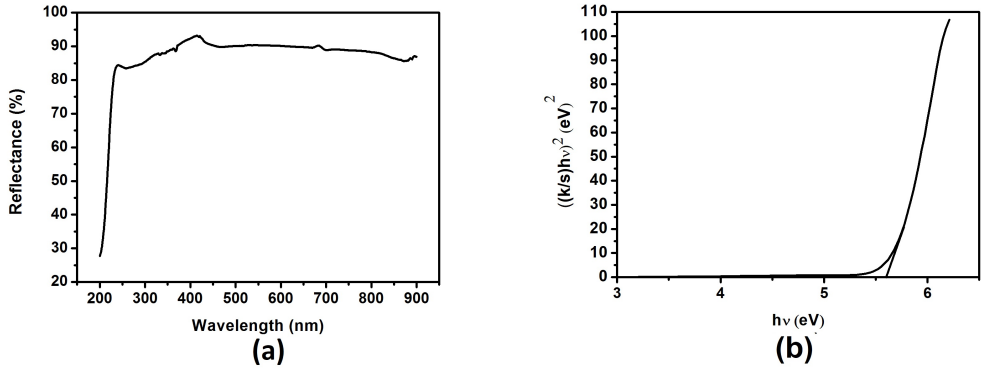

Figure 3.22: (a) Diffuse reflectance spectrum of ZnA (b) Plot of $[(k/s)h\nu]^2$ versus $h\nu$ for ZnA.

band gap is 5.66 eV.

3.7 Dielectric property studies

3.7.1 CaAMH crystals

Various polarization mechanisms in a material can be studied by dielectric property studies. One of the important electrical properties of dielectric materials is permittivity (dielectric constant). The crystal samples were finely ground and made in the form of pellets using a hydraulic press. The dielectric constant is calculated using the relation

$$\varepsilon_r = \mathrm{Cd}/\varepsilon_0 \mathrm{A} \tag{3.2}$$

and the a c conductivity is calculated from the relation

$$\sigma_{ac} = \varepsilon_0 \varepsilon_r \omega \tan\delta \tag{3.3}$$

Where C is the capacitance (F), ε_0 is the free space dielectric constant value (8.854×10^{-12} F/m), A is the capacitor area (m^2) and d is the thickness (m) of the material.

Electrical conductivity is an effective tool to probe the internal purity and structural defects of crystalline solids. Hence we have studied electrical characterization on these crystals at room temperature. The variations of dielectric constant with the frequency of the applied field at room temperature are shown in Figure 3.23 (a). It is observed that the dielectric constant decrease with increasing frequency, at the lower range of frequencies dielectric constant decreases drastically, becoming a constant at larger frequencies, is a normal dielectric behavior and can be explained on the basis of various polarization mechanisms. There are four major mechanisms of electric polarization which are electronic, ionic, orientational and space charge polarization. At moderate electric field (low frequency) and for materials with a very low conductivity, these mechanisms of polarization contribute to the dielectric constant and with the further increase in the frequency of the applied field the contributions from different polarization starts reducing [26]. The polarization occurs due to the local displacement of electrons, which is the effect of the electronic exchange of the number of ions in the crystal. As the frequency increases the electron exchanges cannot follow the dielectric field and the polarization becomes independent of frequency. The contribution towards polarization from space charge effects depends on the purity and perfection of crystals. The impurities or other forms of imperfection create potential barriers, limiting the transport of charge carriers and hence increasing the value of ε_r. The high value of dielectric constant at low frequencies is attributed to space charge and dipolar polarization. In CaAMH crystal, at frequency 100 Hz to 5 KHz the dielectric constant decreases drastically, becoming a constant at higher frequencies, the value of dielectric constant at higher frequency is 4.01. As the frequency increases, the dipoles do not comply with the varying external field. Therefore, the polarization decreases and hence, the dielectric constant decreases as the frequency increases [27, 28].

Dielectric absorption in a material is characterised by dielectric loss and loss tangent ($tan\delta$) values. Figure 3.23 (b) shows variation of dielectric loss with frequency. It is clear that dielectric loss decreases with increasing frequency. At low frequencies the dipoles can easily switch alignment with the changing field. As the

frequency increases the dipoles are less able to rotate and maintain phase with the applied field, thus they reduce their contribution to the polarization field [30]. When polarization lags behind the applied field, causing an interaction between the field and the dielectrics polarization that results in heating.

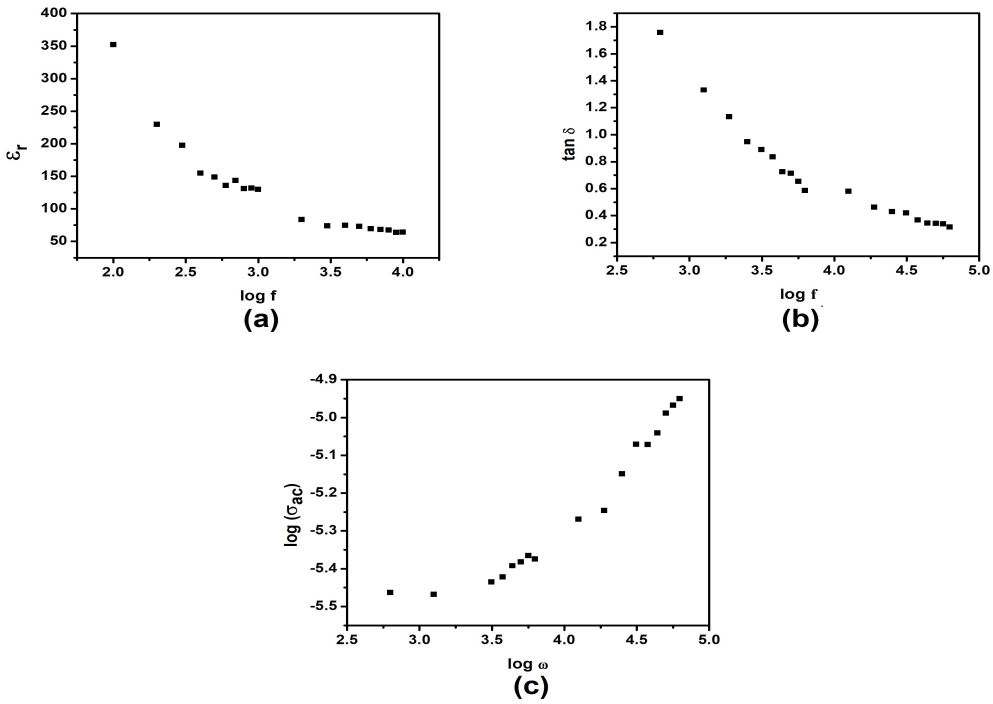

Figure 3.23: (a) Variation of ε_r with frequency (b) Variation of dielectric loss with frequency (c) Variation of ac conductivity with frequency of CaAMH crystal.

Figure 3.23 (c) shows variation of log (σ_{ac}) with log ω of CaAMH crystal in the frequency range of 100Hz to 5MHz. The conductivity of the crystal at room temperature region is determined by intrinsic defects caused by thermal fluctuations in the crystal. For any substance, more and more defects are produced as the temperature increases which, in turn, increase the conductivity. It is reported that the conduction mechanism in adipate crystals is due to rotation of the adipate ions. When the temperature of adipate crystals approaches 300 K, there is a possibility of weakening of the hydrogen bonding system due to the rotation of adipate ions. This results in an enhanced conduction in these materials.

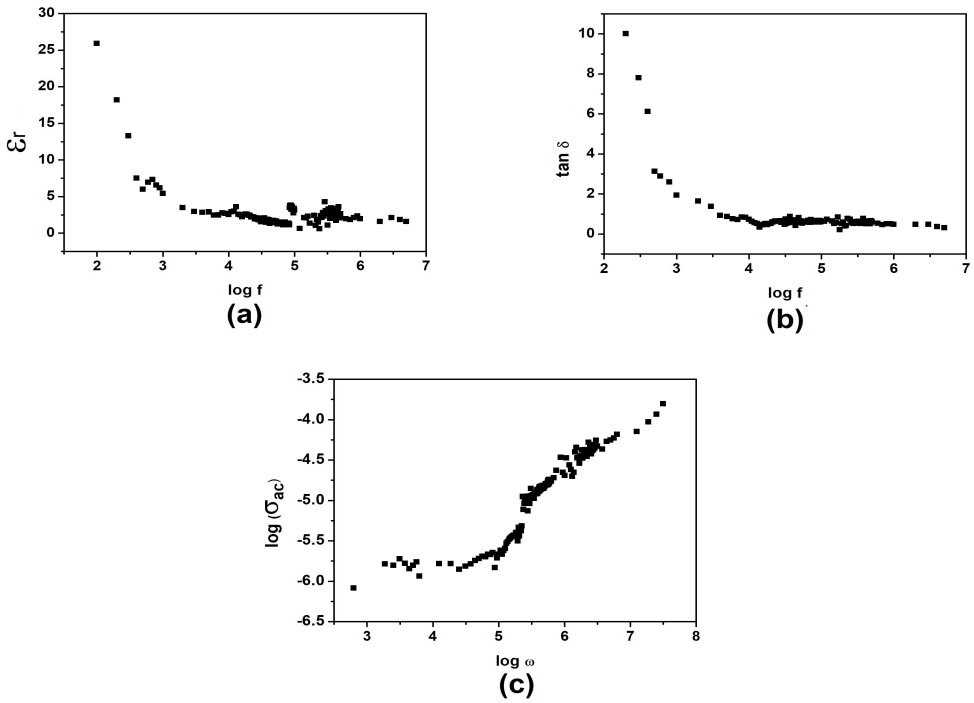

Figure 3.24: (a) Variation of ε_r with frequency (b) Variation of dielectric loss with frequency (c) Variation of ac conductivity with frequency of CoATH crystal.

3.7.2 CoATH crystals

The variations of dielectric constant with the frequency of the applied field are shown in Figure 3.24 (a). It is observed that the dielectric constant decrease with increasing frequency, at the lower range of frequencies (100 Hz - 5 KHz) dielectric constant decreases drastically with frequency, becoming a constant at higher frequencies, the value of dielectric constant at higher frequency is 6.18. This high value of dielectric constant at low frequencies is attributed to space charge and dipolar polarization. As the frequency increases, the dipoles do not comply with the varying external field. Therefore, the polarization decreases and hence, the dielectric constant decreases as the frequency increases

Dielectric absorption in a material is characterised by dielectric loss tangent ($tan\delta$) values [32]. At low frequencies the dipoles can easily switch alignment with the changing field. As the frequency increases the dipoles are less able to rotate and maintain phase with the applied field, thus they reduce their contribution to the

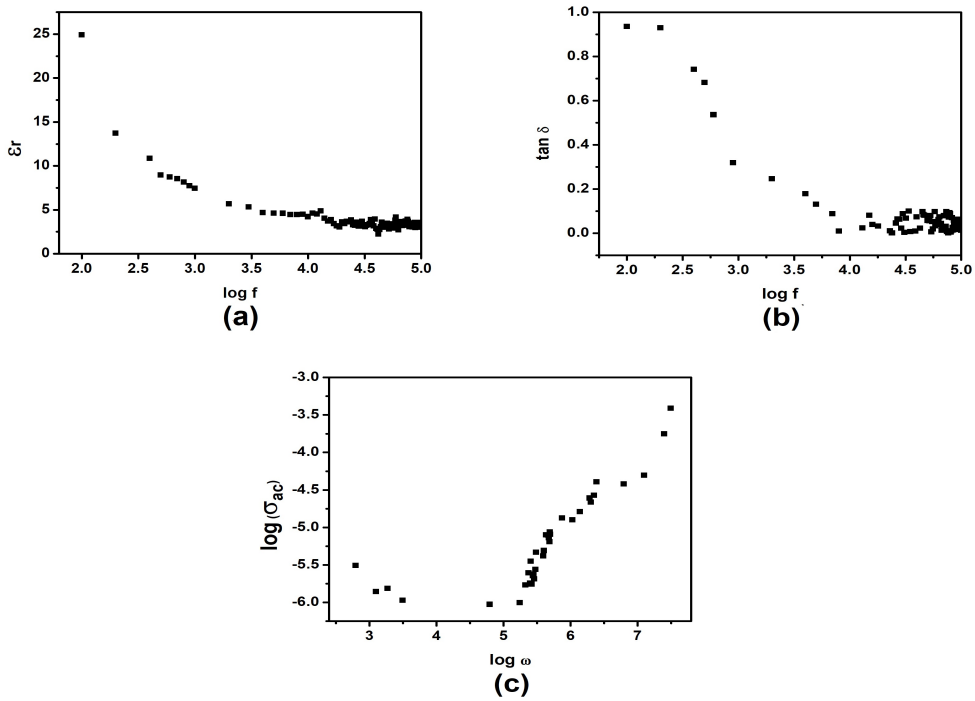

Figure 3.25: (a) Variation of ε_r with frequency (b) Variation of dielectric loss with frequency (c) Variation of ac conductivity with frequency of CuAMH crystal.

polarization field (Figure 3.24 (b))[33]. Variation of ac conductivity (Figure 3.24 (c)) is same as observed in CaAMH crystal.

3.7.3 CuAMH crystals

The variation of dielectric constant with the frequency of the applied field at room temperature is shown in Figure 3.25 (a). It is observed that the dielectric constant decreases with increasing frequency for CuAMH crystals. It is a normal dielectric behaviour and can be explained on the basis of various polarization mechanisms such as electronic, ionic, orientational and space charge polarization. At the moderate electric field, for materials with low conductivity these mechanisms of polarization contribute to the dielectric constant. On further increase in the frequency of the applied field, the contributions from different polarization starts reducing [34, 35]. The variation of ac conductivity and dielectric loss (Figure 3.25 (b) and 3.25 (c)) of the crystal is also showing similar trend discussed for CaAMH crystal.

3.7.4 ZnA crystals

The variation of dielectric constant with the frequency of the applied field at room temperature is shown in Figure 3.26 (a). It is observed that the dielectric constant decrease with increasing frequency, and at the lower range of frequencies, dielectric constant decreases drastically with frequency (100 Hz - 5 KHz), becoming a constant at larger frequencies, is a normal dielectric behavior and can be explained on the basis of various polarization mechanisms. The contribution towards polarization due to space charge effects depends on the purity and perfection of crystals, because the impurities or other forms of imperfection create potential barriers, limiting the transport of charge carriers and lead to higher value of ε_r. The high value of dielectric constant at low frequencies is attributed to space charge and dipolar polarization. In ZnA crystal, at the lower range of frequencies the dielectric constant decreases drastically, becoming a constant at larger frequencies. As the frequency increases, the dipoles do not comply with the varying external field. Therefore, the polarization decreases and hence, the dielectric constant decreases as the frequency increases. The similar behaviour , exhibited by CaAMH crystal discussed occure in the case of ZnA crystal also., for the variation of dielectric loss and ac conductivity (Figure 3.26 (b) and (c)).

3.8 Conclusions

Growth of four different adipate crystals CaAMH, CoATH, CuAMH and ZnA were accomplished by single gel diffusion technique. The crystal structure has been confirmed and the spectroscopic, thermal, optical and dielectric properties were investigated for four novel crystals. The combination of metal cation with the carboxylate ligand leads to the formation of crystals. The co-ordinated water molecules and the carboxylate oxygen atoms bonded with hydrogen make the chains into the 3D frame work. Optical band gaps of crystals are determined from optical absorption studies. The FT-IR and micro Raman spectral studies, reported the modes of vibration of different functional groups present in the crystal.

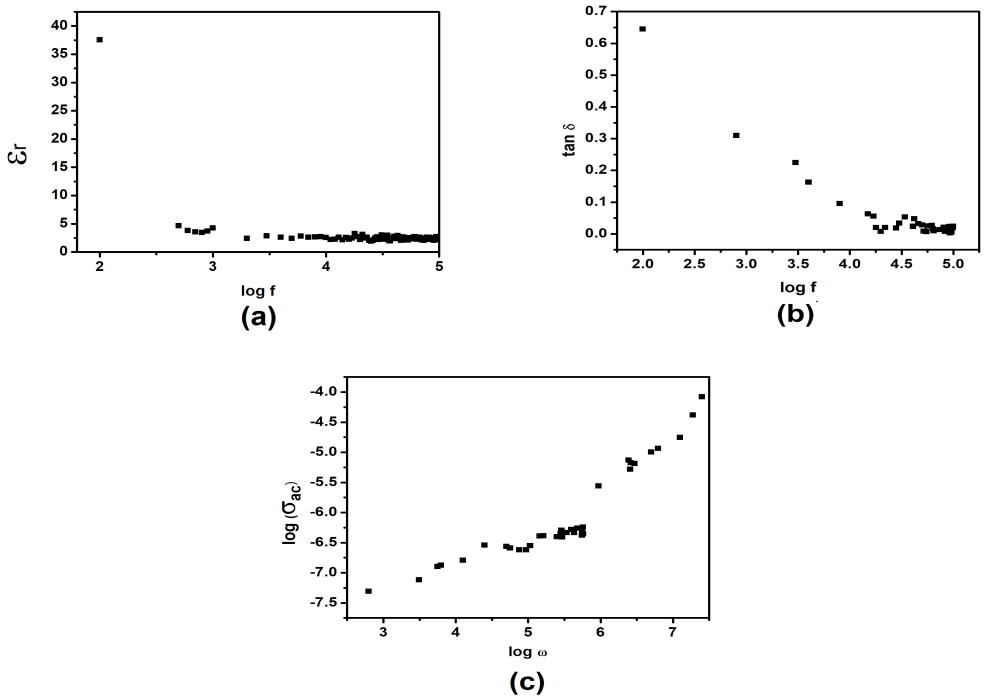

Figure 3.26: (a) Variation of εr with frequency (b) Variation of dielectric loss with frequency (c) Variation of ac conductivity with frequency of ZnA crystal.

In the case of CaAMH crystals, which belongs to the triclinic system with space group P-1 (2). The thermo gravimetric analysis suggested that the grown CaAMH crystal is associated with one molecule of water of hydration. The results of thermal analysis proved that the gel grown CaAMH starts decomposition at about 103 °C. CaAMH decomposed to calcium oxide through calcium oxalate and basic carbonate. The stoichiometric composition of the crystals was established to be $Ca(C_6H_8O_4)$ H_2O. From DRS spectrum cutoff wavelength and optical band gap of the material were found to be 216 nm and 5.3 eV respectively. The dielectric constant of CaAMH decreased gradually with increasing frequency of the applied ac field. Dependence of σ_{ac} on frequency suggests that the conduction phenomenon is ac type which could be due to the hopping of charge carriers. The wide optical transparency, low dielectric response and good thermal stability value obviously endorsed the grown crystal as a promising candidate for developing electro-optical application.

Cobalt adipate single crystals were grown successfully by the single gel diffusion

technique and the effects of different parameters like pH, concentration of reactants, gel density and gel aging on the growth were discussed. It was found that experimental conditions, such as pH, density of gel, concentration of reactants and gel aging, have strong influence on the nucleation kinetics and growth of the crystals. From single crystal X-ray diffraction and powder X-ray diffraction studies the structure of the crystal is determined to be monoclinic. The thermal decomposition pattern of the material suggests the different stages of degradation and the DSC curve confirms the presence of water molecules in the crystal lattice. The water of crystallization is completely lost well before the onset of anion decomposition. The optical band gap of the material is found to be 2.18 eV. The variation of dielectric constant with frequency confirms the contribution of dipolar polarization towards total polarization of the material.

Growth of CuAMH crystals was accomplished by allowing diffusion of Cu^{2+} through silica gel impregnated with adipic acid in the single gel tube system. X-ray diffraction reveals that the crystals belong to the monoclinic system with space group C2/c (15). The thermo gravimetric analysis suggests that the grown CuAMH crystal is associated with one molecule of water of hydration, the crystal is thermally stable upto a temperature of about 278 ^{o}C and decomposes to copper oxalate. The optical band gap of the material is found to be 3.45 eV. The stoichiometric composition of the crystals is established to be $Cu(C_6H_8O_4)$ H_2O. The dielectric constant of CuAMH decreases gradually with increasing frequency of the applied ac field.

ZnA crystals belong to the monoclinic system with space group P21/c (14). The thermo gravimetric analysis suggests that the grown ZnA crystal is anhydrous and suggest that the gel grown ZnA is thermally stable up to a temperature of about 387 ^{o}C and decomposes to zinc oxide. The stoichiometric composition of the crystals is established to be $Zn(C_6H_8O_4)$. The optical band gap of the crystal is found to be 5.66 eV. The dielectric constant of ZnA decreases gradually with increasing frequency of the applied ac field.

References

[1] Yoshiki Chujo, Organic – Inorganic hybrid materials,Current openion in solid state and materials **1** (1996) 806-811.

[2] T. Maity, D. Saha, S. Das, S. Koner, Eur. J. Inorg. Chem. (2012) 4914–4920.

[3] B.-H. Ye, M.-L. Tong, X.M. Chen, Coord. Chem. Rev. **249** (2005) 545– 565.

[4] A. Ducruix R. Giegé. Crystallization of Nucleic Acids and Proteins: A Practical Approach 2nd edition, Oxford University Press (1999).

[5] M.Mathew, S.Takagi, H.L.Ammon Journal of crystallographic and spectroscopic research. **23** (1993) 617-621.

[6] E.G.Bagalbasis et.al. J. Chem. Soc., Dalton Trans., (2001) 850–857.

[7] Jian Cai, La-Sheng Long, and Lan-Sun Zheng, main group metal chemistry **25** 8 (2002).

[8] H. Sus; Spectrochemica Acta **59** 1063–1071.

[9] Masko Suzuki Infrared and Raman Spectra of Adipic Acid Crystal, Takehiko Shimanouchi journal of molecular spectroscopy **20** (1969)415-425.

[10] E.C. Jumanath and P.P. Pradyumnan Journal of Crystal Growth, **479** (2017) 83–88

[11] V. Ananthanarayanan; Spectrochemica Acta; **20** (1964) 197-210.

[12] Barbara Stuart, Infrared spectroscopy: fundamentals and applications, John Wiley Sons, Ltd ISBNs: 0-470-85427-8 (HB); 0-470-85428-6 (PB)(2004).

[13] Jean-Joseph Max† and Camille Chapados, J. Phys. Chem. A, **108** (2004) 3324-3337.

[14] B. Stuart, Infrared Spectroscopy: Fundamentals and Applications, Wiley, NewYork, (2004).

[15] Want B, Ahamed F, Kotru PN, J Mater Sci. **42** (2007) 9324-30.

[16] Rahimkutty MH, Babu KR, Pillai KS, Sudarsana Kumar MR, Nair CMK, Bull Mater Sci. **24** (2001) 249-52.

[17] Want B, Ahamed F, Kotru PN; J Mater Sci. **42** (2007) 9324-30.

[18] Rahimkutty MH, Babu KR, Pillai KS, Sudarsana Kumar MR, Nair CMK. Bull Mater Sci. **24** (2001) 249-52.

[19] J R llen and B R Barson, Thermochemica Acta, **161** (1990) 105-109.

[20] Oscar E. Pecho, Razvan Ghinea, Ana M. lonescu, Juan C.Cardona, Alvaro Della Bona, Maria del Mar Perez, **31** (2015) 60-67.

[21] P.J. Bahad, Ph.D Thesis, Chelate polymers of transition metal ions with Schiff base ligands Amaravati University (1998).

[22] Hong Woo Lee, Bull.Korean Chem. Soc., **29** (2008) 1711.

[23] R.N.Patel, N.Sing, D K Patel and V L N Gundla , Indian J.Chem., **46** (2007) 422.

[24] C P Pradeep, P S Zacharias and S.K Das, J.Chem. Sci., **117** (2005) 133.

[25] Nazir Ahmad a, M.M. Ahmad a and P.N. Kotru, Journal of Crystal Growth **412** (2015) 72–79.

[26] Soosen Samuel, JijiKoshy, AnoopChandran, K.C. George Current Applied Physics. **11** (2011) 1094.

[27] B.Rajagopal, A.V.Sharma and M.V.Rmana; Journal of Minerals Material Characterization Engineering; **10** (2011) 1487.

[28] B. Rajagopal 1, A.V. Sarma 2 and M.V. Ramana, Journal of Minerals Materials Characterization Engineering; **10** (2011) 1487.

[29] S.K. Arora, V. Patel, R.G. Patel, B. Amin, A Kothari, J. Phys. Chem. Solids **65** (2004).

[30] B. Rajagopal 1, A.V. Sarma 2 and M.V. Ramana, Journal of Minerals Materials Characterization Engineering **10** (2011) 1487.

[31] Sagadevan Suresh, Optik **125** (2014) 1223– 1226.

[32] M.P. Binitha, P.P. Pradyumnan, J. Therm. Anal. Calorim. **114** (2013) 665.

Chapter 4

Growth and Characterization of Metal Citrate Crystals

4.1 Introduction

Biomineralisation is a process which involves the controlled deposition and ordered growth of molecular materials in biological systems. This natural occurring process, produces organic-inorganic solids with fascinating inner and outer shapes, such as shells, bone, teeth etc. [1]. The reason for crystallization in blood vessels, gall bladder, kidney, urinary tract of animals and human beings were explained and reported in several studies [2]. Though the form, type and function of bio minerals are extremely varied and all of them share a common theme in the control mechanism, this determines the crystal deposition, morphology and the production of biominerals [3]. Over the last few decades, our ability to identify a large number of macromolecules and their interactions involved in the process of biomineralisation has grown and expanded [4-6].

As mentioned in the chapter 1 citric acid is a tricarboxylic acid, naturally found in citrus fruits. Mineral citrates are formed by the bonding of a mineral cation to citrate anion. This research work reports the single crystal growth, characterization and property studies of the citrates of calcium, copper and cadmium. To study the

nature of crystallization and morphology of these crystals, we have chosen hydro silica gel as a medium for the growth. Since hydrosilica gel is a medium which mimics the internal secretions in the organs in animals and plants, the medium were used for the growth of citrate crystals.

Calcium is one of the most important element, mainly found in the bones and teeth of the living beings. Over consumption of citric acid contained food or medicine may lead to the excess growth of crystalline metallic citrates in organs. Calcium citrate is the calcium salt of citric acid, and is an important chemical used in medicines, flavouring extracts, food candies, and in the manufacture of ink and dyes. Calcium citrate is also used as a water softener because the citrate ions can chelate unwanted metal ions and is found in some dietary calcium supplements [7].

Copper is considered a vital element to all living organisms as a trace dietary mineral because it is an important component of the respiratory enzyme complex cytochrome c oxidase [8]. The main organs where copper is found in human beings are liver, muscle and bone. The vitamin C reacts directly or indirectly with ceruloplasmin, a serum copper protein; specifically labilizing the bound copper atoms and facilitating their cross membrane transport [9]. The excess amount of cations like copper and citrate anion may lead to the formation of metallic citrates including copper (II) citrate in animal/human organisms. This may reduce the presence of copper like elements in the biological systems.

Cadmium is an element in the category of heavy metals. It has been attracted in various research due to its considerable toxicity with destructive impacts on organisms, including plants and animals [10]. Being a toxic metal, Cd is absorbed by the liver, finding its way to the kidney and may cause crystallization [11]. Presence of cadmium in plants depends on many factors such as pH of the water, temperature, concentration of minerals in the soil, etc. [12]. In recent decades, quantities of Cd in the atmosphere, hydrosphere and lithosphere of the planet have been significantly increased, which resulted in rising of solubility and mobility of cadmium in the environment [13]. Initially, Cd reached in soils and plants through its interactions with micro-organisms and eventually entered into human beings through

the food chain. Direct human contact through professional exposure and drinking of cadmium rich water also causes the intake of cadmium in the body. The excess amount of cadmium cation and citrate anion may lead to the formation of metallic citrates including cadmium citrate in animals and human beings. The literature survey reveals that the complex forms of Cd(II) with citrate do not transport into the bacterial cells and are consequently not degraded by bacteria [14]. Therefore, citric acid appears to be a good target for Cd(II), and their interactions are of chemical interest with potential biological outcome. The available solution studies carried out in the past on the Cd(II)-citrate system proposed various species of 1:1 (Cd(II)/citrate) stoichiometry, but were limited to further insight on their nature and properties [15].

4.2 Growth of crystals

The single crystals of metal citrates were grown by single diffusion gel technique. Initially, the stock solution (specific gravity ranging from 1.02 - 1.06) was prepared by dissolving an appropriate quantity of sodium metasilicate powder in double distilled water. After making this the gel was set by adding stock solution to citric acid (molarity ranging from 0.5 - 2 M) drop by drop with continuous stirring which may otherwise result in premature local gelling and make the final medium inhomogeneous and turbid. The gel of given pH (3 - 8) was then allowed to set for a given time (24 - 168 hrs) at room temperature. Once the gel got set, chloride solutions of Ca, Cu and Cd (molarity ranging from 0.5 - 2 M) were poured as upper reactant over the gel along the sides of the test tube separately, without disturbing the gel. The supernatant ions of Ca^{2+}, Cu^{2+} and Cd^{3+} are separately diffused into the gel medium where it reacts with citrate ions $(C_6H_5O_7)^{3-}$ encapsulated in the gel as lower reactant giving rise to the formation of calcium citrate pentahydrate (CaCPH), copper citrate dihydrate (CuCDH) and cadmium citrate hexahydrate (CdCHH) crystals inside and interface of the gel. The following chemical reaction was expected to take place for the formation of the title compounds.

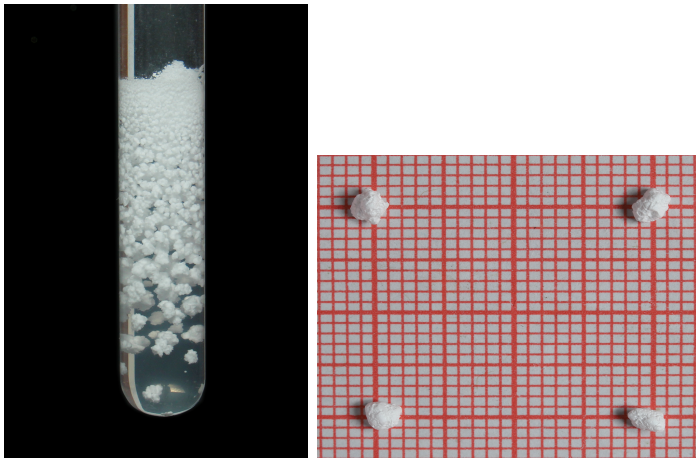

Figure 4.1: CaCPH crystals during growth and grown crystals

$3CaCl_2 + 2(C_6H_8O_7) + 5H_2O \rightarrow Ca_3(C_6H_5O_7)_2\ 5H_2O + 6HCl$

$3CuCl_2 + 2(C_6H_8O_7) + 2H_2O \rightarrow Cu_3(C_6H_5O_7)_2\ 2H_2O + 6HCl$

$3Cd(NO_3)_2 + 2(C_6H_8O_7) + 6H_2O \rightarrow Cd_3(C_6H_5O_7)_2\ 6H_2O + 6HNO_3$

4.2.1 CaCPH crystals

When the concentration of the diffusant is optimum, a few critical-sized nuclei are produced and due to the subsequent diffusion of Ca^{2+} ions, the habits of the crystals formed within the gel were spherulitic. The growth setup and harvested crystals of CaCPH are shown in Figure 4.1.

4.2.2 CuCDH crystals

The supernatant solution of $CuCl_2$ diffuses into the gel column and reacts with citric acid in the gel to produce necessary supersaturation for the slow precipitation of $Cu_3(C_6H_5O_7)_2\ 2H_2O$. When the concentration of the added $CuCl_2$ solution, the gel density and the acid concentration are optimum, a few critical-sized nuclei were produced. The grown crystals are spherulitic in nature and is shown in Figure 4.2.

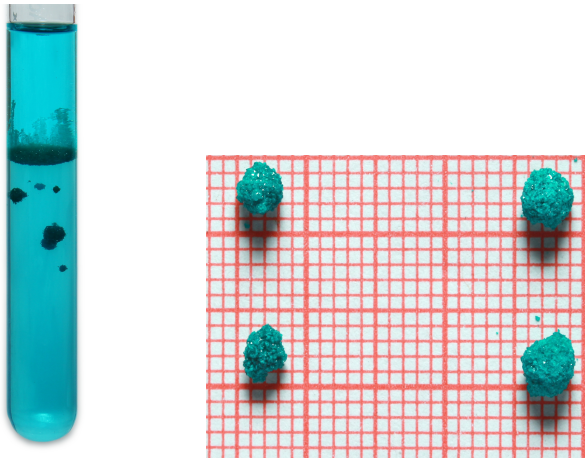

Figure 4.2: CuCDH crystals during growth and grown crystal

4.2.3 CdCHH crystals

To determine the optimum conditions for the growth of CdCHH crystal, separate experiments were performed, particularly in regard to the effect of gel density, gel pH and concentration of cadmium nitrate. The details like the effect of basic parameters of gel on the nucleation and the number of single crystals formed were also studied.

Dependence of crystal growth on gel density and pH

Nucleation control attained by the controlled diffusion of the cation is the key element for the success of crystal growing mechanism by gel method. There are two parameters which depend on nucleation: (1) the size of the diffusing ions relative to the pore size in the gel and (2) the amount of interaction between solute and the internal gel surfaces. Preliminary experiments were done to determine particular conditions for the preparation of silica gel. It was noted that high density gels took lesser time to set and they were mechanically stronger than the lower density gels. But the transparency of the gel was found to decrease with increase in gel density. It is also observed that the crystal count decreased with increase in gel concentration. Higher the gel density, smaller the pore sizes which diminishes nucleation and tends to increase contamination of the crystals by silicon and thereby affect their perfection and shape adversely. Gels of insufficient density have taken a long time to set and are mechanically unstable [16, 17]. So the optimisation of gel density

for growing crystal is attained by several experiments to get good quality and sized crystal.

pH during gelling has significant influence on gel structure. Effect of pH of silica gel was studied by different ratios of sodium meta silicate and citric acid. As pH increases the gel structure changes from a distinctly box like network to a structure consisting of loosely bound platelets, which appear to lack cross linkages and the cellular nature becomes less distinct. It is noted that the time required for the gelation is very sensitive to pH. At very low pH values the tendency towards polymerization is diminished and chain formation is slowed. The gel structure affects the crystal growth characteristics, including growth rate and ultimate crystal size. The crystal count increases with increase in the pH value of the gel. Gel pH is an important parameter of growth, which controls the pore size of the gel and in turn governs the diffusion rate of the reactant [18, 19].

Effect of concentration of $Cd(NO_3)_2$

The concentration of reactants plays an important role in the growth of crystals. Maintaining constancy of gel specific gravity 1.03 and gel pH as optimum conditions of growth as described above, then the nature of the growth of crystals will depend on the concentration of the reactants. Solution of $Cd(NO_3)_2$, of different concentrations ranging from 0.25 M to 1.5 M was poured above the set gel and crystal growth was observed. It was found that by increasing the concentration of Cd^{3+}, the nucleation density increases. The increase in nucleation with increase in concentration is because of the enhanced availability and the probability of Cd^{3+} ions to react with the citrate $(C_4H_5O_7)^{3-}$ ions in the medium [20]. Good quality crystal is obtained at a concentration of 1M with gel density 1.03. The experiment resulted in the formation of crystals of maximum size $2\times\ 2\times 2$ mm^3. They were platy, colorless and transparent. The grown crystals of CdCHH are shown in Figure 4.3.

The effect of various growth parameters such as gel pH, gel density, gel age and concentration of reagents on the growth of CaCPH, CuCDH and CdCHH crystals

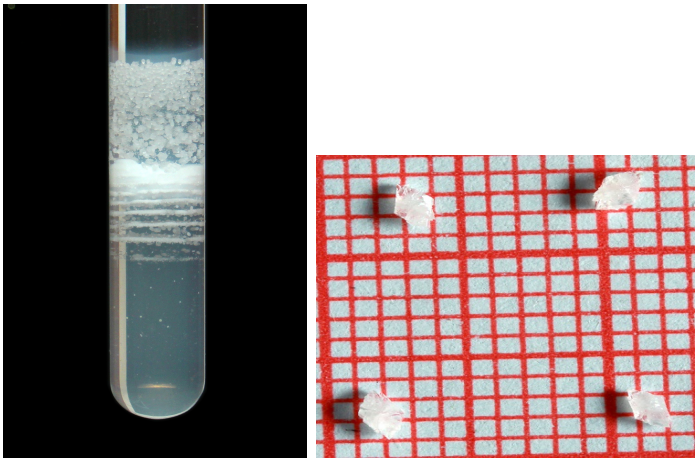

Figure 4.3: Growth of CdCHH crystals in testube and harvested crystals

Table 4.1: Optimum conditions for the growth of citrate crystals

Paramaeters	CaCPH	CuCDH	CdCHH
Gel density	1.05	1.03	1.03
pH	6	6	6
Gel set time	1 day	1 day	1 day
Growth period	35 days	40 days	21 days
Concentration of citric acid	1M	1M	1M
Concentration of upper reactant	1M	1M	1M

were investigated from different experiments. The optimum growth conditions for the growth of good-quality crystals of are summarized in Table 4.1.

Well grown crystals were separated from the gel medium after ensuring their maximum growth and structural, spectroscopic and thermal characterization were performed.

4.3 Structural studies

4.3.1 CaCPH crystals

Figure 4.4 shows the powder XRD pattern of the CaCPH crystal. The crystallinity of the material is quite clear from this diffraction pattern. Since the well faceted good quality crystals are not grown, the authors are not able to perform the single crystal characterization. The powder XRD data revealed that the crystal belonging

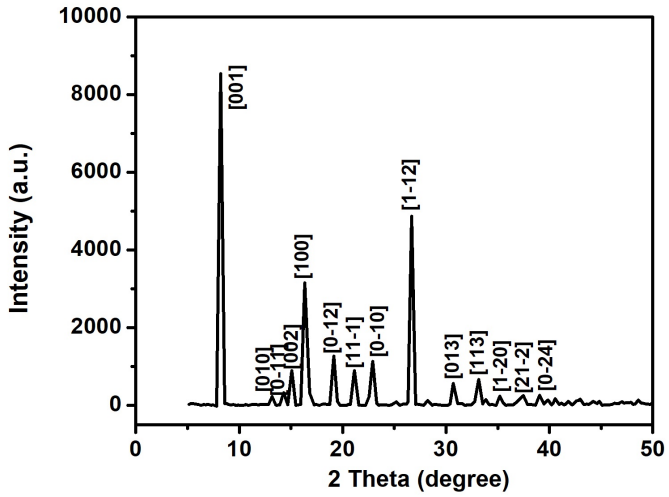

Figure 4.4: Powder XRD pattern of CaCPH crystal

to triclinic system with space group P-1. The cell parameters are a = 5.4630 Å, b= 6.5058 Å, c = 11.1573 Å, $\alpha = 101.121^{o}, \beta = 88.855^{o}, \gamma = 81.382^{o}$.

4.3.2 CuCDH crystals

The powder XRD patterns of CuCDH is shown in Figure 4.5. The well defined Bragg peaks reveal the crystalline nature. The data were compared with the standard values in the ICDD card 00-050-2490. The calculated cell parameters reveal that the crystal belongs to the monoclinic system having space group I4/m(87). The unit cell parameters of the crystal calculated by PDXL software by matching with the above ICDD card are a = 16.176 Å, b= 9.732 Å, c = 6.921 Å, $\alpha = \gamma = 90.00^{o}, \beta = 116.570^{o}$ and unit cell volume = 974.469 $(Å)^3$, and are in agreement with the literature [21].

4.3.3 CdCHH crystals

The single crystal structure was determined by direct methods at 296 K and found to correspond to a monoclinic system and P21/n space group. A unit cell consisting of two crystallographically independent citrate ions, three Cd^{2+} ions and six water molecules. The powder X-ray pattern of the bulk crystal grown to be identical to one another and to the powder XRD pattern simulated from the single crystal

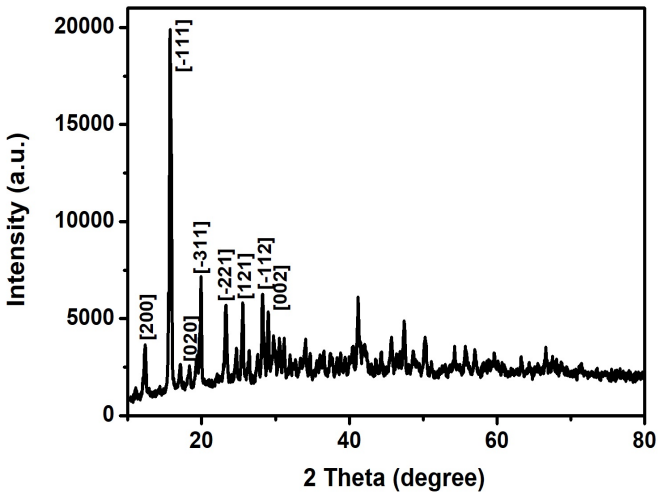

Figure 4.5: Powder XRD pattern of CuCDH crystal

structure, thereby confirming the presence of only one citrate salt phase under the growth condition (CCDC No: 1881999). The powder XRD pattern of the grown crystal is presented in Figure 4.9. The sharp peaks at specific Bragg's angles confirm the crystallinity of the entire sample.

Atoms in each of the cadmium citrate hexahydrate units are numbered according to Figure 4.6. Each cadmium ion exists an octahedral geometry through short contacts with the citrate ions, the bond lengths of Cd – O (oxygen present in the citrate molecule) bonds are Cd(1)...O5, 2.3329 Å; Cd(1)...O10, 2.2700 Å; Cd(2)...O6, 2.3329 Å; Cd(3)...O11, 2.2980 Å; Cd(3)...O16, 2.3492 Å; and bond lengths of Cd – O (oxygen present in the water molecules) bonds are Cd(1)...O9, 2.2817 Å; Cd(2)...O6, 2.2682 Å; Cd(3)...O12, 2.3048 Å; Cd(3)...O13, 2.2993 Å; Cd(3)...O17 2.2798 Å.

The six apices of the oxygen co-ordination octahedron are occupied as follows: 3 co-ordination positions are occupied by one citrate ligand, which employs both the central alcoholic and carboxylate oxygen atoms as well as one of its terminal carboxylate oxygens to bind Cd(1). The other two co-ordination positions are occupied by two additional citrate ligands from two adjacently located octahedral Cd(2) and Cd(3) ions are reaching out and co-ordinate to Cd(1) through the oxygen atoms

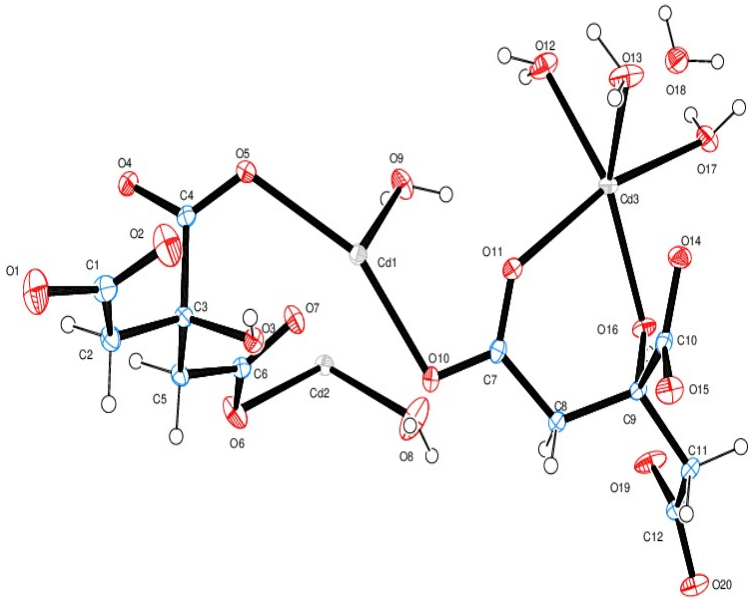

Figure 4.6: ORTEP image of CdCHH single crystal

of their respective central carboxylate groups. The remaining co-ordination site is occupied by a water molecule. The second terminal carboxylate group of the citrate ligand is protonated so not participate in any co-ordination. It remains free, moving away from the Cd sites.

The Cd-O bond distances vary between 2.270 and 2.576 Å and O-Cd-O bond angles vary in a very wide range from 85.14 to 180 Å. The crystal data and structure refinement parameters are presented in Table 4.2. The six water molecules present in the crystal involve the extensive network of hydrogen bond amongst themselves and are responsible for the stability of the structure. Table 4.3 gives the parameters of hydrogen bonding. Figure 4.7 shows the 2D layer network and Figure 4.8 is the three dimensional polymeric structure of CdCHH single crystal. The single crystal XRD results are very similar to other reported structure of cadmium (II) complexes were grown by slow evaporation and hydrothermal methods [22-24].

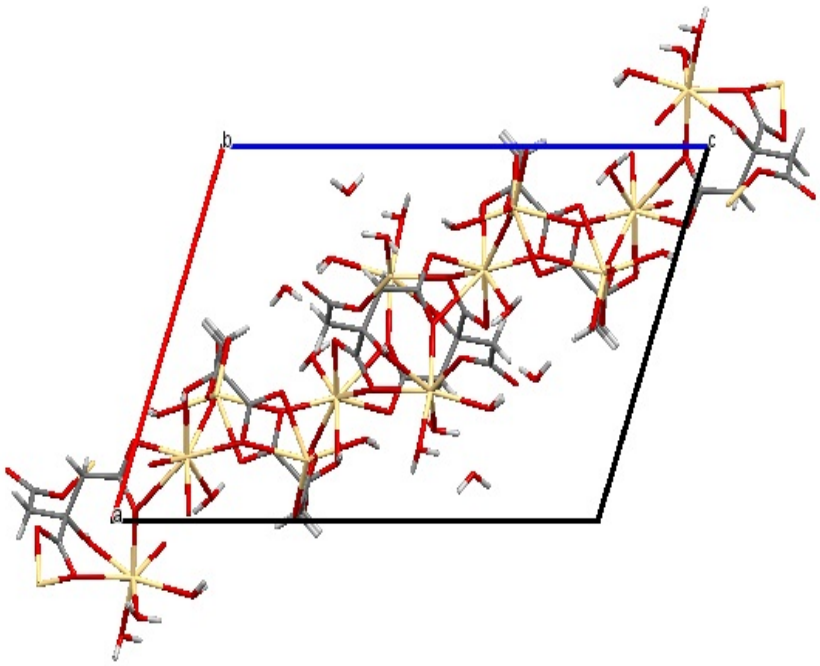

Figure 4.7: The 2D layer network, showing packing along the b axis.

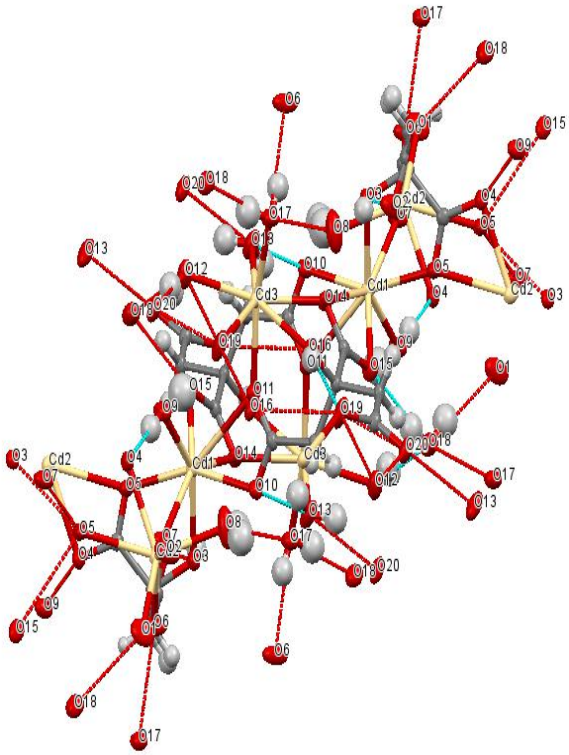

Figure 4.8: Three dimensional polymeric structure of CdCHH single crystal.

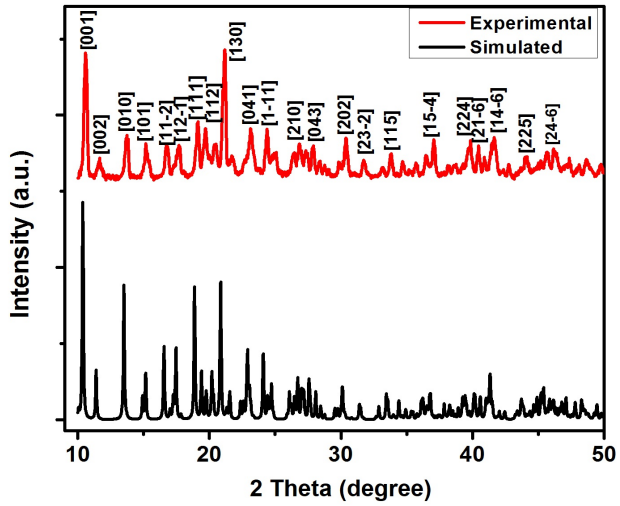

Figure 4.9: Powder XRD Pattern of CdCHH crystal

Table 4.2: Crystal data and structure refinement for CdCHH crystal

Parameter	CdCHH crystal
Identification code	Shelxl
Emperical formula	$C_{12}H_{22}Cd_3O_9$
Formula weight	823.49
Temperature	296(2)K
Wavelength	0.71073 Å
Crystal system, Space group	Monoclinic, P21/n
Unitcell dimensions	a = 12.5515 Å, b = 10.2656 Å, c = 18.0063 Å, $\alpha = \gamma = 90^0$, $\beta = 109.0150^0$
Volume	2193.75 (12) $Å^3$
Z, Calculated density	4, 2.494 Mg/m^3
Absorption coefficient	2.980 mm^{-1}
F(000)	1592
Theta range for data collection	2.623 to 28.316 deg
Limiting indices	-16$\leq h \leq$ 16, $-13 \leq h \leq 13, -23 \leq h \leq 23$,

Table 4.3: Geometries of H-bonds in CdCHH crystal; D = donor, A = acceptor

D-H...A	d(D-H) [Å]	d(H...A)[Å]	D(D...A) [Å]	DHA [^{0}]
O(3)-H(3)...O(2)	0.80(3)	2.07(3)	2.737(2)	141(3)
O(3)-H(3)...O(14)1	0.80(3)	2.41(3)	2.834(2)	115(2)
O(12)-H(12A)...O(18)7	0.88	1.96	2.819(3)	162.0
O(12)-H(12B)...O(20)4	0.88	1.80	2.656(2)	163.2
O(13)-H(13A)...O(10)1	0.87	2.10	2.892(2)	151.2
O(13)-H(13B)...O(20)8	0.87	1.93	2.698(2)	145.9
O(16)-H(16)...O(19)	0.79(3)	1.92(3)	2.606(2)	145(3)
C(5)-H(5B)...O(3)9	0.95(3)	2.48(3)	3.426(2)	171(2)
C(11)-H(11A)...O(4)10	0.96(3)	2.64(3)	3.434(2)	139.9(19)
O(18)-H(18A)...O(15)8	0.830(18)	1.96(2)	2.757(2)	162(3)
O(18)-H(18B)...O(1)11	0.831(18)	1.99(2)	2.789(3)	161(3)
O(17)-H(17A)...O(6)12	0.832(17)	1.95(2)	2.744(2)	160(3)
O(17)-H(17B)...O(18)	0.833(18)	1.87(2)	2.684(2)	167(3)
O(9)-H(9A)...O(4)3	0.822(17)	1.917(18)	2.735(2)	173(3)
O(9)-H(9B)...O(11)	0.834(18)	2.42(4)	2.928(2)	120(3)
O(9)-H(9B)...O(19)4	0.834(18)	2.46(2)	3.234(3)	155(4)
O(8)-H(8A)...O(17)4	0.821(18)	2.04(2)	2.827(3)	160(4)
O(8)-H(8B)...O(10)	0.832(19)	2.32(3)	3.074(3)	151(4)

4.4 FTIR and micro Raman studies

4.4.1 CaCPH crystals

The FTIR and micro Raman spectra of the prepared sample are given in Figure 4.10 (a) and (b) respectively. The spectra are analyzed by comparing with those of related compounds available in literature [25-27]. The assignments of some selected wave numbers are given in Table 4.4. The internal vibrations are due to the carboxylate group, methylene group and internal water.

FTIR studies

Spectrum exhibit strong characteristic absorption bands for the carbonyls from the carboxylate rich citrate ligands in both the asymmetric and symmetric vibration regions with water of crystallization. The broad absorption band centered at 3425 cm^{-1} is expected for the stretching vibration of the hydroxyl group. The absorption bands appear at 1551 cm^{-1} and 1436 cm^{-1} are asymmetric stretching vibrations of

the carbonyl group (COO-). The corresponding symmetric stretching vibrations of carbonyl group are observed at 1275 cm^{-1}. The difference between symmetric and asymmetric stretches $\triangle[\nu_{as}$(COO-)-ν_s(COO-)] is of the order of 200 cm^{-1}, indicating that the carbonyl groups are either free or coordinated to the metal in monodentate fashion [28].

Micro Raman studies

The observed spectrum (figure 4.10 (b)) consists of 9 Raman lines. The line of frequency shifts observed at 3455 cm^{-1} corresponding to OH stretching vibration. The frequency shifts 2926 cm^{-1} may be attributed to C-H oscillations. The vibrations corresponding to asymmetric and symmetric stretching are observed at 1462 cm^{-1} and 1275 cm^{-1}. The Raman line corresponding to bonding of calcium and oxygen is observed at 196 cm^{-1}. All of the bands are shifted to lower wave numbers compared to the free citric acid.

The proposed assignments obtained from both spectroscopic studies are presented in table 4.5. From the spectroscopic studies, it may be concluded that some of the observed vibrations in both Raman and IR are active so the CaCPH crystal is noncentre of symmetric in nature. The functional groups present in the crystal are exactly same as in the citrate ligand, and also confirm the presence of water of crystallization. The aforementioned spectral assignments for citrate complexes are in agreement with results reported in the literature [28].

4.4.2 CuCDH crystals

The recorded FTIR and Micro Raman spectra of powdered CuCDH crystal is shown in the Figure 4.11 (a) and (b). Spectrum exhibits strong characteristic absorption bands for the carbonyls from the carboxylate rich citrate ligands in both the asymmetric and symmetric vibration regions with water of crystallization. The proposed assignments obtained from both spectroscopic studies are presented in Table 4.5.

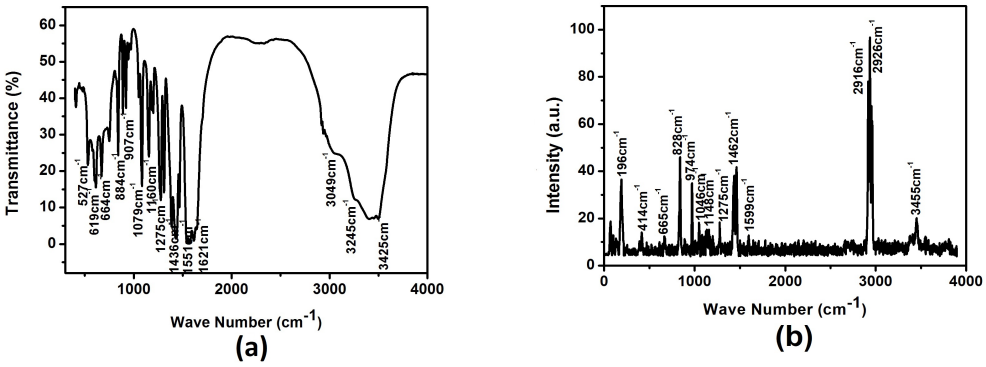

Figure 4.10: (a) FTIR spectrum of CaCPH crystal (b) Micro Raman spectrum of CaCPH crystal.

Table 4.4: Assignment of some selected FTIR and Raman wave numbers of CaCPH crystal

FTIR band (cm^{-1})	Raman band (cm^{-1})	Assignment of peaks per band
3425	3455	ν(OH)
3245	2926	ν_{as}(C-H)
3049	2916	ν_{s}(C-H)
1551	1572	ν_{as}(COO-)
1436	1462	ν_{s}(COO-)
1275	1275	ν_{as}(C-O)
1160	1148	ν_{in}(C-CO_2)
1079	1046	ν_{as}(C-C)
907	974	ν_{s}(C-C)
884	828	ρ_{r}(H_2O)
664	665	δ(OCO)
619	414	ν(Ca-O)
527	196	ν(Ca-O)

OH stretching: The OH stretching frequency has been used for many years as a test and measure of hydrogen bonds. The stronger the hydrogen bond the longer the OH bond, the lower the vibrational frequency and the broader and more intense the absorption band [29]. For CuCDH crystals at 3409 cm^{-1}. This indicated that the water molecule is present in the grown crystals.

CH_2 stretching: The IR spectrum of copper citrate exhibit a weak peak at 2929 cm^{-1} which are assigned to asymmetric stretching vibrations of the C-H bonds. Corresponding vibrations in the Raman spectrum observed at 2988 cm^{-1}. The medium peaks observed in IR spectrum at 855 cm^{-1} of CuCDH suggesting the rocking vibrations of CH_2 group. Similarly 912 cm^{-1} is the peak observed in Raman spectrum.

COO- and C-O stretching: The C-O stretching absorption in aliphatic compounds generally occurs at 1725 - 1700 cm^{-1} [30]. The C-O absorption in carboxylic acids appears at 1700 cm^{-1} [31]. If carboxylic acid is converted into its soluble salts, then carboxylate anion is formed [32]. In CuCPH crystals the IR vibrations observed at 1258 cm^{-1} and Raman shift observed at 1236 cm^{-1} are assigned to C-O vibrations. The COO- absorption has a possible higher wave number for an acid as compared to that in carboxylate anion. In citrate crystals COO- asymmetric stretching appears at 1566 cm^{-1} in the IR spectrum and 1236 cm^{-1} in Raman spectrum. Symmetric stretching vibrations of COO- appears at 1585 cm^{-1} in the CuCDH crystals. This indicates the presence of carboxylate anions (citrate) in crystal.

C-C stretching: The band at 1321 cm^{-1} in FT-IR and 1313 cm^{-1} in Raman specifies C-C asymmetric stretching in copper citrate and IR bands at 1153 and 946 cm^{-1} and Raman shift at 913 and 970 cm^{-1} specifies C-C symmetric stretching in CuCPH crystal, which shows the presence of carboxylate anion. This confirms the existence citrate group in CuCPH crystal.

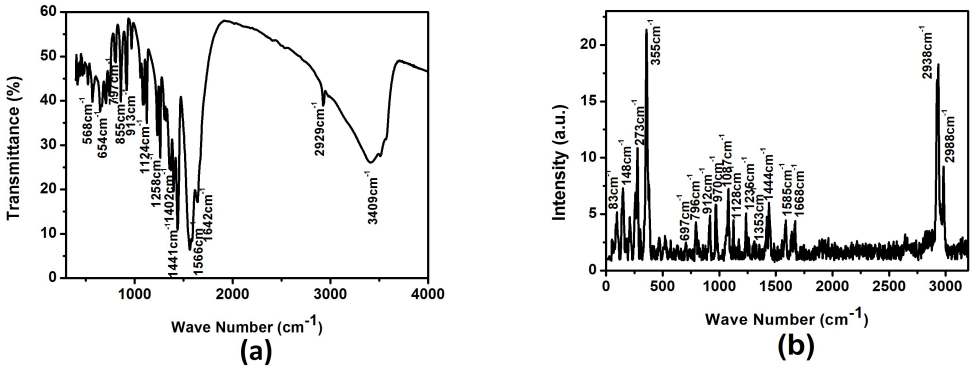

Figure 4.11: (a) FTIR spectrum of CuCDH crystal (b) Micro Raman spectrum of CuCDH crystal.

Metal-O stretching: All the bands observed at below 500 cm^{-1} are assigned to Metal-O bonding, which confirms the metal carboxylate bonding in grown crystals.

4.4.3 CdCHH crystals

FTIR spectrum of cadmium citrate crystal is shown in the Figure 4.12 (a). Spectrum exhibit the broad absorption band centered at 3390 cm^{-1} is expected for the stretching vibration of the hydroxyl group which confirm the presence of water of hydration in the crystal. The strong absorption bands appear at 1599 cm^{-1} and 1427 cm^{-1} are asymmetric stretching vibrations of the carbonyl group (COO-). The corresponding symmetric stretching vibrations of carbonyl group are observed at 1259 and 1206 cm^{-1}. Medium IR peaks at 922 cm^{-1} and 1082 cm^{-1} are due to the central C-C stretching. Bending and rocking vibrations of CH_2 are observed at 688 cm^{-1} and 625 cm^{-1} respectively [28].

Micro Raman Studies: The observed spectrum (Figure 4.12 (b)) consists of 12 Raman lines. The two lines of frequency shifts observed at 3331 and 3528 cm^{-1}, in which the first is comparatively broad and diffuse. The frequency shifts 2978 and 2916 cm^{-1} may be attributed to C-H oscillations. The vibrations corresponding to asymmetric and symmetric stretching are observed at 1452 cm^{-1} and 1390 cm^{-1}.

Table 4.5: Assignment of some selected FTIR and Raman wave numbers of CuCDH crystal

FTIR band (cm^{-1})	Raman band (cm^{-1})	Assignment of peaks per band
3409	-	ν(OH)
2929	2988	ν_{as}(C-H)
	2938	ν_{s}(C-H)
1642	1668	ν_{as}(H-O-H)
1566	1585	ν_{as}(OCO)
1441	1444	ν_{s}(OCO)
1402	1353	$\delta(CH_2)$
1258	1236	ν_{as}(C-O)
1124	1128	ν_{out}(C-CO_2)
	1087	ν_{in}(C-CO_2)
913	970	ν_{s}(C-C)
855	912	$\rho_{r}(CH_2)$
791	796	$\rho_{r}(H_2O)$
654	697	δ(OCO)
568	355	ν(Cu-O)
-	273	ν(Cu-O)
-	148	ν(Cu-O)

The Raman line corresponding to bonding of Cd and oxygen is observed at 124 cm^{-1}. Larger masses of the metals give Raman line at a very low stretching frequency of 124 cm^{-1} corresponding to Cd-O stretching. All of the bands are shifted to lower wave numbers compared to the free citric acid. The aforementioned spectral assignments for citrate complexes are in agreement with results reported in the literature [33, 34]. The proposed assignments obtained from both spectroscopic studies are presented in Table 4.6.

4.5 Thermal decomposition studies

4.5.1 CaCPH crystals

TG–DTA and DSC curves of CaCPH crystals are depicted in Figures. 4.13 (a) and (b) respectively. The TGA was carried out from room temperature to a maximum of 700 ^{o}C at a heating rate of 10 ^{o}C/min in an atmosphere of nitrogen. A slight weight

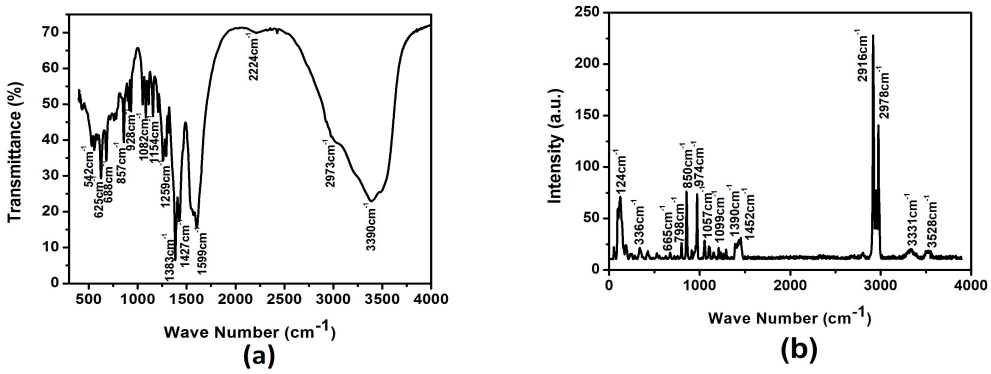

Figure 4.12: (a) FTIR spectrum of CdCHH crystal (b) Micro Raman spectrum of CdCHH crystal.

Table 4.6: Assignment of some selected FTIR and Raman wave numbers of CdCHH crystal

FTIR band (cm^{-1})	Raman band (cm^{-1})	Assignment of peaks per band
3390	3528 and 3331	ν(OH)
2973	2978	ν_{as}(C-H)
2224	2918	ν_s(C-H)
1599	1452	ν_{as}(COO-)
1427 and 1383	1390	ν_s(COO-)
1259	1099	ν_s(O-C)
1154	1057	(C-C-C) bending
922 and 1082	974	ν_s(C-C)
857	850	CH bending
688	798	$\rho_t(CH_2)$
625	665	C-H deformation
542	124	ν(Metal-O)

increased in the early stage of degradation could be explained due to buoyancy effect of TGA equipment. There are few fundamental thermal analysis textbooks and papers explained about the buoyancy effect in TGA equipment [35-37]. In TGA analysis buoyancy is the upward force on the sample produced by the surrounding atmosphere, which will affect the apparent mass during TGA experiment. The buoyancy effect occurs as the density of the atmosphere in the balance decreases with increasing temperature, resulting in an apparent mass gain. Consequently, it depends on the volume of the sample and the density of the atmosphere. The first stage of decomposition (43 - 151 °C) results in the elimination of five water molecule and the formation of anhydrous CaCPH crystal. The calculated and observed mass loss corresponding to this is 14.85% and 15.31% of the total mass taken. This dehydration occurring at low temperature range suggests the presence of water of crystallization, this is matched by the observations made by E. Herdtweck et. al. [38]. Corresponding to this dehydration, there are two endothermic peak in the DTA curve at about 78 and 145 °C.

The second stage of decomposition between 348 and 532 °C, there occurs a loss of one water molecule and 10H, 2O and 6C, thereby reducing the calcium citrate pentahydrate to calcium oxalate. The measured and theoretical values of mass loss at this stage are 22.89% and 25.58% of the total mass taken. Corresponding to these losses there is an endothermic peak in DTA at about 499 °C. The figure 4.15 (b) shows the DSC profile of CaCPH crystal in nitrogen at 10 °C min^{-1}. The profile displayed three exothermic peaks at 70, 105 and 138 °C, accounts for the dehydration step. The DTA portion of the thermal curve is consistent with the description of DSC results. Critical examination of the TG and DSC curves indicates that the decomposition pattern is typical of a hydrated CaCPH and transformations are associated with mass changes and there are no physical (crystallographic) transformations independent of mass change or decomposition of the material. Following is the stoichiometry of the different intermediates involved in the decomposition process of CaCPH.

1. $Ca_3(C_6H_5O_7)_2.5H_2O$ - $5H_2O \rightarrow Ca_3(C_6H_5O_7)_2$

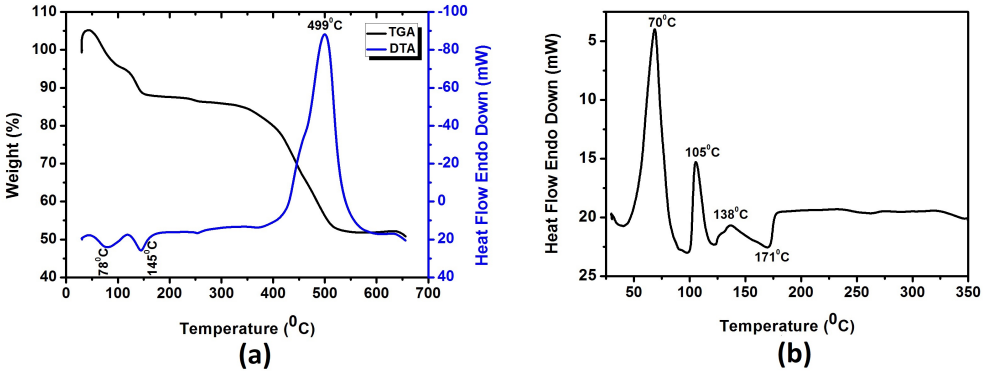

Figure 4.13: (a) TG-DTA curves of grown crystals (b) DSC thermogram of CaCPH crystal.

2. $Ca_3(C_6H_5O_7)_2$ - (10H + 6C + 2O) $\rightarrow$ 3 ($Ca(C_2O_4)$

4.5.2 CuCDH crystals

Thermal characterization of the samples is carried out by the thermo gravimetric analysis in the temperature range of 50 - 700 °C under nitrogen atmosphere at a heating rate of 10 °C/min. DSC analysis of grown crystals was also performed. Figure 4.14 (a) shows the observed thermal degradation curve. The compound displays mainly two thermal processes in the temperature range of 50 - 700 °C. The compound losses two water molecule in the temperature range 51 - 109 °C corresponding to an exothermic DTA peak at 103 °C with a weight loss of 5.59% (calculated weight loss 5.95%). After the dehydration, the compound remains nearly stable until 219 °C, beyond which it decomposes. In the temperature range of 219 - 307 °C corresponding to an endothermic DTA peak at 49.87 °C, the weight loss of 34.82% during the second thermal process attributes to the liberation of nine carbon, ten hydrogen and five oxygen from the anhydrous CuCDH crystal. Thus the the final product may be 3($CuCO_3$). The formation of carbonates of other citrate compounds is also reported in the literature [39]. Therefore the temperature range of 50 - 700 °C, the experimentally observed weight loss of 50.39% is much closer to the calculated weight loss of 40.77% for the formation of copper carbonate.

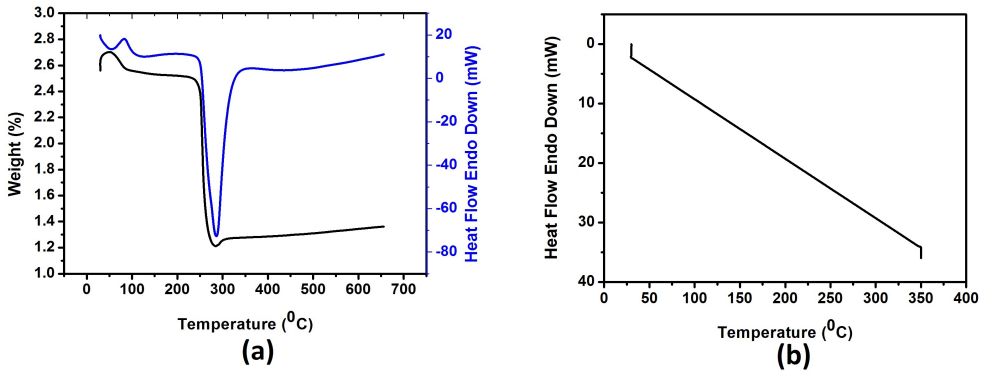

Figure 4.14: (a) TG-DTA curves of grown crystals (b) DSC thermogram of CuCDH crystal.

From the TG-DTA plot, only two chemical reactions have been proposed to take place during the thermal decomposition of the compound. Figure 4.14 (b) shows the thermogram obtained from DSC, it is observed that there are no peaks.

1. $Cu_3(C_6H_5O_7)_2\ 2H_2O$ - $2H_2O \rightarrow Cu_3(C_6H_5O_7)_2$
2. $Cu_3(C_6H_5O_7)_2$ - (9C + 5O + 10H) $\rightarrow 3(CuCO_3)$

4.5.3 CdCHH crystals

TG–DTA and DSC curves of CdCHH crystals are depicted in Figure 4.15 (a). The TGA was carried out from room temperature to a maximum of 700 °C at a heating rate of 10 °C/min in an atmosphere of nitrogen. The material remains stable up to a temperature 67 °C and starts decomposing at about 67 °C, after which it reduces to its carbonaceous compound at 456 °C and process continue.

The first stage of decomposition (67 - 299 °C) leads to the elimination of six water molecules and results in the formation of anhydrous CdCHH. The calculated and observed mass loss corresponding to this is 13.089 and 15.131% of the total mass taken. The dehydration occurring at this temperature range suggests the presence of water of crystallization [40]. Corresponding to this dehydration, there are three endothermic peaks in the DTA curve at about 125 °C, 152 °C and 221 °C.

During the second stage of decomposition between 299 °C and 456 °C, there occurs a loss of 12H, 10C and 8O, thereby reducing the anhydrous cadmium citrate

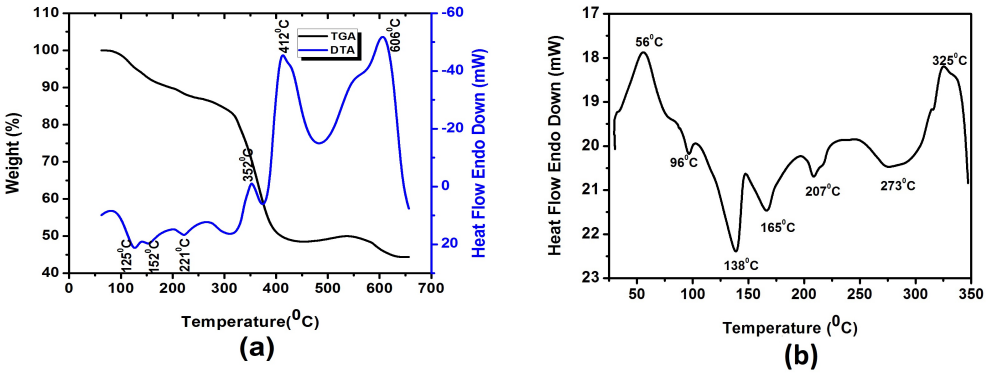

Figure 4.15: (a) TG-DTA curves of grown crystals (b) DSC thermogram of CdCHH crystal.

to cadmium carbonate. The measured and theoretical values of mass losses at this stage are 51.31 and 49.34% of the total mass taken. Corresponding to these losses there are endothermic peaks in DTA at about 352 °C and 412 °C. In the third step, we are expecting that the material may continue to decompose and reduces to cadmium oxide. The thermal decomposition reactions are usually endothermic. However, some of the DTA peaks are exothermic, this is due to the concomitant oxidation reactions taking place along with decomposition reactions. The final solid products of thermal compositions of the investigated are oxides [41].

The Figure 4.15 (b) shows the DSC profile of CdCHH crystal in nitrogen at 10 °C min^{-1}. The profile displayed five endothermic peak at 96 °C, 138 °C, 165 °C, 207 °C and 273 °C accounts for the dehydration step. The DTA portion of the thermal curve is consistent with the description of DSC results. Critical examination of the TG and DSC curves indicates that the decomposition pattern is typical of a hydrated CdCHH and transformations are associated with mass changes and there are no physical (crystallographic) transformations independent of mass change or decomposition of the material.

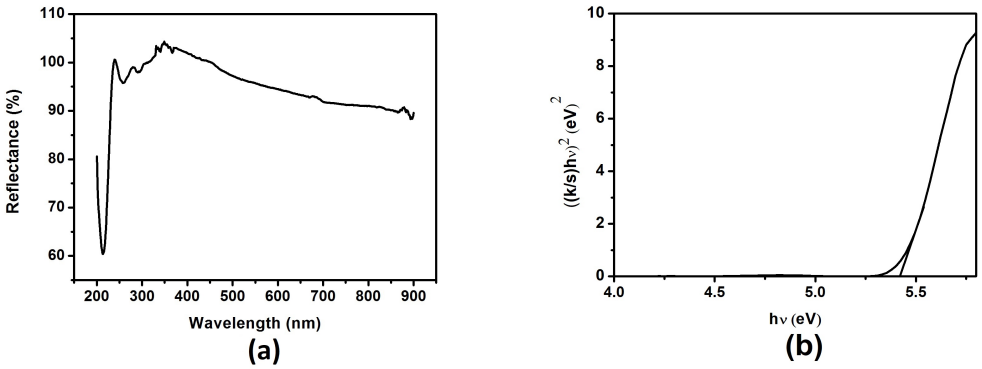

Figure 4.16: (a) Diffuse reflectance spectrum of CaCPH (b) Plot of $[(k/s)h\nu]^2$ versus $h\nu$ for CaCPH crystals.

4.6 Optical property studies

4.6.1 CaCPH crystals

Optical absorption measurement of the powdered sample of CaCPH crystal was carried out in the range 200 – 900 nm at room temperature and is shown in Figure 4.16 (a). The spectrum shows maximum absorption in the near UV range (200 - 300 nm) at 216 nm for which percentage of reflectance is 59.83. The crystal shows the absence of absorption in the entire visible range and that is an essential parameter to an NLO crystal. This crystal is used for suitable optical applications due to its wide transparency window in the part of visible region above 216 nm. From Kubelka-Munk function [42]

$$F(R) = (1\text{-}R)^2/2R = k/s \tag{4.1}$$

where R is reflectance, k is absorption coefficient and s is scattering coefficient. The optical band gap of the material was determined by extrapolating the linear portion of the plot of $[(k/s)h\nu]^2$ versus $h\nu$ (Figure 4.16 (b)). The calculated band gap is 5.33 eV.

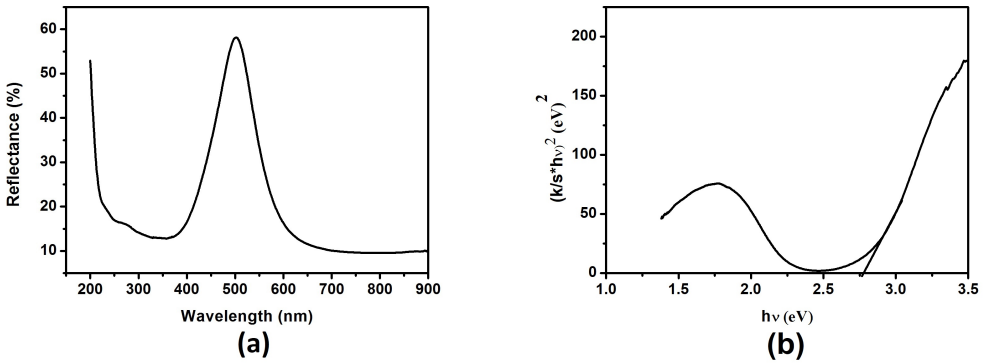

Figure 4.17: (a) Diffuse reflectance spectrum of CuCDH (b) Plot of $[(k/s)h\nu]^2$ versus $h\nu$ for CuCDH crystals.

4.6.2 CuCDH crystals

The diffuse reflectance measurements for copper citrate crystal at room temperature is shown in Figure 4.17 (a). CuCDH crystal highly reflecting in the region between 450 and 550 nm. The optical band gap of the material was determined by extrapolating the linear portion of the plot of $[(k/s)h\nu]^2$ versus $h\nu$ (Figure 4.17 (b)), where k is the absorption coefficient evaluated from the Kubelka–Munk function and s is the scattering coefficient. The calculated band gap of CuCMH crystal is 2.78 eV.

4.6.3 CdCHH crystals

The finely ground powder of cadmium citrate crystal is used for the optical measurement in the wavelength range of 200 - 900 nm. The variation of diffuse reflectance for cadmium citrate crystal at room temperature is shown in Figure 4.18 (a). The optical band gap of the material was determined by Kubelka Munk function, extrapolating the linear portion of the plot of $[(k/s)h\nu]^2$ versus $h\nu$ (figure 4.18 (b)). The calculated band gap is 5.15 eV.

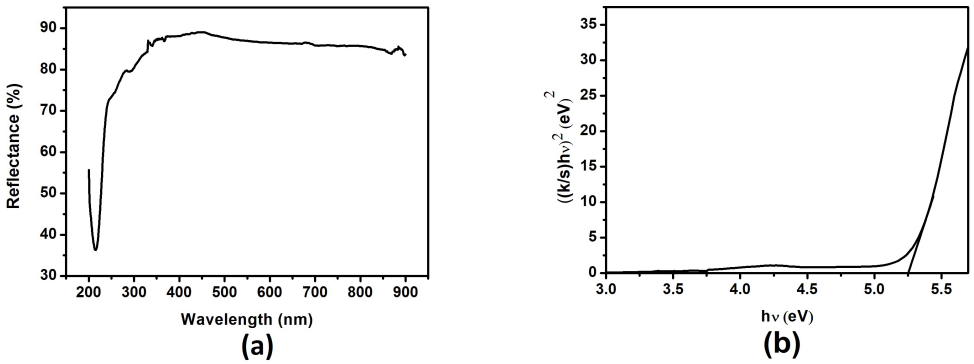

Figure 4.18: (a) Diffuse reflectance spectrum of CdCHH (b) Plot of $[(k/s)h\nu]^2$ versus $h\nu$ for CdCHH crystals.

4.7 Dielectric property studies

4.7.1 CaCPH crystals

The variation of dielectric constant with the frequency of the applied field at room temperature is shown in Figure 4.19 (a). It is observed that, at lower range of frequencies dielectric constant decreases drastically, becoming a constant at higher frequencies. Naturally dielectric behaviour of a material can be explained on the basis of four mechanisms of electric polarization, which are electronic, ionic, orientational and space charge polarization. At moderate electric field (low frequency) for materials with a very low conductivity, these mechanisms of polarization contribute to the dielectric constant. The further increase in the frequency of the applied field the contributions from different polarization starts reducing [43]. The high value of dielectric constant at low frequencies is attributed to space charge and dipolar polarization [44, 45]. In CaCPH crystal, the dielectric constant is found drastically decreased with increasing frequency (800 Hz - 20 KHz) and becoming a constant at MHz range of frequencies. The value of dielectric constant at high frequency is 1.35.

The dielectric loss studied as a function of frequency at room temperature is shown in Figure 4.19 (b). The dielectric loss is strongly dependent on the frequency of the applied field, similar to that of the dielectric constant. The dielectric loss

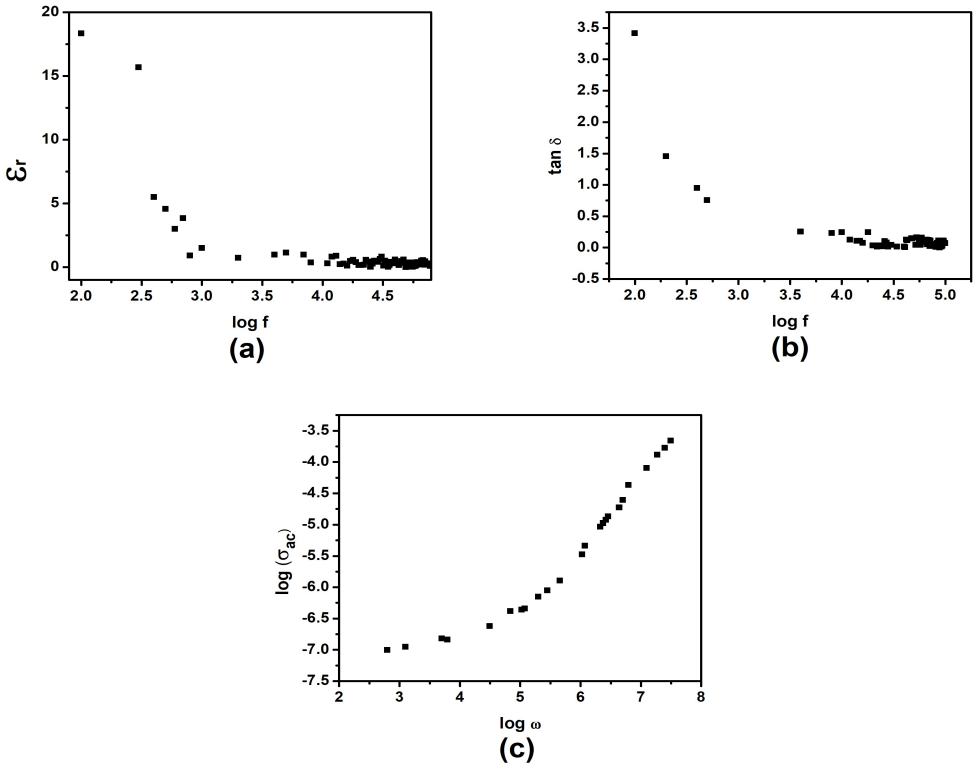

Figure 4.19: (a) Variation of ε_r with frequency (b) Variation of dielectric loss with frequency (c) Variation of ac conductivity with frequency of CaCPH crystal.

decreases with an increase in frequency, but appears to achieve saturation in the higher frequency and above room temperature. In the low frequency region (800 Hz - 20 KHz), high energy loss is observed, which may be due to the dielectric polarization, space-charge and rotation-direction polarization [46]. The characteristic of low dielectric loss at high frequency of the sample suggests that the crystal possesses an enhanced optical quality with lesser defects and this parameter plays a vital role in the construction of devices from nonlinear optical materials. It is also observed that the ac conductivity (Figure 4.19 (c)) also increases with increasing frequency as reported in previous chapter.

4.7.2 CuCDH crystals

The variation of dielectric constant with the frequency of the applied field at room temperature is shown in Figure 4.20 (a) It is observed that the dielectric constant

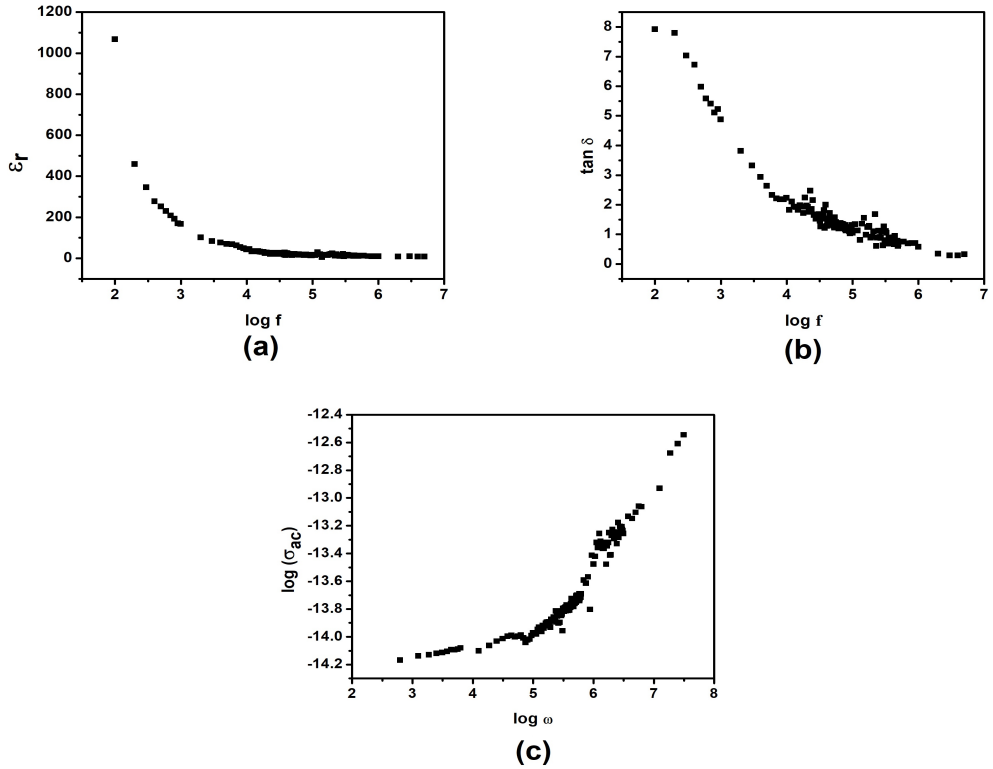

Figure 4.20: (a) Variation of ε_r with frequency (b) Variation of dielectric loss with frequency (c) Variation of ac conductivity with frequency of CuCDH crystal.

decreases with increasing frequency for CuCDH crystal. The value of dielectric constant decreases drastically at lower range of frequencies (100 Hz - 2 KHz), and then decreases gradually (2 KHz - 400 KHz) and become constant at 5 MHz, value of dielectric constant at 5 MHz is 9.620. It is a normal dielectric behaviour and can be explained on the basis of various polarization mechanisms such as electronic, ionic, orientational and space charge polarization. At the moderate electric field for materials with low conductivity these mechanisms of polarization contribute to the dielectric constant. The further increase in the frequency of the applied field the contributions from different polarization starts reducing.

Figures 4.20 (b) and (c) show the variation of dielectric loss and ac conductivity with frequency. This is also similar to observed results of adipate crystals as described in the previous chapter.

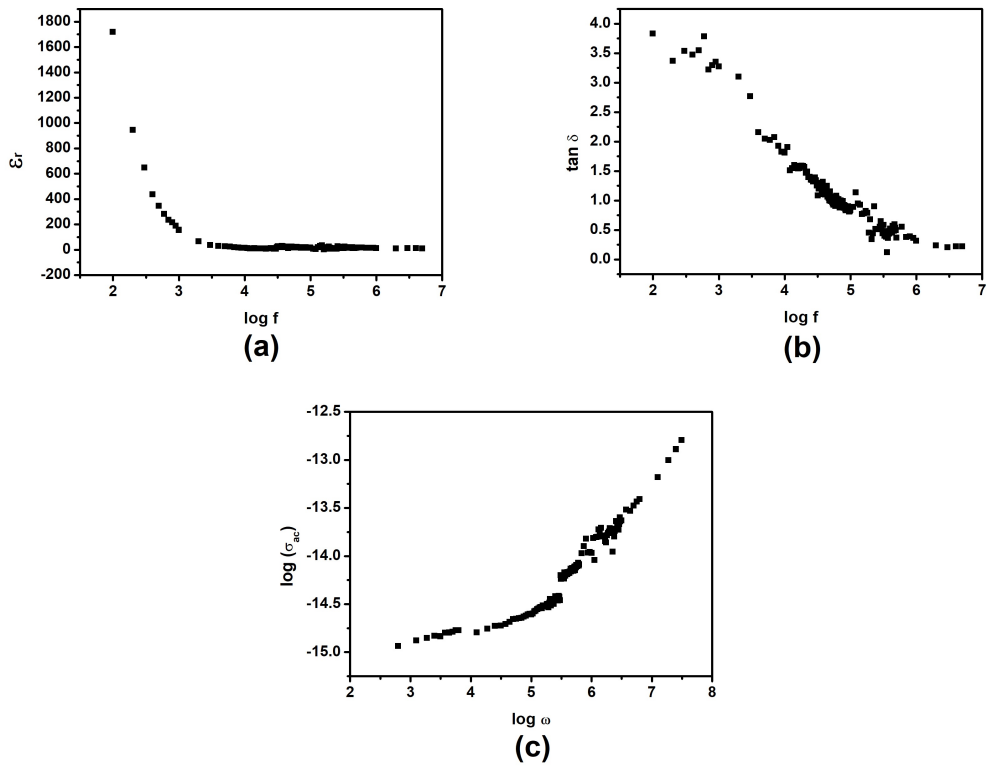

Figure 4.21: (a) Variation of ε_r with frequency (b) Variation of dielectric loss with frequency (c) Variation of ac conductivity with frequency of CdCHH crystal.

4.7.3 CdCHH crystals

In the case of CdCHH crystal the value of the dielectric constant is higher at lower frequencies, and this is attributed to space charge polarization. Also at a lower range of frequencies (100 Hz - 30 KHz) the dielectric constant decreases drastically from 1717 to 70 and becomes a constant at larger frequencies (30 KHz - 5 MHz), value of dielectric constant is 9.57 (Figure 4.21 (a)). Due to the effect of the electronic exchange of the number of ions in the crystal, local displacement of electrons occurs, resulting in polarization. As frequency increases, this electron exchange cannot follow the electric field and the polarization becomes independent of frequency.

The ac conductivity is found to be increasing with frequency and the loss tangent is decreases with frequency as shown in Figure 4.21 (b) and (c).

4.8 Conclusions

Growth of citrate crystals of calcium, copper and cadmium were achieved by single gel diffusion technique. Structure and properties of crystals were studied by different characterization methods. Growth of CaCPH crystals was accomplished by allowing diffusion of calcium chloride solution through silica gel impregnated with citric acid in the single gel tube system. X- ray diffraction revealed that the crystal belongs to the triclinic system with space group P-1(2). The IR spectra showed all the important peaks as is expected of citrate compounds associated with water of hydration. The thermo gravimetric analysis suggested that the grown CaCPH crystal is associated with five molecules of water of hydration. The results of thermal analysis proved that the gel grown CaCPH is thermally unstable even at low energies. Decomposition started at about 103 °C. CaCPH decomposed to calcium oxide through calcium oxalate and basic carbonate. Comparison of TG and DSC curves suggested that the transformations are associated with mass changes and there is a known physical (crystallographic) transformation independent of mass change. The stoichiometric composition of the crystals was established to be $Ca_3(C_5H_6O_7)_2$ $5H_2O$. From DRS spectrum cutoff wavelength and optical band gap of the material were found to be 216 nm and 5.33 eV respectively. The dielectric constant of CaCPH decreased gradually from 18.33 to 1.35 with increasing frequency of the applied ac field. Dependence of σ_{ac} on frequency suggests that the conduction phenomenon is ac type which could be due to the hopping of charge carriers.

Copper citrate crystals were grown and characterized by XRD, FTIR, Micro Raman, TG-DTA, DSC, UV-DRS and dielectric property studies. Controlled reaction of copper chloride with citric acid through silica gel medium leads to formation of CuCDH as spherulitic morphology. The optimum conditions for the growth of good quality crystals were determined. X- ray diffraction reveals that the crystal belongs to the monoclinic system with space groups I4/m(87) for CuCDH crystal. The IR spectrum shows all the important peaks as is expected of citrate compounds associated with water of hydration. The results of thermal analysis suggest that the gel grown CuCDH crystals starts decomposing at 51 ^{0}C and form cop-

per carbonate. The stoichiometric composition of the crystal is established to be $Cu_3(C_6H_5O_7)_2.2H_2O$. FTIR and Raman results also support the findings of thermal studies. The optical band gap (Eg) of CuCDH crystals is determined from optical absorption studies is found to be 2.78 eV. The dielectric constant of grown crystal decreases gradually with increasing frequency of the applied ac field and the value of dielectric constant at high frequency is 9.62. The dielectric loss decreases slowly with increasing frequency of the applied ac field.

Controlled reaction of cadmium nitrate with citric acid through silica gel medium leads to formation of three dimensional layered framework of CdCHH as single crystals. The crystals are well faceted and have a definite morphology. The optimum conditions for the growth of single crystals of CdCHH are determined. X- ray diffraction reveals that the crystal belongs to monoclinic system with the cell parameters as a = 12.552 Å, b = 10.266 Å, c = 18.006 Å and $\alpha = 90.00^o, \beta = 109.02^o, \gamma = 90.00^o$, space group P21/n and with volume 2193 $Å^3$. The IR spectra shows all the important peaks as is expected of citrate compounds associated with water of hydration. The results of thermal analysis suggest that the gel grown CdCHH is thermally unstable even at low energies. Decomposition starts at about 67 ^oC. CdCHH decomposes to cadmium oxide through cadmium oxalate and basic carbonate. The stoichiometric composition of the crystals is established to be $Cd_3(C_6H_5O_7)_2\ 6H_2O$. FTIR and Raman results also support the findings of thermal studies. The optical band gap (Eg) of CdCHH crystals is determined from the diffuse reflectance studies is found to be 5.152 eV. Less absorption in the entire visible range with a wide band gap projects these crystals as a potential candidate for optoelectronics applications. The value of dielectric constant of CdCHH decreases gradually from 1717 to 9.57 with increasing frequency of the applied ac field, also the dielectric loss decreases slowly with increasing frequency of the applied ac field. The characteristic of low dielectric loss with high frequency is indicative of CdCHH having enhanced optical quality with lesser defects which is vital for the construction of devices from non-linear optical materials.

References

[1] Robert R. Crichton, Biomineralization, Biological inorganic chemistry, 2nd edition (2012).

[2] Jiang Hu, Peter X.Ma, Biomineralization and bone regeneration, Principles of regenerative Medicine, 2nd edition (2011).

[3] Jinhui Tao, Research methods in Biomineralization Science, Methods in Enzymology, (2013).

[4] Salgaonkar M, Nadar SS, Rathod VK, Journal of Environmental Chemical Engineering (2019), https://doi.org/10.1016/j.jece.2019.102969.

[5] M. Tavakkoli-Gilavan, H. Abdizadeh, M. Reza Golobostanfard, Applied Surface Science Biomineralization (2018), doi: https://doi.org/10.1016/j.apsusc.2018.07.168.

[6] Boskey, Adele L., Villarreal-Ramirez, Eduardo, Matrix Biology, (2016), doi: 10.1016/j.matbio.2016.01.007.

[7] Mark G. Papich, Calcium Citrate, Saunders Handbook of Veterinary Drugs (Fourth Edition), (2016) 101-102.

[8] Araya M, Pizarro F, Olivares M, Arredondo M, Gonzalez M et al. Biol Res **39** (2006) 183-187.

[9] Edward D Harris and Susan S Percival, Adv Exp Med Biol. **258** (1989) 95-102

[10] Mitsuo Kakei, Toshiro Sakae and Masayoshi YoshikaWA, Proc. Jpn. Acad., Ser. B **85** (2009).

[11] E C Foulkes, Toxicology Lettere **53** (1990) 29-31.

[12] S.L.di. Toppi and R. Gabbriels, Environmental and Experimental Botany, **41** (1999) 105-130.

[13] Robin A. Bernhoft, The Scientific World Journal Volume (2013) doi: http://dx.doi.org/10.1155/2013/394652.

[14] M. Dakanali, E. T. Kefalas, C. P. Raptopoulou, A. Terzis, T. Mavromoustakos, and A. Salifoglou, Inorg. Chem. **42** (2003) 2531-2537.

[15] Jean-Francois Boily and Jeremy B. Fein , Geochimica et Cosmochimica Acta, **60** (1996) 2929-2938.

[16] M.P. Binitha, P.P. Pradyumnan, Growth, Bull. Mater. Sci. **37** (2014) 491–495.

[17] H.K. Henisch, Crystal Growth in Gels, Pennsyllvania state University Press, University Park, PA, (1973).

[18] A.M. Ezhil Raj, D.D. Jayanthi, V.B. Jothy, M. Jayachandran, C. Sanjeeviraja, Cryst. Res. Technol **43** (2008) 1307.

[19] Sushma Bhat, P.N. Kotru, Mater. Sci. Eng., **23** (1994) 73.

[20] R. Roop Kumar, G. Raman, F.D. Gnanam, J. Mater. Sci. **24** (1989) 124535.

[21] Donald Mastropaolo, D.A. Powers, J.A. Potena, and H.J Schcgar. Inorganic Chemistry, **15**(6) (1976) 1445 .

[22] Yu-Mei Daia,b,c, Jian-Kai Chenga, Jian Zhanga, En Tangb, Zhao-Ji Lia, Yi-Hang Wena, Yuan-Gen Yao, Journal of Molecular Structure **740** (2005) 223–227.

[23] E. T. Kefalas, M. Dakanali, P. Panagiotidis, C. P. Raptopoulou,§ A. Terzis, T. Mavromoustakos, I. Kyrikou, N. Karligiano, A. Bino, and A. Salifoglou, Inorg. Chem. **44** (2005) 4818.

[24] Guoqi Zhang, Guoqiang Yang, and Jin Shi Ma, Cryst Growth Des. **6** (2006) 375.

[25] Jean-Joseph Max and Camille Chapados, Phys. Chem. **108** (2004) 3324-3337.

[26] B.R.Lakshmanan, J.Ind.Inst. of Sci. (1956).

[27] S. M. Tsimbler, L. L. Shevchenko and V. V. Grigor'eva; Journal of Applied Spectroscopy; **11** (1969) 1096–1101.

[28] C. Djordjevic, M. Lee, Sinn E. Oxoperoxo(citrato)- and Dioxo(citrato)vanadates(V): Inorg. Chem. **28** (1989) 719-723.

[29] D. F. Coker, J. R. Reimers and R. O. Watts, Aust. J. Phys., **35** (1982) 623-38.

[30] John Coates, Interpretation of Infrared Spectra, A Practical Approach, Encyclopedia of Analytical Chemistry R.A. Meyers (Ed.) John Wiley Sons Ltd.

[31] Zh Nockolov, G Georgiev, D Stoilova, I Ivanov, J. Mol. Struct., **354** (1995) 119.

[32] D Valarmathi, Leela Abraham S Gunasekaran, Indian Journal of Pure Applied Physics **48** (2010) 36-38.

[33] T. S. Krishnan, Raman spectrum of crystalline sodium citrate, (1953).

[34] Quantitative determinant of citric acid in seminal plasma by using raman spectroscopy **67** (2017) 757-60.

[35] Gabbott, P.. Principles and applications of thermal analysis. (Ed.),UK, John Wiley Sons (2008).

[36] Menczel, J. D., Prime, R. B. Thermal analysis of polymers: fundamentals and applications. (Eds.). UK, John Wiley Sons (2014).

[37] Vaimakis, Tiverios C. "Thermogravimetry (TG) or Thermogravimetric Analysis (TGA).

[38] Eberhardt Herdtweck, Tobias Kornprobst, Roland Sieber, Leo Straver, and Johann Plank, Z. Anorg. Allg. Chem. **637** (2011) 655–659.

[39] Guoqi Zhang, Guoqiang Yang, and Jin Shi Ma, Crystal growth Design, **6** (2006) 375-381.

[40] Want B, Ahamed F, Kotru PN , J Mater Sci. **42** (2007) 9324-30.

[41] Rahimkutty MH, Babu KR, Pillai KS, Sudarsana Kumar MR, Nair CMK, Bull MaterSci. **24** (2011) 249-52.

[42] Oscar E. Pecho, Razvan Ghinea, Ana M. lonescu, Juan C.Cardona, Alvaro Della Bona, Maria del Mar Perez, **31** (2015) 60-67.

[43] Sagadevan Suresh, Optik **125** (2014) 1223– 1226.

[44] M.P. Binitha, P.P. Pradyumnan, J. Therm. Anal. Calorim. **114** (2013) 665.

[45] Soosen Samuel, JijiKoshy, AnoopChandran, K.C. George Current Applied Physics. **11** (2011) 1094.

[46] Firdous A, Quasim I, Ahmad M and Kotru P N, Bull.Mater. Sci. **33** (2010) 377.

Chapter 5

Growth and Characterization of Copper Ascorbate Dihydrate Crystals

5.1 Introduction

Biomineralization involves the controlled deposition and regulated growth of material in biological systems. It occurs throughout nature, producing bioinorganic and organic solids. The research interest is to understand the mechanisms of formation and dissolution of biological crystal. A number of previous studies have partly shown the hierarchical structures and the related organic macromolecules in biominerals. However, in the present technology, the biomineral replicas cannot be synthesized. Gels commonly promote the growth of high-quality crystals of small molecules. In the last few decades, the crystallization of biological macromolecules were tested with different types of gels - agarose, silica or polyacrylamide. Although these gels possess many advantages in the crystal production over the other growth technique for the crystal handling, they have been rarely used. Gels are semi solid in nature and rich in liquids and porosity. When gel is introduced in the crystallization medium, the convection is reduced and the molecule transport towards the crystal

is more regular and operates in a diffusive mode. It is clear that the understanding and mimicking of the processes involved in biomineralization may provide new approaches to the growth of particular organic-inorganic hybrid materials. Crystals of copper and its derivatives are playing major role in inorganic as well as organic materials [1-8].

The outstanding chemical property of ascorbic acid is that it is a good reducing agent that may reduce ferric or cupric ions to ferrous or cuprous forms [9]. Larger consumption of ascorbic acid contained food or medicine can cause for the excess growth of metallic crystals in organs. The higher amount of cations like copper and ascorbate anion may lead to the formation of copper ascorbate dihydrate (CADH) crystals in animal or human organisms. These may reduce the presence of copper like elements in the biological systems [10, 11]. Mineral ascorbates are a group of salts of ascorbic acid. They are composed of a mineral cation and ascorbate anion. These are highly reactive oxidants and used as dietary supplements and food additives [12]. Therefore the structure and property study of copper ascorbate crystal are becoming important. To study the behavior of crystallization and shape of this crystal we chose hydro silica gel as a medium for the growth. Since hydrosilica gel is a medium which mimics the secretions in the organs in animals and plants, we utilized this medium for the growth of ascorbate crystals. In this study, we report the growth of CADH crystal in the hydro silica gel medium for the first time. To date no information exist on structurally characterized copper ascorbate dihydrate crystal grown by controlled diffusion of cation with ascorbate anion. The detailed characterizations of grown crystals were studied by using different advanced experimental methods like powder and single crystal X-ray diffraction (XRD), Fourier Transform Infra-red (FTIR), micro Raman, Thermo Gravimetric Analysis (TGA), Differential Thermo Gravimetric (DTG), Differential Scanning Calorimetry (DSC), UV-visible and ac conductivity .

5.2 Crystallization mechanism of CADH crystal

Single crystals of CADH were grown in hydro silica gel medium by the controlled chemical reaction method [13-15]. The pure sodium metasilicate powder was dissolved in double distilled water and the solution was filtered out. After making this solution at a particular specific gravity, the gel was set by acidification of sodium metasilicate solutions by ascorbic acid as one of the reactants, so that the pH of the solution was brought to the desired value. This mixture was taken in test tubes and kept for gelation. After proper setting and aging of the gel, it is ready for accepting cations. Then, copper chloride solution, acting as an upper reactant, was poured over the gel without disturbing the gel surface. The well-developed greenish blue coloured pyramidal shaped crystals with reasonable dimensions were appeared inside the gel within a period of one week.

To observe the changes in crystallization, the experiment was performed by changing the growth parameters such as concentration of ascorbic acid and copper chloride between 0.25 - 1 M, pH of the gel from 4 to 7 and the specific gravity of the gel between 1.02 and 1.06. It is observed that the gelation time is highly dependent on the initial pH of the gel, the gelation time found is higher for lower pH values. The polymerization reaction was slow at low pH values, and the gel with initial pH value 4 took nearly 1 week for proper setting, whereas, the gel with pH above 5 found set within a day. The optimum pH yielding maximal crystal size was found to be equal to 6. Multiple and twinned growth was observed at higher concentration of the copper chloride and the number of crystals was reduced at lower reactant concentrations [16].

The following chemical reaction was expected to take place for the formation of the title compound.

$$CuCl_2\ H_2O + (C_6H_8O_6) + H_2O \rightarrow Cu(C_6H_6O_6)\ 2H_2O + 2HCl$$

We have taken applicable measures to fix the growth depending parameters. CADH crystals were grown at various gel specific gravities of 1.02, 1.03, 1.04 and

Figure 5.1: Growth of CADH crystals with specific gravities 1.02, 1.03, 1.04 and 1.05

1.05 (Figure 5.1). The pH of the gel medium was adjusted to 7 by using 1-Molar (M) ascorbic acid. It took about 24 h for gel setting and 1 M copper chloride solution was added above the gel as upper reactant. After a week period, small pyramidal shaped crystals were formed inside the gel of specific gravity of 1.03. Similar observations were found in other samples with specific gravities of 1.02, 1.04 and 1.05 within a period of two weeks. But the samples with 1.04 and 1.05 yielded relatively small crystals. After three weeks, we were noticed an apparent color change in gel media and Figure 5.1 depicts these color changes. The results can be interpreted in terms of gel specific gravities. If specific gravity of gel is above the optimal value (1.03), the presence of ascorbic acid per unit volume decreases and it results in decreased number of crystals inside the gel [17]. The higher specific gravities of the gel also cause a decrease in pore size which enable lower sized crystals [18].

The best transparent single crystals of CADH have maximum size of $2\times2\times0.5$ mm^3. The molecular structure of copper ascorbate, growth setup and grown crystals are shown in Figure 5.2. The optimum conditions for the growth of good quality crystals are given in Table 5.1.

5.3 Structure determination and description

From single crystal XRD studies, it is found that the structure of the grown crystal is cubic. The phase purity of the samples is controlled by powder XRD analysis. The

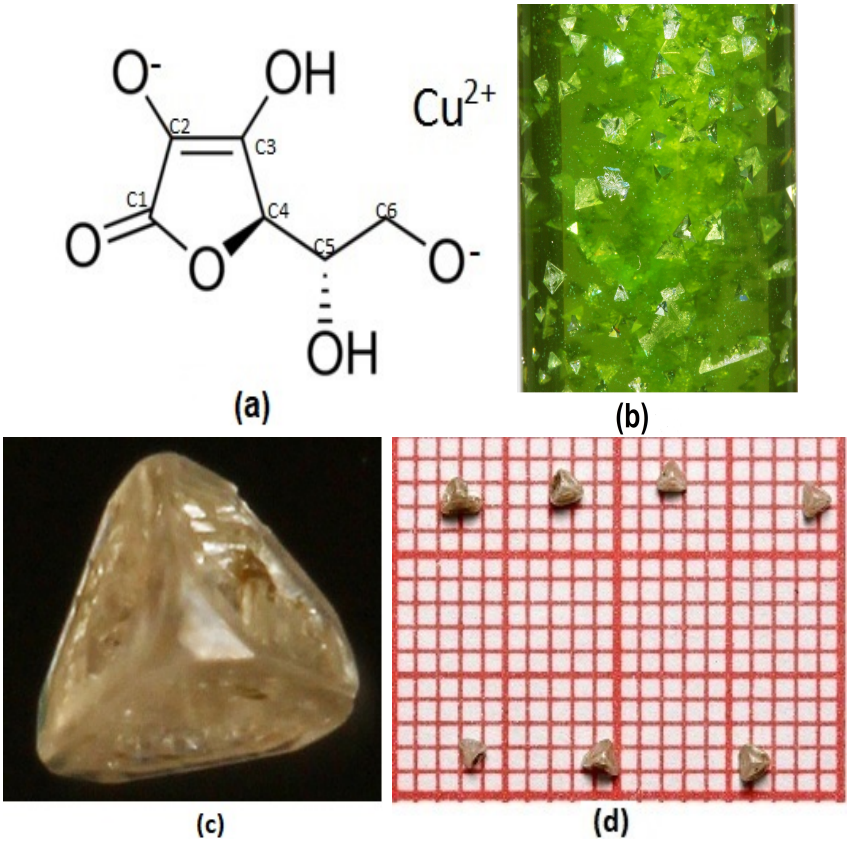

Figure 5.2: (a) Molecular structure of a single unit of copper ascobate (b) Crystals in the growth apparatus (c) Harvested single crystal (d) Crystal placed on graph sheet.

measured cell parameters are a = b = c = 5.412 Å, $\alpha = \beta = \gamma = 90^0$. ORTEP Image and 3D packing of the grown crystal are shown in Figures 5.3 and 5.4 respectively. The crystal data and structure refinement parameters are presented in Table 5.2. The atomic coordinates and equivalent thermal parameters for all the non-hydrogen atoms are given in Table 5.3.

Table 5.1: Optimum conditions for the growth of CADH crystal

Parameters	Value
Gel density	1.03
pH	7
Gel set time	1 day
Growth period	28 days
Concentration of ascorbic acid	1 M
Concentration of $CuCl_2$	1 M

Table 5.2: Crystal data and structure refinement for CADH crystal

Parameter	CADH crystal
Identification code	Shelxl
Emperical formula	Cu
Formula weight	285.07
Temperature	273(2) K
Wavelength	0.71073 Å
Crystal system, Space group	Cubic, Fd-3m
Unitcell dimensions	a = b = c = 5.412 Å
	$\alpha = \beta = \gamma = 90^0$
Volume	158.47(18) $Å^3$
Z, Calculated density	1, 2.511 Mg/m^3
Absorption coefficient	3.438 mm^{-1}
F(000)	121
Theta range for data collection	6.53 to 24.54 deg
Limiting Indices	-6$\leq h \leq 6, -6 \leq h \leq 6, -6 \leq h \leq 6,$

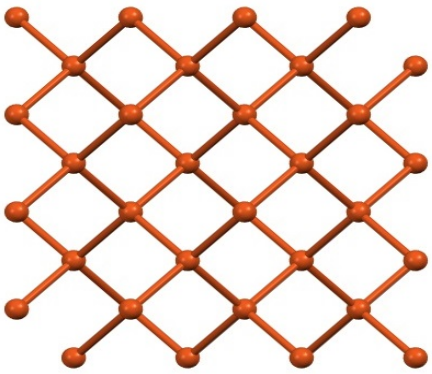

Figure 5.3: ORTEP of the grown CADH crystal.

Table 5.3: Atomic coordinates (Å$\times 10^{-4}$) and equivalent isotropic displacement parameters (Å$^2 \times 10^3$)for grown crystals

Atoms	X	Y	Z	U(eq)
Cu	0.625	0.625	0.623	0.036(10)

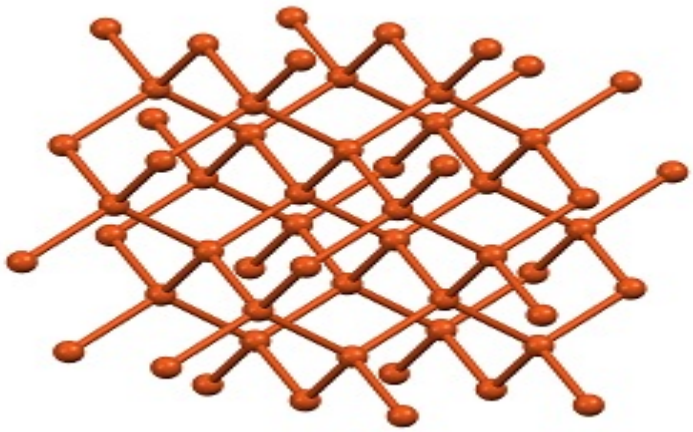

Figure 5.4: 3D packing of the grown CADH crystal.

The degree of crystallinity and phase identification of the grown crystal was determined by comparing its powder diffraction pattern with the ones for CADH. The calculated powder XRD pattern obtained from the single-crystal study were also included (Figure 5.5). The presence of characteristic reflections in the diffraction pattern of the CADH crystal reveals the newness of its crystalline phase. Even though the result obtained from single crystal XRD as copper crystal, the powder patterns obtained was observed to be different from the pattern of reported copper crystal [19]. In addition, the experimental and the calculated diffraction patterns are in agreement, thus confirming the novelty and the phase purity of the grown ascorbate crystal. Since the ICDD/JCPDS data of grown ascorbate crystal is not available, the structural data obtained from powder XRD are given in Table 5.4.

Single crystal XRD studies of the grown crystal reveals that the material obtained was metallic copper which contradicts all the other characterizations including powder XRD results. So the reason for the data obtained from single crystal XRD maybe the resultant of the continuous impingement of high energy X-ray photons with the smaller sized single crystal fixed at the goneometer head of the single

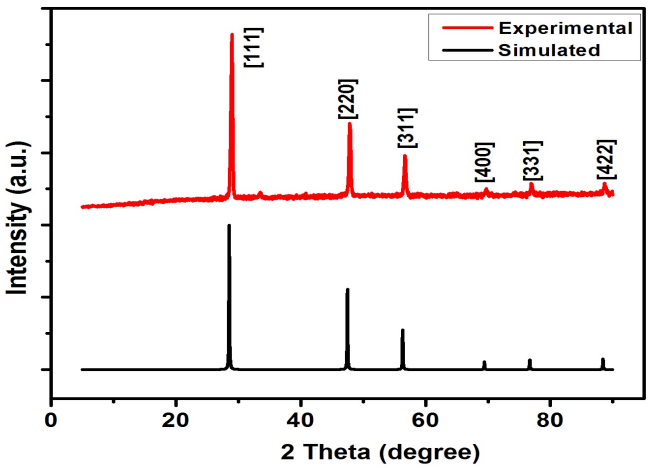

Figure 5.5: Powder XRD pattern of CADH crystal.

Table 5.4: Powder XRD data of CADH crystals

2Θ (degree)	D (Å)	FWHM(degree)	I/I_0
28.689	3.1092	0.1468	100
33.237	2.6934	0.152	2.21
47.601	1.90877	0.168	30.01
56.452	1.62871	0.169	14.08
69.453	1.35221	0.133	2.49
76.750	1.2408	0.154	3.36
88.462	1.10428	0.186	3.48

crystal XRD equipment. For getting more reflections may lead for the dissociation of copper ascorbate to copper metal [20]. It is observed that the initial simulated powder data matched with the obtained powder XRD data.

5.4 FTIR and micro Raman studies

5.4.1 FTIR studies

The FTIR spectrum of $Cu(C_6H_6O_6)\ 2H_2O$ crystals grown in silica gel is shown in Figure 5.6. The infrared spectrum in the range of 400-4000 cm^{-1} gives the different bands corresponding to ascorbate anion.

Since there is a ring closure in the structure of CADH between C2(OH) and

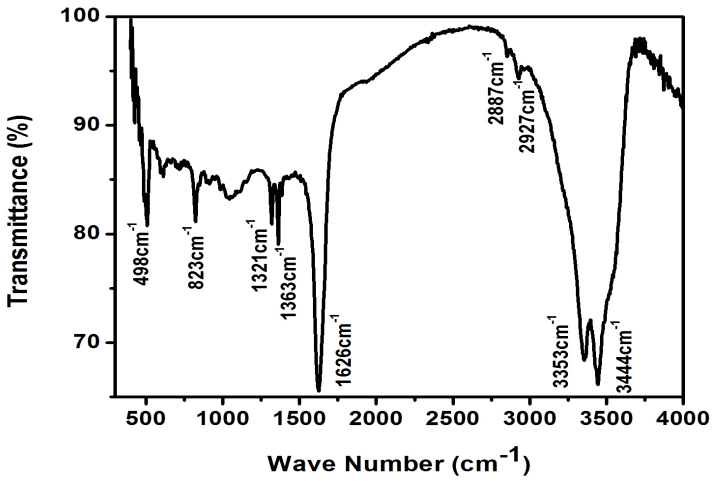

Figure 5.6: FTIR spectrum of CADH crystals.

C3(OH) resulting in a disappearance of the O-Hs at carbon 2 and 3 in the spectrum. The two remaining bands in CADH were assigned to C(5)-OH (3353 cm^{-1}) and C(6)-OH (3444 cm^{-1}). During the formation of CADH, the C=C (1675 cm^{-1}) band of ascorbic acid host is shifted towards 1626 cm^{-1}. The shift to lower frequency of the C=C stretching band suggests a reduction of the double bond character of C(2)=C(3). This result qualifies the reports for sodium ascorbate elsewhere [20]. It is also observed that the absorption band of C=O is at 2887 cm^{-1}. The absorption bands at 2927 cm^{-1} and 1362 cm^{-1} represent the strong stretching and bending vibrations of -CH_2 group, respectively. The C-C ring stretching is observed at 823 cm^{-1}.

5.4.2 Micro Raman studies

Micro Raman spectrum of the crystal is given in the Figure 5.7. Spectrum exhibit a peak at 1619 cm^{-1} which are assigned to symmetric stretching vibrations of C=C bond. Medium bands at 687 cm^{-1} correspond to bending of O-C-O groups, and a band at 514 cm^{-1} is ascribed to the wagging mode of water. Weak band at 406 cm^{-1} is due to rocking vibrations of O-C-O bonds. Larger mass of the metal give Raman line at a very low stretching frequency of 214 cm^{-1} and 114 cm^{-1} corresponding to CuO stretching [21].

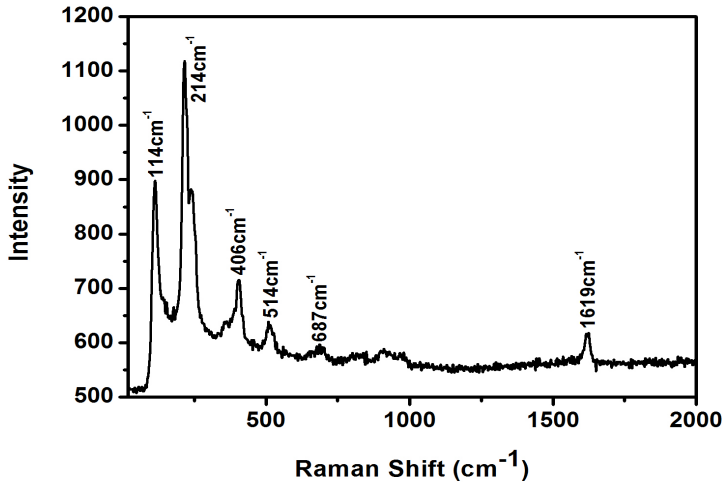

Figure 5.7: Micro Raman spectrum of CADH crystals.

The proposed assignments obtained from both spectroscopic studies are presented in Table 5.5. From the spectroscopic studies, it may be concluded that some of the observed vibrations in both Raman and IR are active so the CADH crystal is non-centre of symmetric in nature. The functional groups present in the crystal are exactly the same as in the ascorbate ligand and also confirm the presence of water of crystallization. The aforementioned spectral assignments for ascorbate complexes are in agreement with results reported in the literature [22].

5.5 Thermal decomposition studies

Thermo analytical studies play significant role in the development and characterization of different materials [23-28]. The TG-DTA curves of CADH crystals in the temperature range 30 to 700 ^{0}C are shown in Figure 5.8 (a), whereas the DSC curve recorded in the temperature range 50 to 400 ^{0}C is shown in Figure 5.8 (b). The TG curve gives information regarding the thermal stability and composition of the sample under investigation. The recorded curve is first analyzed for obtaining the percentage mass loss at different temperatures and hence the thermal stability and dissociation of the compound. The TG curve exhibits mass losses in three stages which indicate that the decomposition takes place continuously. The first stage of

Table 5.5: FTIR and micro Raman band assignment of CADH crystal

FTIR band (cm^{-1})	Micro-Raman band(cm^{-1})	Assignment
3444	-	ν(OH)
3353	-	ν(OH)
2927	-	ν_{as}(C-H)
2887	-	ν_s(C-H)
1626	1619	ν_s(C=C)
1362	-	ν_{as}(O-C)
1315	-	ν_s(O-C)
823	-	ν_s(C-C)
-	687	δ(OCO)
595	514	$\rho_\omega(H_2O)$
498	406	ρ_r(OCO)
-	240	ν(Cu-O)
-	214	ν(Cu-O)
-	114	ν(Cu-O)

decomposition is due to partial dehydration of the crystal which starts at 67 ^{0}C and ends at 107 ^{0}C. This is due to the loss of one water molecule and two hydrogen ions present in the crystal, causing an effective mass loss of 8.7%. The second decomposition stage starts at 236 - 256 ^{0}C and the loss of other water molecule occurs during this stage. This mass loss is attributed to the complete dehydration of the sample by eliminating the remaining one water molecule from the structure of the compound. The third stage of decomposition is in between 297 ^{0}C and 322 ^{0}C which corresponds to the elimination of one oxygen, 2C and 4H from the anhydrous copper ascorbate. The last stage of decomposition is in between 401 ^{0}C and 566 ^{0}C which correspond to the elimination of remaining four CO molecules resulting the new phase CuO. The calculated and observed mass loss values are tallied with proposed molecular formula. The thermal decomposition at all the stages and the corresponding mass loss is given in Table 5.6 below. The thermal decomposition at all the stages can be depicted as

$Cu(C_6H_6O_6)\ 2H_2O$ - $(H_2O + 2H)$ - (H_2O) - $(O + 2C + 4H)$ - $4CO \longrightarrow CuO$

DSC monitors heat effects associated with phase transitions or chemical reactions as a function of temperature [29]. The DSC analysis of the grown crystals was performed with a heat flow from 50 ^{0}C to 400 ^{0}C at the rate of 10 ^{0}C/minute. The

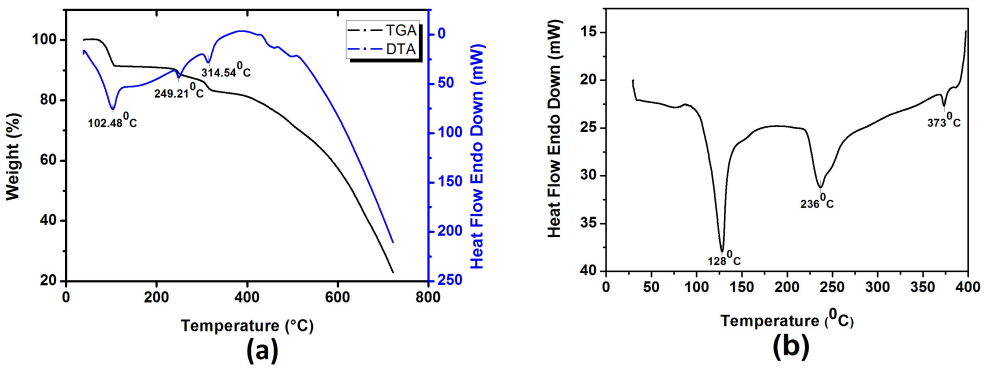

Figure 5.8: (a) TG-DTA curves of CADH crystal (b) DSC thermogram of CADH crystal.

Table 5.6: The results of the decomposition process of $Cu(C_6H_6O_6)\ 2H_2O$

steps	Temperature range/^0C	Observed mass loss/%	Calculated mass loss /%	Loss of molecules in the step	Corresponding peak in DTG/^{0}C
I	76-107	8.72	7.31	1H2O+2H	102
II	236-256	11.77	13.16	1H2O	249
III	297-321	16.89	16.09	1O+2C+4H	314
III	401-566	36.65	36.55	4CO	-

thermogram of the grown crystals shows three endothermic peaks (Figure 5.8 (b)). The first peak observed at 128 ^{0}C, is accounted for the dehydration step of the sample and the complete dehydration occurs at 236 ^{0}C. The peak at 373 ^{0}C is due to the reduction of anhydrous copper ascorbate to copper oxide, as observed in TG results. The DTA portion of the thermal curve is consistent with the description of DSC results.

5.6 Optical property studies

Optical absorption measurement of the powdered sample of CADH was carried out in the range of 200 - 900 nm at room temperature and the spectrum is shown in Figure 5.9 (a). The CADH crystals are transparent in the range 380 - 550 nm so the absorption is less. The band gap of the material is calculated using Kubelka Munk function, the Figure 5.9 (b) shows the plot of $[(k/s)h\nu]^2$ versus $h\nu$, where (k/s) is the absorption coefficient. The optical band gap of the material was determined by

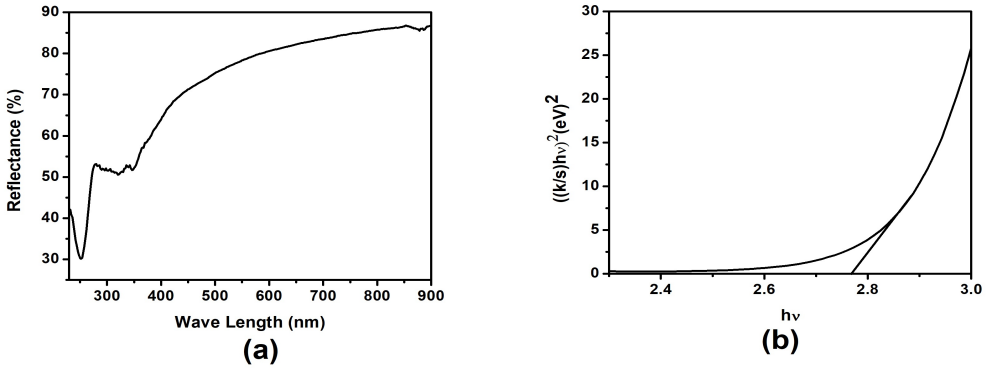

Figure 5.9: (a) Diffuse reflectance spectrum of CADH (b) Plot of $[(k/s)h\nu]^2$ versus $h\nu$ for CADH crystals.

extrapolating the linear portion of the plot [30] and the calculated band gap is 2.76 eV.

5.7 Dielectric property studies

The variations of dielectric constant, ac conductivity and dielectric loss with the applied field frequency at room temperature are shown in Figure 5.10 (a), (b) and (c) respectively. In Figure 5.10 (a), it is observed that the dielectric constant decreases drastically from 6781 to 818 with increase in frequency from 100 Hz to 3 KHz and becoming a constant at higher frequencies(mega hertz range). The value of dielectric constant at higher frequency is 27.21. Frequency dependence of a dielectric material is due to the different polarization mechanisms in the presence of electric field. The theory of polarisation mechanism in the CADH crystal is similar to that of the crystals discussed in the previous chapter.

The variation of $\sigma_{ac}(\omega)$ as a function of frequency (1×10^3 - 5×10^6 Hz) at room temperature is shown in Figure 5.10 (c) for CADH crystals. It is seen that $\sigma_{ac}(\omega)$ remains almost constant at low frequency and, after a certain characteristic crossover frequency, ω_0, it increases with power law fashion. Similar behaviour was observed in many organic materials in bulk and thin film forms [31-33].

Dielectric absorption in a material is characterised by dielectric loss and loss tangent ($\tan\delta$) values [34-36]. The variation of dielectric loss with frequency is shown

in Figure 5.10 (b). It is clear that dielectric loss decreases with increasing frequency. At low frequencies, the dipoles can easily switch alignment with the changing field. As the frequency increases, the dipoles are less able to rotate and maintain phase with the applied field, and, thus, they reduce their contribution to the polarization field [37]. When polarization lags behind the applied field, causing an interaction between the field and the dielectrics polarization that results in heating.

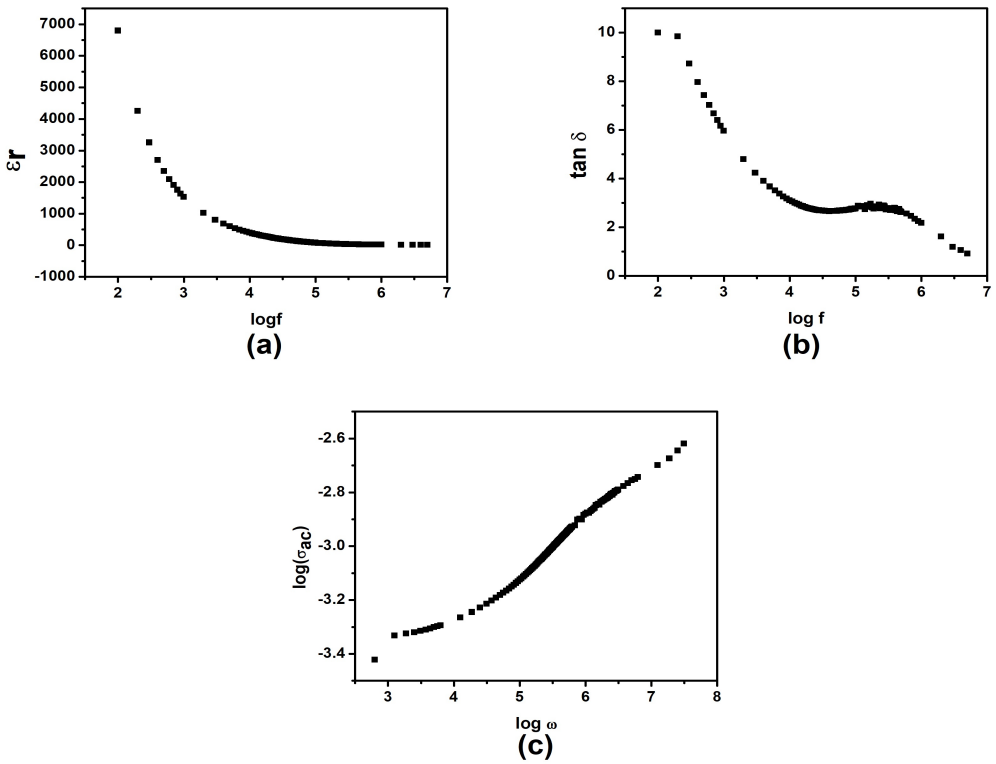

Figure 5.10: ((a) Variation of ε_r with frequency (b) Variation of dielectric loss with frequency (c) Variation of ac conductivity with frequency of CADH crystal.

5.8 Conclusions

CADH single crystals have been grown by copper ion diffusion through hydro silica gel medium impregnated with ascorbic acid anion. The well faceted triangular pyramidal shaped crystals having an average size of $2\times2\times2$ mm^3 were harvested. X- ray diffraction reveals that the structure of the grown crystal as cubic copper with single

crystalline phase. The IR spectra show all the representative peaks expected for ascorbate compounds associated with hydration. . The results of thermal analysis suggest that the gel grown CADH is thermally unstable even at low temperatures. The decomposition starts at 67 ^{0}C and material undergoes four-stage decomposition process and the end product is copper oxide. Comparison of TG and DSC curves suggests that the transformations are associated with mass changes and there is a known physical (crystallographic) transformation independent of mass change. The stoichiometric composition of the grown crystals is confirmed to be $Cu(C_6H_6O_6)$ $2H_2O$. FTIR and Raman results also support the findings of thermal studies. The optical band gap (E_g) of CADH crystals, as determined from optical absorption studies, is found to be 2.76 eV. The dielectric constant of CADH decreases gradually with increasing frequency of the applied ac field. The ac conductivity increases with frequency and dielectric loss decreases slowly with increasing frequency of the applied ac field. The characteristic of low dielectric loss with high frequency is indicative of CADH having enhanced optical quality with lesser defects which is vital for the construction of devices from non-linear optical materials. In conclusion, the X-rays may dissociates CADH crystals into copper crystals, so the obtained data are resembled with that of metallic copper. Also the results of spectroscopic, thermal, optical and dielectric studies were support the grown crystal as copper ascorbate dihydrate.

References

[1] Kosuke Sato , Yuya Oaki and Hiroaki Imai; Chem. Commun, **51** (2015) 7919-7922.

[2] Lia Addadi and Steve Weiner; Phys. Scr. **89** (2014) 098003.

[3] H. C. W. Skinner and A. H. Jahren, Treatise on Geochemistry, **8** (2003) 117-184. .

[4] Karim Benzerara, Encyclopedia of Astrobiology, (2014) doi: 10.1007/978-3-642-27833-4-185-5.

[5] M.-C. Robert, O. Vidal, J.-M. Garcia-Ruiz F. Otalora; Crystallization in gels and related methods In Crystallization of Nucleic Acids and Proteins: A Practical Approach (second edition). A. Ducruix R. Giegds., IRL Press 149-175 (1999).

[6] Stupp, S. I.; Mejicano, G. C.; Hanson, J. A. J. Biomed. Mater. Res., **27** (1993) 289.

[7] Heinz K. Henisch, Helvetica; Physica Acta, **41** (1968).

[8] A.R Patel andVenkateswara Rao, Bull.Mater.Sci., **4** (1982) 527-548.

[9] Juan Du, Joseph J. Cullen, and Garry R. Buettner, Biochim Biophys Acta. **1826** (2012) 443-457.

[10] Edmnund M. Mystkowski, Clinical Laboratory, Royal Infirmary, Edinburgh, The Oxidation of Ascorbic Acid in the Presence of Copper (1942).

[11] Canan Unaleroglu , Yuksel Mert Birgul Zumreoglu-Karan, Synthesis and Reactivity in Inorganic and Metal-Organic Chemistry **1532** (2006) 0094-5714.

[12] EFSA ANS Panel (EFSA Panel on Food Additives and Nutrient Sources added to Food), EFSA Journal; **13** (2015) 4087.

[13] E.C.Jumanath and P.P.Pradyumnan; Journal of Molecular Structure **1193** (2019) 231-238.

[14] A.M. Ezhil Raj, D.D. Jayanthi, V.B. Jothy, M. Jayachandran, C. Sanjeeviraja, Cryst. Res. Technol; **43** (2008) 1307 .

[15] Sushma Bhat, P.N. Kotru, Mater. Sci. Eng., **23** (1994) 73.

[16] Ernst Graf, J. Agric. Food Chem. **42** (1994) 161.

[17] SushmaBhat, P.N. Kotru. Mater. Sci. Eng., **23** (1994) 73.

[18] M.R. Shedam, A. VankateshwaraRao. Bull. Mater. Sci.; **16** (1993) 309.

[19] A.Umar, S.Naveed and N.Ramzan; Revistha; Materia, (2014) 197-203 .

[20] Jose Brandao Neto, Crystal, **273** (2018).

[21] Wolfgang LOHMANN, Detlef PAGEL, and Volker PENKA. Eur. J. Biochem; **138** (1984) 479.

[22] Mathew V, Joseph J, Jacob S and Abraham K E ; Bulg. J. Phys. **35** (2008) 303.

[23] Brown ME. Handbook of thermal analysis and calorimetry, vol. 1. Amsterdam: Elsevier; 2003.

[24] Pradyumnan PP, Ittyachan. J Therm Anal Calorim. **61** (2000) 243-7.

[25] N.N. Golovnev, M.S. Molokeev, S.N. Vereshchagin V.V. Atuchin; J. Coord. Chem. **66** (2013) 4119-4130.

[26] V.V. Atuchin at. al.; J. Phys. Chem. C, **118** (2014) 15404-15411 .

[27] Nicolay N. Golovnev, Maxim S. Molokeev, Maxim K. Lesnikov, Victor V. Atuchin; J. Phys. Org. Chem. **31** (2018) 3773.

[28] V.V. Atuchin, A.K. Subanakov, A.S. Aleksandrovsky, B.G. Bazarov, S.Yu. Stefanovich; Mater. Des. **140** (2018) 488-494.

[29] Katarzyna Drozdzewska, V. Kestens, A. Held, G. Roebben and T. Linsinger, Journal of Thermal Analysis and Calorimetry, **88** (2007) 757.

[30] M P Binitha and P P Pradyumnan, Phys. Scr. **87** (2013) 065603 .

[31] A.A. Hendi, Structure, Life Science Journal, **8** (2011) 554.

[32] S.K. Arora, V. Patel, R.G. Patel, B. Amin, A Kothari, J. Phys. Chem. **65** (2004).

[33] Firdous A, Quasim I, Ahmad M and Kotru P N, Bull.Mater. Sci. **33** (2010) 377.

[34] Soosen Samuel, Jiji Koshy, Anoop Chandran, K.C. George, Current Applied Physics **11** (2011) 1094.

[35] V.V. Atuchin at. al.; J. Phys. Chem. C; **116** (2012) 10162-10170.

[36] Vinnik, D.A.; Klygach, D.S.; Zhivulin, V.E.; Malkin, A.I.; Vakhitov, M.G.; Gudkova, S.A.; Galimov, D.M.; Zherebtsov, D.A.; Tro-mov, E.A.; Knyazev, N.S.; et al. J. Alloys Compd. **755** (2018) 177-183.

[37] B. Rajagopal, A.V. Sarma and M.V. Ramana, Journal of Minerals Materials **10** (2011) 1487.

Chapter 6

Biomimetic Growth of Alkaline Earth Metal Oxalates

6.1 Introduction

Biomimetic growth is the process which involves the controlled precipitation and ordered growth of molecular mineral materials in biological systems. The process creates heterogeneous accumulations, composites composed of organic and inorganic compounds, with inhomogeneous distributions [1]. The human body fluids contain minerals at various levels of saturation. When the body fluids get supersaturated with minerals, crystallization takes place [2]. These crystals are beneficial and they produce pathological effects on humans. The major beneficial role of mineralization is formation of bones and teeth, which consists of oriented micro crystals of hydroxyapatite [3]. Biomineral formation process under controlled conditions inspires researchers to develop designed single crystals [4]. Crystals play major role in biology and most of the living beings form crystals. Our sense of balance and acceleration is dependent upon small calcium carbonate (calcite) crystals present in the inner ear [5]. The pathological effects result in the crystal deposition diseases. The increasing incidence of crystal deposition diseases, such as heart disease, gout, gallstones, urinary stones etc., over the last few dacades, has resulted in an extensive

research on the above. Gallstones consist mainly of cholesterol with some quantities of calcium phosphates and calcium carbonates [6]. The clusters of small crystals formed in the urinary system give rise to urinary (renal) calculi, which consist primarily of different forms of calcium, such as calcium oxalates, calcium phosphates etc. [7].

The stone formation in our body is similar to the crystal growth and can be grown synthetically. The gel method is most versatile and simple technique for growing urinary stones [8]. Gels promote the growth of high-quality crystals of small molecules. Crystallization of biological macromolecules were tested with different types of gels; agarose, silica and polyacrylamide in the last few decades. Although these gels possess many advantages in the crystal production over the other growth technique for the crystal handling they are not much been used [9]. Crystal growth in the gel is a simple and inexpensive technique for growing single crystals of materials which show poor solubility in water and other organic solvents. It has obtained considerable importance due to its simplicity and effectiveness in growing single crystals of various biologically important compounds. When a gel is introduced in the crystallization medium, the convection is reduced and the molecule transport towards the crystal is more regular and operates in a diffusive mode. It is clear that the understanding and mimicking of the processes involved in biomineralization may provide new approaches to the growth of particular organic-inorganic hybrid materials [10, 11].

As mentioned in the first chapter, oxalic acid and its salts play an important role in human body, animals, plants and micro-organisms. Ascorbic acid, a form of vitamin C, is an essential nutrient found in citrus fruits and vegetables [12]. Most of the plants and animals are able to produce vitamin C from glucose. However, humans, other primates, guinea pigs and fruit bats require it to get from their nutrition [13]. During the process of metabolism, it decomposes into oxalic acid. This compound is photosensitive and has least thermal stability. The decomposition of ascorbic acid has been studied in various conditions [14-17]. It is reported that decomposition of ascorbic acid in presence of Cd^{2+} ions leads to the formation of

cadmium oxalate crystals [18].

In the present study, alkaline earth metal oxalate (AEMO) crystals are grown by single diffusion gel technique. In gel method, the gel acidified with ascorbic acid provides a controlled medium for the diffusion of supernatant cations into it, leading to the formation of crystals. In this technique, silica gel is used as a medium to grow crystals. Slow diffusion of reactants in the gel medium can be considered to mimic the growth of crystals in the human body. The structural characterizations including powder XRD, FTIR, micro Raman and thermal analysis were done to confirm that the grown crystals are oxalates.

6.2 Crystal growth

Alkaline earth metal oxalate (AEMO) crystals were grown by single diffusion gel method using ascorbic acid. Previously the technique was used and described elaborately to grow AEMO crystals by using oxalic acid as one of the reactant [19-22]. Here the silica gel was used as the medium of growth. The hydrosilica gel was prepared by using sodium meta silicate solution with different specific gravity. Ascorbic acid with different concentrations was mixed with the sodium meta silicate solution in an appropriate amount to set the gel with specific pH values of the mixture. The solution were transferred into test tubes and kept undisturbed for gelation. After the gelation took place, supernatant solutions of chlorides of Mg, Ca, Sr and Ba with different concentration were slowly poured along the walls of the test tube over the set gels. The supernatant ions slowly diffused into the gel medium, in the presence of these ions the ascorbate anions in the gel medium decomposed into oxalate ions and reaction took place. That giving rise to the formation of AEMO single crystal.

The supernatant solutions of chlorides diffuses into the gel column and reacts with oxalic acid (formed by the reduction of ascorbic acid) in the gel to produce necessary supersaturation for the slow precipitation of respective oxalates. When the concentration of the added chloride solution, the gel density and the ascorbic acid concentration are optimum, a few critical sized nuclei were produced and due

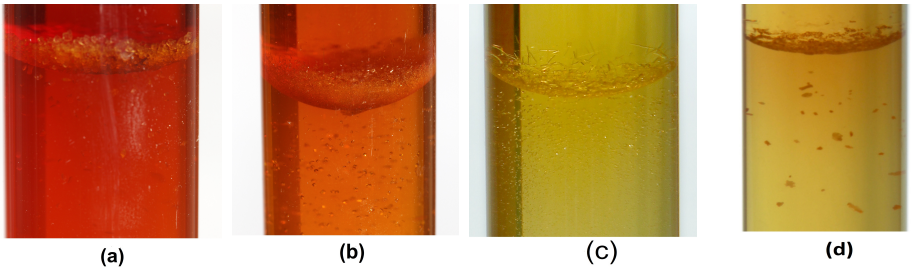

Figure 6.1: Grown crystals of a) Magnesium oxalate dihydrate b) Calcium oxalate dihydrate c) Strontium oxalate dihydrate d) Barium oxalate monohydrate.

Table 6.1: Optimum conditions for the growth of AEMO crystals

Parameters	Mg	Ca	Sr	Ba
Gel density	1.03	1.03	1.03	1.03
pH	6	6	7	7
Gel set time	1 day	1 day	1 day	1 day
Growth period	45 days	40 days	28 days	28 days
Concentration of ascorbic acid	1M	1M	1M	1M
Concentration of upper reactant	1M	1M	1M	1M

to the subsequent diffusion of this diffusant, crystals with definite faces and good sizes were formed. The grown crystals in growth apparatus is shown in Figure 6.1. The gel grown magnesium oxalate dihydrate and calcium oxalate dihydrate crystals are rectangular in shape and strontium oxalate dihydrate and barium oxalate monohydrate crystals are in stick like fashion. The optimum growth conditions for the growth of good-quality crystals of AEMO are summarized in Table 6.1.

6.3 X-Ray diffraction studies

The powder XRD patterns of Mg, Ca, Sr and Ba oxalates are shown in Figure 6.2 (a), (b), (c) and (d) respectively. The well-defined Bragg peaks reveal the crystalline nature. The data were compared with the standard values in the ICDD cards and literature [23-26]. The cell parameters, volume and space groups of different crystals obtained are presented in Table 6.2.

Table 6.2: Crystal system and lattice parameters for AEMO crystals

Parameter	Mg Oxalate	Ca oxalate	Sr Oxalate	Ba Oxalate
ICDD Card No:	00-028-0625	00-075-1314	00-020-1204	00-020-0135
Formula	MgC_2O_4 $2H_2O$	CaC_2O_4 $2H_2O$	SrC_2O_4 $2H_2O$	BaC_2O_4 H_2O
Crystal system	Monoclinic	Tetragonal	Tetragonal	Monoclinic
Space Group	C2/c(15)	I4/m(87)	I4/m(87)	C2/c
Unit cell dimension	a = 12.675 Å	a = b = 12.37 Å	a = b = 12.819 Å	c = 8.703 Å
	b = 5.4060 Å	c = 7.35 Å	c = 7.533 Å	b = 7.970 Å
	c = 9.9840 Å	$\alpha = \beta = \gamma = 90^0$	$\alpha = \beta = \gamma = 90^0$	c = 6.868 Å
	$\alpha = \gamma = 90^0$			$\alpha = \gamma = 90^0$
	$\beta = 129.45^0$			$\beta = 100.10^0$
Volume	528.259 $Å^3$	1125.927 $Å^3$	1237.874 $Å^3$	469.002 $Å^3$
Z	4	8	8	4

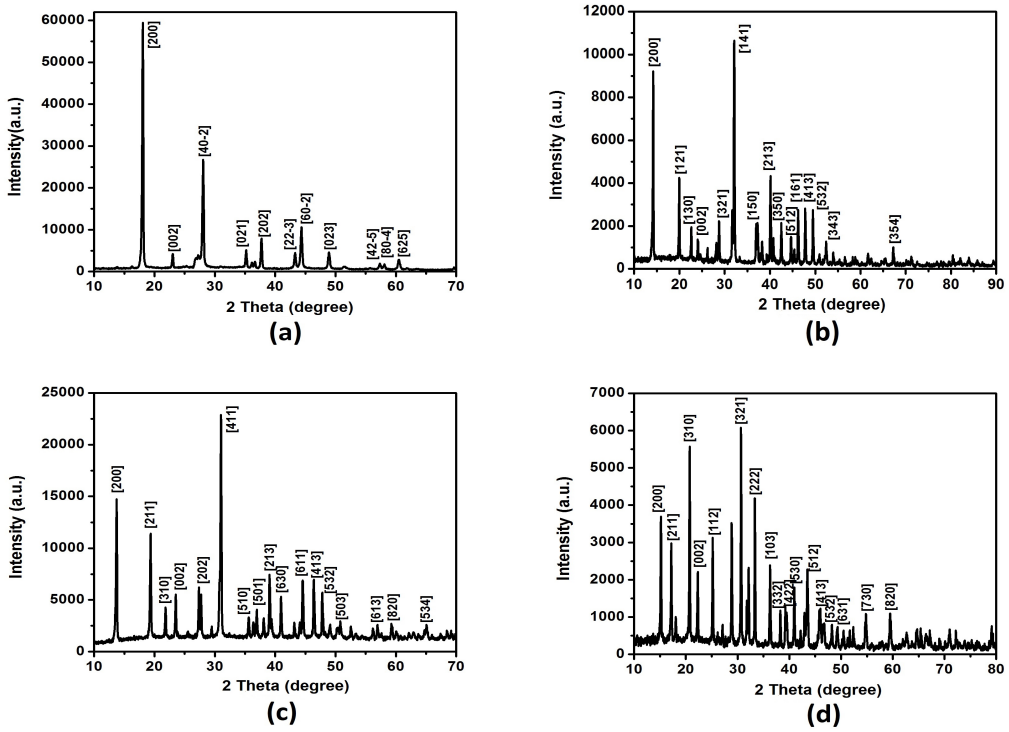

Figure 6.2: Powder XRD pattern of (a) Magnesium oxalate dihydrate (b) Calcium oxalate dihydrate (c) Strontium oxalate dihydrate (d) Barium oxalate monohydrate.

6.4 FTIR and micro Raman studies

6.4.1 FTIR studies

The recorded FTIR spectra of powdered AEMO crystals are shown in Figure 6.3. Spectra exhibit strong characteristic absorption bands of the carbonyl from the oxalate ligand in both the asymmetric and symmetric vibration regions with water of crystallization. The proposed assignments obtained from FTIR study are presented in Table 6.3.

OH stretching: The OH stretching frequency has been used for many years as a test and measure of hydrogen bonds. The stronger the hydrogen bond the longer the OH bond, the lower the vibrational frequency and the broader and more intense the absorption band. For AEMO crystals OH stretching appears at bands 3394, 3478, 3425 and 3398 cm^{-1}. Also bands in Mg and Ba oxalates at 2298 and 2304 cm^{-1} shows intermolecular hydrogen bonded OH stretch. This indicated that water molecule is present in AEMO crystals [27].

C=O and C-O stretching: The C=O stretching absorption in aliphatic compounds generally occurs at 1725-1700 cm^{-1}. The C=O absorption in carboxylic acids appears at 1700 cm^{-1}. If carboxylic acid is converted into its soluble salts, then carboxylate anion is formed. The C=O absorption has possible higher wave number for an acid as compared to that in carboxylate anion. In AEMO crystals C=O asymmetric stretching appears at 1648, 1650, 1628 and 1650 cm^{-1} and symmetric stretching appears at 1367, 1328, 1323 and 1379 cm^{-1}. The bands at 1057, 1039, 1017 and 1052 cm^{-1} show C-O stretching. This indicates the presence of carboxylate anion $(C_2O_4)^{2-}$ in AEMO crystal [28].

C-C stretching: The bands at 828, 908, 901 and 828 cm^{-1} specifies C-C asymmetric stretching and 679, 771, 776 and 679 cm^{-1} specifies C-C symmetric stretching which shows the presence of carboxylate anion. This confirms the existence of oxalate group in AEMO crystals.

Metal-O stretching: The bands observed at 502, 599, 520 and 502 cm^{-1} are assigned to Metal-O bonding,which confirms the metal oxalate bonding in AEMO

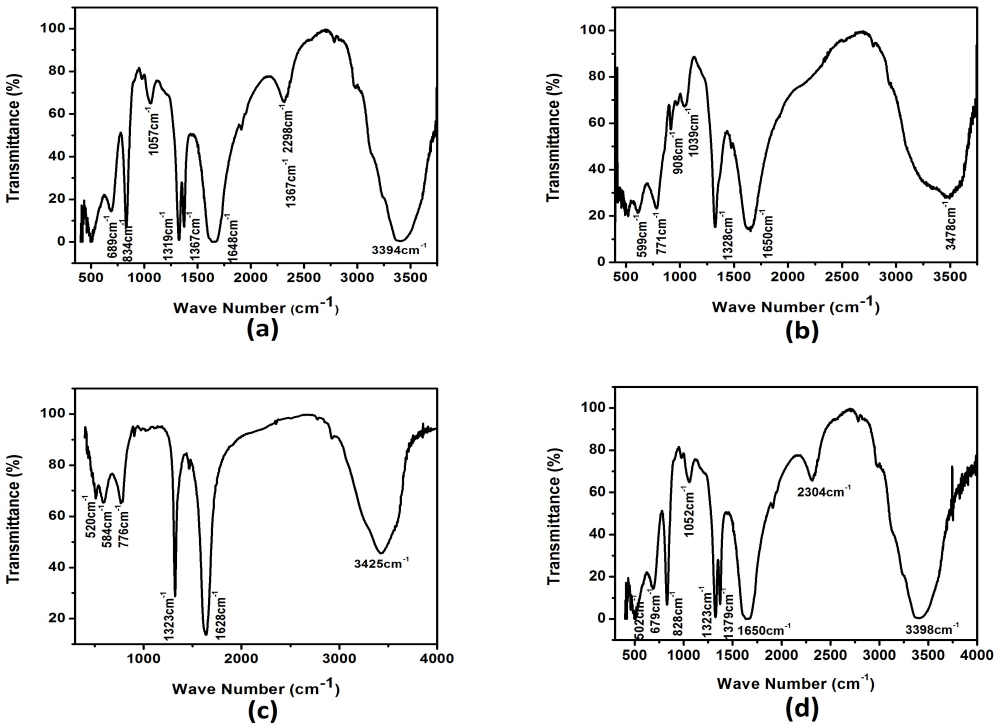

Figure 6.3: FTIR spectrum of (a) Magnesium oxalate dihydrate (b) Calcium oxalate dihydrate (c) Strontium oxalate dihydrate (d) Barium oxalate monohydrate.

crystals.

6.4.2 Micro Raman studies

The observed Raman spectra of AEMO crystals are shown in Figure 6.4, it consists of ten important Raman lines corresponding to asymmetric and symmetric stretching of water of hydration, C=O, C-C and C-O. The O-H stretching vibrations are observed at 2713, 2720, 2720 and 2727 cm^{-1} for magnesium, calcium, strontium and barium oxalates respectively. The Raman line corresponding to metal - oxygen bonding is at 89 cm^{-1} in all four crystals. The other proposed Raman lines are presented in Table 6.4 [29-31].

Table 6.3: Assignment of some selected FTIR wave numbers (cm^{-1}) of AEMO crystals

Mg (cm^{-1})	Ca (cm^{-1})	Sr (cm^{-1})	Ba (cm^{-1})	Assignment
3394	3478	3425	3398	ν_s(OH)
2298	-	-	2304	ν_{as}(OH)
1648	1650	1628	1650	ν_{as}(C=O)
1367	1328	1323	1379	ν_s(C=O)
1319	-	-	1323	ν_{as}(C-O)
1057	1039	1017	1052	ν_s(C-O)
828	908	901	828	ν_s(C-C)
679	771	776	679	ν_s (C-C)
502	599	520	502	ν(Metal-O)

Table 6.4: Assignment of some selected micro Raman wave numbers (cm^{-1}) of AEMO crystals

Mg (cm^{-1})	Ca (cm^{-1})	Sr (cm^{-1})	Ba (cm^{-1})	Assignment
2713	2720	2720	2727	ν_s(OH)
1475	1475	1468	1440	ν_{as}(OH)
1376	1383	1383	1390	ν_{as}(C=O)
1185	1178	1185	1171	ν_s(C=O)
917	-	902	889	ν_{as}(C-O)
598	577	591	570	ν_s(C-O)
528	506	506	492	ν_{as}(C-C)
-	308	393	308	ν_s (C-C)
224	-	210	-	ν(Metal-O)
-	181	146	167	ν(Metal-O)
-	124	-	139	ν(Metal-O)
89	89	89	89	ν(Metal-O)

6.5 Thermal decomposition studies

The thermo gravimetric analysis of AEMO crystals was carried out in the temperature range of 50 - 700 ^{0}C under nitrogen atmosphere at a heating rate of 10 ^{0}C/min. Figure 6.5 (a), (b), (c) and (d) depicts the thermal properties of the magnesium oxalate dihydrate, calcium oxalate dihydrate, strontium oxalate dihydrate and barium oxalate monohydrate, respectively. The compounds display mainly two thermal processes in the temperature range of 50 - 700 ^{0}C. Dehydration of the AEMO crystals occurs below 250 ^{0}C.

In the case of magnesium oxalate (Figure 6.5 (a)), after the dehydration the

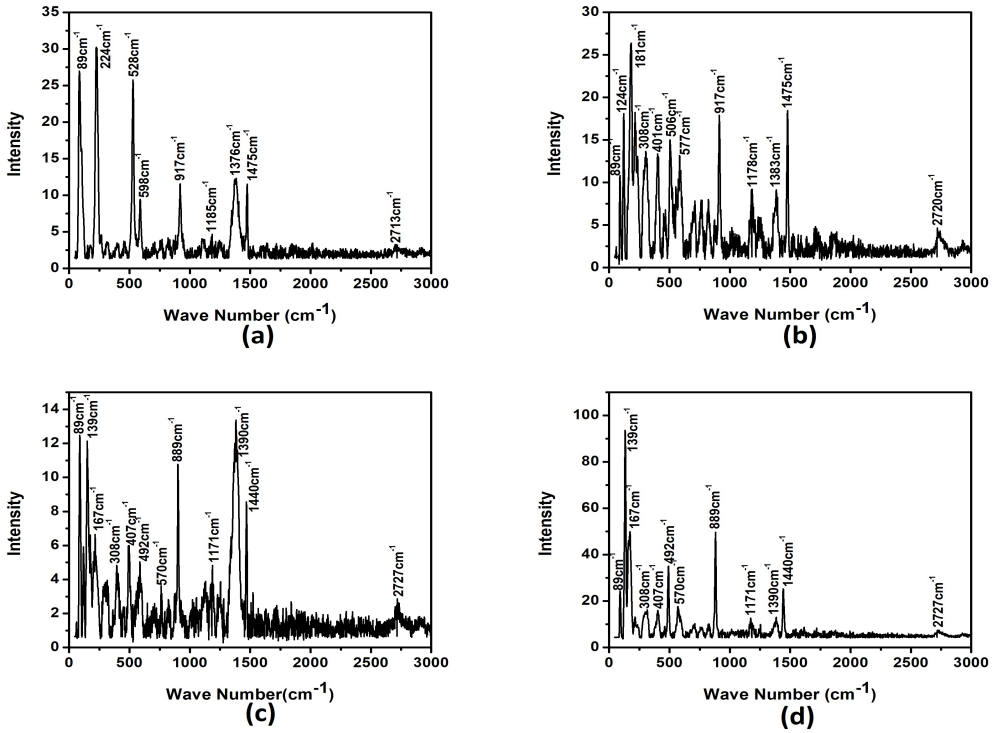

Figure 6.4: Micro Raman spectrum of (a) Magnesium oxalate dihydrate (b) Calcium oxalate dihydrate (c) Strontium oxalate dihydrate (d) Barium oxalate monohydrate.

compound remains nearly stable until 413 ^{0}C, beyond which it decomposes. In the temperature range of 413 - 505 ^{0}C, corresponding to this, an exothermic DTA peak is observed at 490 ^{0}C, the weight loss of 67.61% during the second thermal process attributes to the liberation of two molecule carbon monoxide and one oxygen from the anhydrous magnesium oxalate. Thus, the remaining weight of 32.39% indicates that the final product is $MgCO_3$ [32].

The Figure 6.5 (b), anhydrous calcium oxalate remains stable up to a temperature of 402 ^{0}C, starts second stage of decomposition and it became calcium carbonate at 490 ^{0}C. This decomposition has an endothermic peak at 484 ^{0}C. The percentage of calculated and experimental mass loss are 21.88 and 21.95% of the total mass taken [33].

Strontium oxalate dihydrate (Figure 6.5 (c)) also shows two stages of decomposition, in which the first step dehydration occurs at the temperature range of 143-223 ^{0}C. After the dehydration, the compound remains nearly stable until 294 ^{0}C, be-

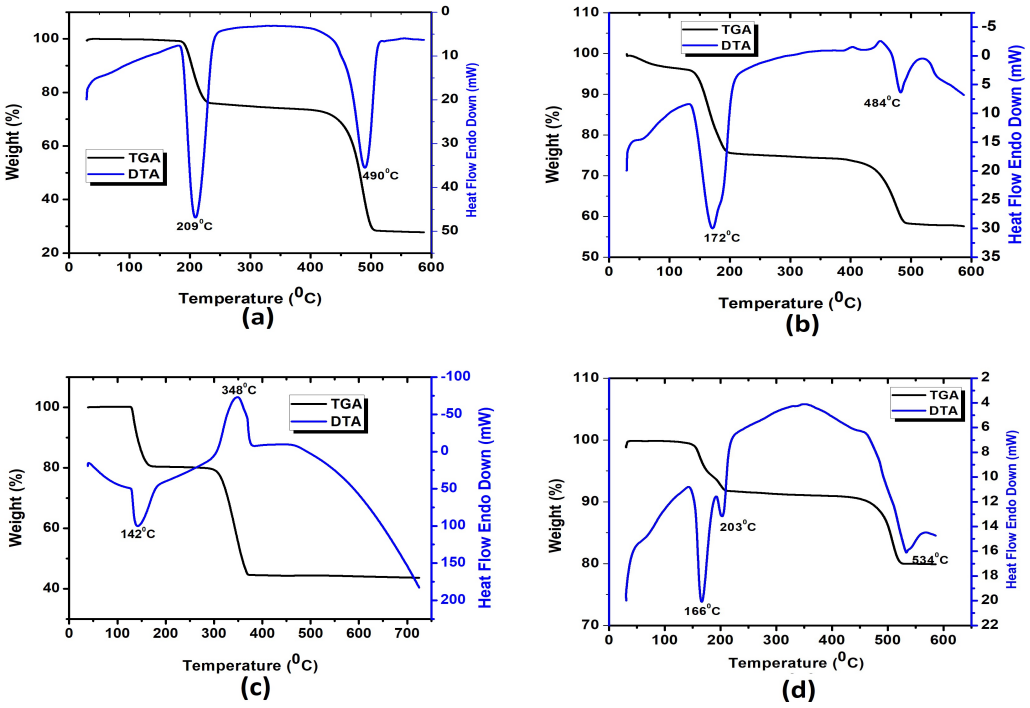

Figure 6.5: TG-DTA curves of (a) Magnesium oxalate dihydrate (b) Calcium oxalate dihydrate (c) Strontium oxalate dihydrate (d) Barium oxalate monohydrate.

yond which it decomposes. In the temperature range of 294-373 ^{0}C corresponding to an exothermic DTA peak at 348 ^{0}C, the weight loss of 35.11% during the second thermal process attributes to the liberation of one molecule of carbon dioxide and one molecule of carbon monoxide from the anhydrous strontium oxalate. Thus the remaining weight of 45.63% indicates that the final product may be strontium carbonate. [34].

In barium oxalate monohydrate (Figure 6.5 (d)), decomposition starts at about 143 ^{0}C and dehydration occurs. Then it remains stable up to a temperature of 459 ^{0}C, starts second stage of decomposition and it became barium carbonate at 523 ^{0}C by loss of one carbon monoxide. The percentage of calculated and experimental mass loss are 12.42 and 10.06% of the total mass taken [35].

DSC curves of AEMO crystals are shown in Figure 6.6. The analysis was done with a heat flow from 323 to 648 K at 10 ^{0}C/min. Figure 6.6 (a) and (d) are the thermogram of magnesium oxalate and barium oxalate and the sharp peaks at 223

^{0}C and 183 ^{0}C corresponding to single step of dehydration. Figure 6.6 (b) and (c) shows the two peaks corresponding to dehydration.

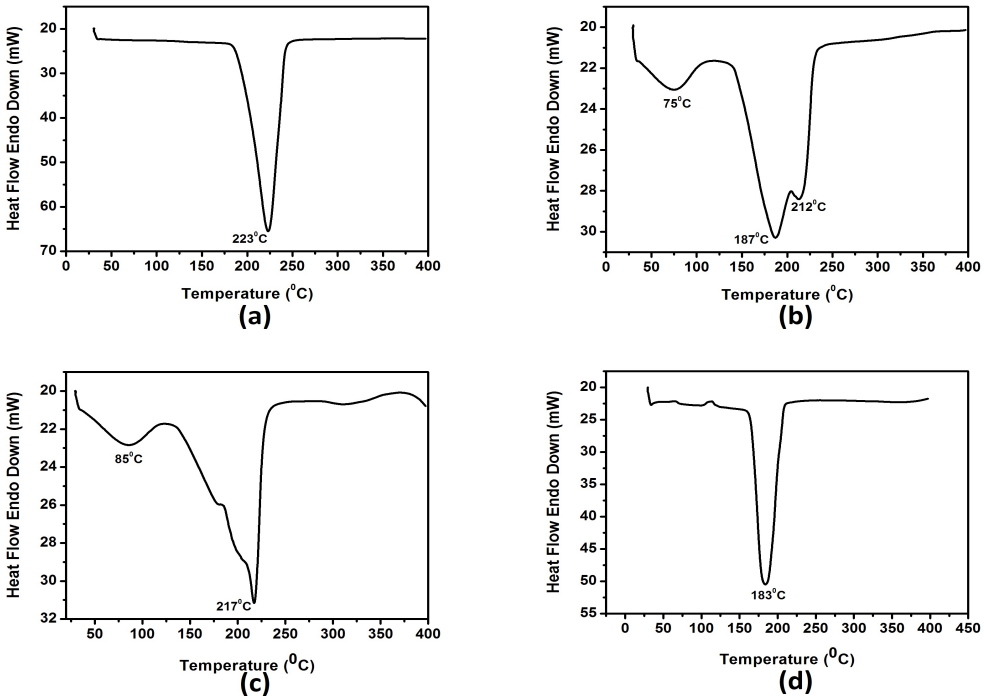

Figure 6.6: DSC thermogram of (a) Mg oxalate dihydrate (b) calcium oxalate dihydrate (c) Strontium oxalate dihydrate (d) Barium oxalate monohydrate.

6.6 UV visible spectroscopy

UV-Visible/NIR spectrum of reflectance of AEMO crystals were carried out between 200 - 900 nm at room temperature and is shown in Figure 6.7. In which, magnesium oxalate dihydrate crystal shows a wide reflectance (85%) window ranging from 400 - 900 nm (Figure 6.7 (a)). But in other three AEMO crystals percentage of reflectance increases with wavelength and become 70 - 80% at 900 nm.

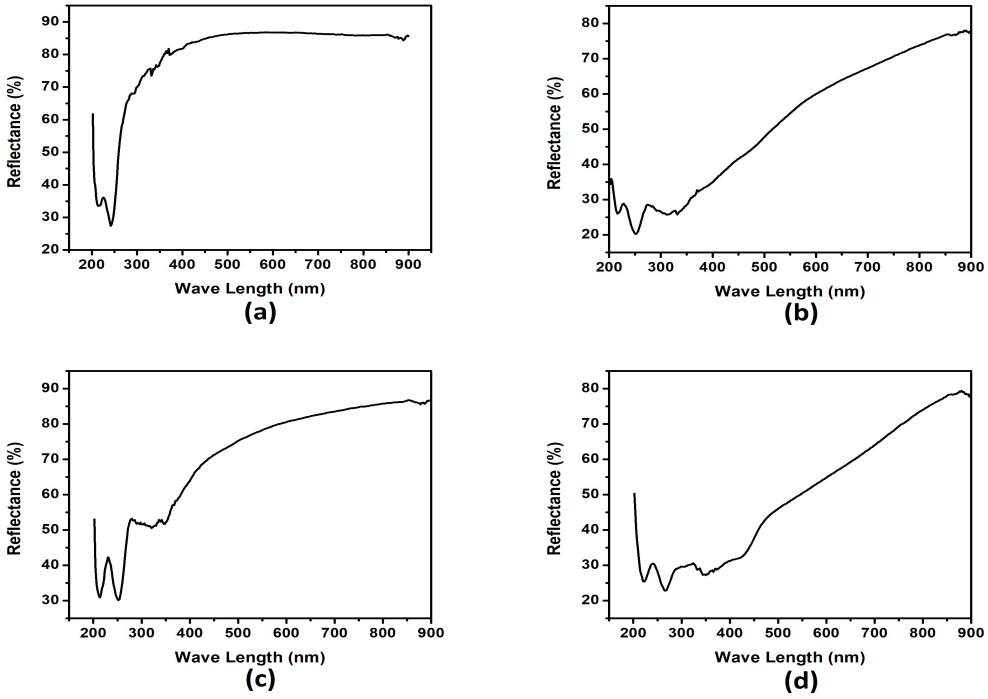

Figure 6.7: DRS Spectrum of (a) Magnesium oxalate dihydrate (b) Calcium oxalate dihydrate (c) Strontium oxalate dihydrate (d) Barium oxalate monohydrate.

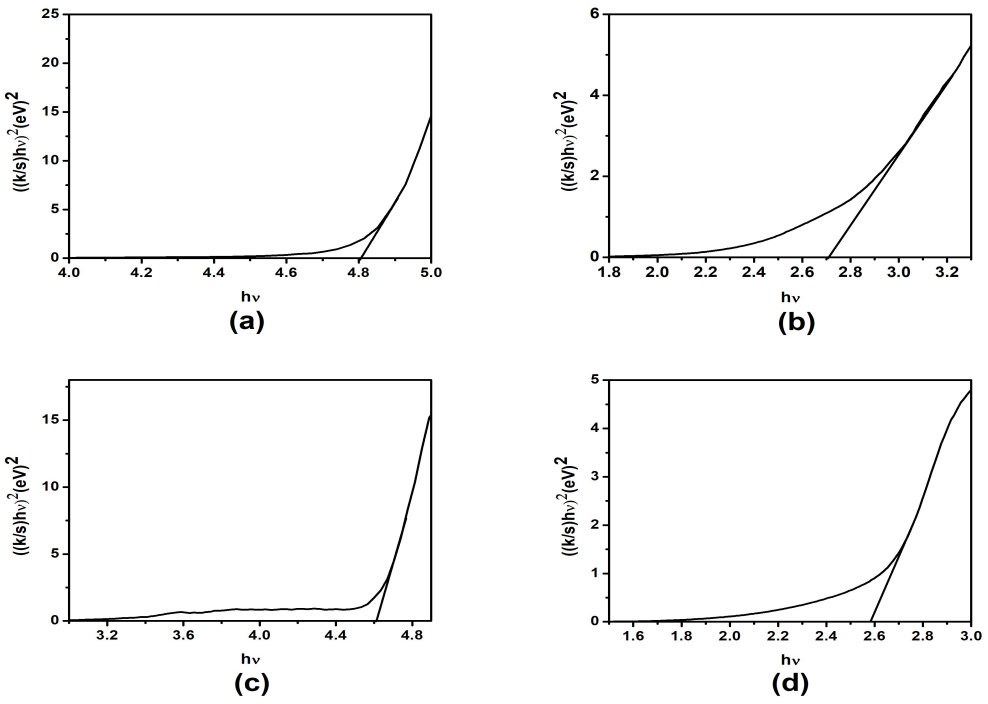

Figure 6.8: Plot of $[(k/s)h\nu]^2$ versus $h\nu$ for (a) Magnesium oxalate dihydrate (b) Calcium oxalate dihydrate (c) Strontium oxalate dihydrate (d) Barium oxalate monohydrate.

Extrapolation of the linear portion of the plot of photon energy (hν versus $[(k/s)h\nu]^2$ (Figure 6.8) gives optical band gap of the material. The band gap of magnesium, calcium, strontium and barium oxalates are estimated as 4.72, 2.71, 4.62 and 2.58 eV.

6.7 Dielectric property studies

Figure 6.9 shows the variations of the real part of dielectric constant ϵ_r with frequency f at room temperature for all investigated samples. It is clear that ϵ_r decreases gradually and then slowly with increasing frequency which is a normal dielectric behaviour and can be explained on the basis of four basic polarization mechanisms as given in the previous chapters.

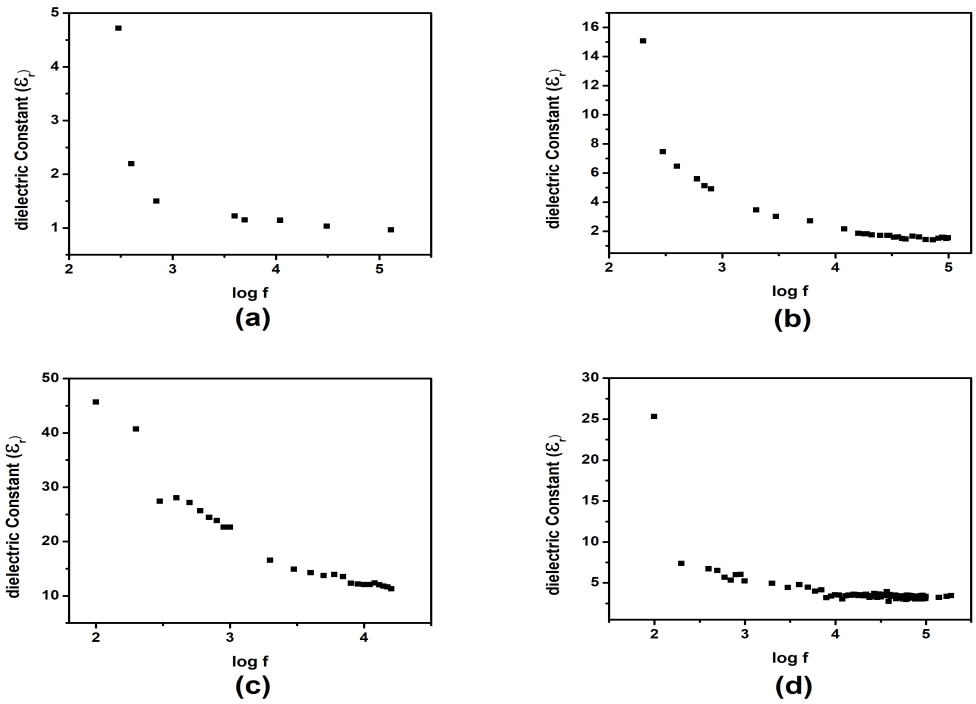

Figure 6.9: Variation of ϵ_r with frequency of (a) Magnesium oxalate dihydrate (b) Calcium oxalate dihydrate (c) Strontium oxalate dihydrate (d) Barium oxalate monohydrate.

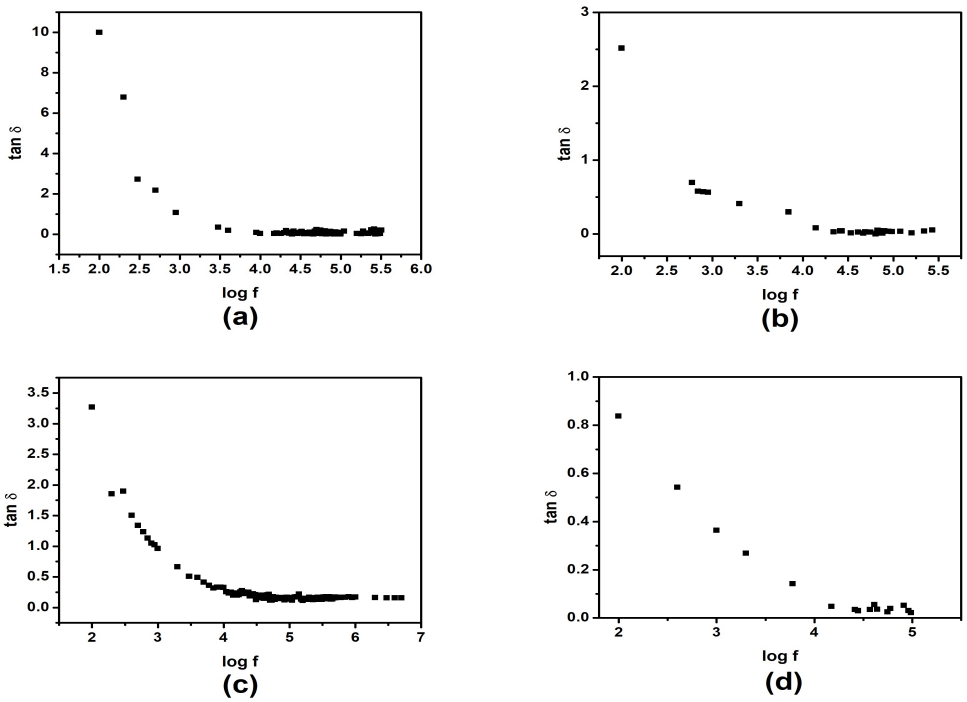

Figure 6.10: Variation of tangent loss with frequency of (a) Magnesium oxalate dihydrate (b) Calcium oxalate dihydrate (c) Strontium oxalate dihydrate (d) Barium oxalate monohydrate.

Figure 6.10 illustrates the dependence of the electrical conductivity σ_{ac} on the frequency. It is observed that the electrical conductivity is generally increased with increasing the frequency. For frequency greater than 17 KHz, there is a linear relation between log σ_{ac} and log f, i.e. the conductivity follows the relation [36].

$$\sigma_{ac} = A\omega^n \tag{6.1}$$

where $\omega = 2\pi$f , n is a dimensionless exponent and A has the dimensions of $\Omega^{-1}\text{cm}^{-1}$. The deviation of σ_{ac} from linearity at lower frequencies may be due to a change in the conduction mechanism.

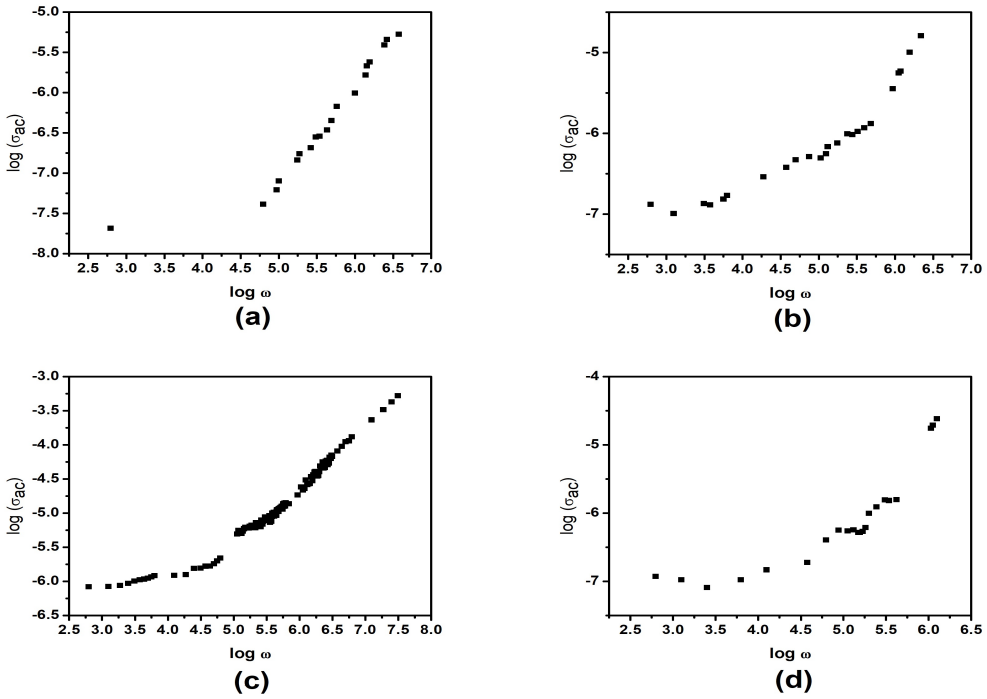

Figure 6.11: Variation of σ_{ac} with frequency of (a) Magnesium oxalate dihydrate (b) Calcium oxalate dihydrate (c) Strontium oxalate dihydrate (d) Barium oxalate monohydrate.

The variation of tanδ with frequency for various samples is shown in Figure 6.11. It is clear that tanδ is in close relation with the conductivity. The increase of the conductivity σ is accompanied by an increase of the eddy current which in turn increases the energy loss tanδ.

6.8 Conclusions

AEMO single crystals were grown by the decomposition of L-ascorbic acid in silica gel medium. It was found that the experimental conditions, such as pH, density of gel, concentration of reactants and gel aging have strong influence on the nucleation kinetics and growth of the crystal. Powder X-ray diffraction confirm that the Mg and Ba oxalate are monoclinic and Ca and Sr are tetragonal in structure. The oxalate phase formation was identified using recorded FT-IR and micro Raman spectra and the band assignments were interpreted. The TG-DTA analysis depicted that

the crystals are completely anhydrous below 300 ^{0}C. The optical band gap of the AEMO crystals are found to be 4.72, 2.71, 4.62 and 2.58 eV. The stoichiometric composition of the crystals are established to be $X(C_2O_4)$ nH_2O (where X = Mg, Ca, Sr and Ba; n = 2 for Mg, Ca and Sr; n = 1 for Ba). The dielectric constant of AEMO crystals, decreases gradually with increasing frequency of the applied ac field.

References

[1] Robert R. Crichton, Biomineralization, Biological inorganic chemistry, 2nd edition (2012).

[2] H.C.W. Skinner, A.H. Jahren, Biochemistry; Treatise on Geochemistry, (2007).

[3] Liam C. Palmer, Christina J. Newcomb, Stuart R. Kaltz, Erik D. Spoerke,d Samuel I. Stupp, Chem Rev.; **108** (2008) 475-4783.

[4] Imai, H., Oaki, Y. Kotachi, Bulletin of the Chemical Society of Japan. **79** (2006) 1834-1851.

[5] Adele L. Boskey, Elements , **3** 387-393.

[6] D. June Sutor and Susan E. Wooley; Gut, **14** (1973) 215-220.

[7] Vishal N Ratkalkar, MD and Jack G Kleinman; **9** (2011) 187-197.

[8] K Suguna, M Thenmozhi and C Sekar; Growth, spectral, Bull. Mater. Sci., **35** (2012) 701-706.

[9] M.-C. Robert, O. Vidal, J.-M. Garcia-Ruiz F. Otalora, Crystallization in gels and related methods In Crystallization of Nucleic Acids and Proteins: A Practical Approach (second edition). A. Ducruix R. Gieg, eds., IRL Press (1999) 149- 175.

[10] Stupp, S. I.; Mejicano, G. C.; Hanson, Mater. Res., **27** (1993) 289.

[11] Balcke P, Wien Klin Wochenschr. Suppl. **160** (1985) 1-15.

[12] Huma Tareen et al. Biological Forum An International Journal, **7** (2015) 367.

[13] Ayson, J.Fac.Pharm. **38** (2009) 233.

[14] Jose Luis Silencio Barrita and Mar-a del Socorro Santiago S-nchez, Antioxidant Role of Ascorbic Acid and His Protective Effects on Chronic Diseases, http://dx.doi.org/10.5772/52181.

[15] K. O. Soetan, C. O. Olaiya and O. E. Oyewole, African Journal of Food Science **4**(5) (2010) 200-222.

[16] Luis Villacorta, Angelo Azzi, Jean-Marc Zingg; Molecular Aspects of Medicine, **28** (2007) 507-537.

[17] W.Eugene Knox, M.N.D. Goswami; Advances in Clinical Chemistry, **4** (1961) 121-205.

[18] P. Orioli, B. Bruni, M. Di Vaira, L. Messori, F. Piccioli, V. Uni, V. Lastruccia, **41** (2002) 4312-4314.

[19] Gregory L.W. Simpson , B.J. Ortwerth; Biochimica et Biophysica Acta **1501** (2000) 12-24.

[20] I.T.A.P.F.H. Eilberg, N. Division, U.F. De Sa, **63** (2003) 1066-1071.

[21] John Knight1, Kumudu Madduma-Liyanage1, James A. Mobley, Dean G. Assimos1, and Ross P. Holmes; Urolithiasis. **44** (2016) 289-297.

[22] Mar-a M. Torres, Daniel Palacios, Mar-a C. D'antonio, Ana C. Gonz-lez-Bar Enrique J. Baran, Spectroscopy Letters; An International Journal for Rapid Communication **49** (2016) 1532-2289.

[23] P. V Dalal, K.B. Saraf, Bull. Mater. Sci., **34** (2011) 377-381.

[24] A.R. More, K.B. Saraf, Bull. Mater. Sci., **4** (2011) 2011.

[25] D.J. Price, A.K. Powell, P.T. Wood, Polyhedron; **18** (1999) 2499-2503.

[26] Chen et al. Acta Cryst. (2008) 64.

[27] Maria C. D. Antonioa,b, Mar-a M. Torresa,b, Daniel Palaciosa,b, Ana C. Gonz-lez-Bar-c, Enrique J. Baranc; Spectrochimica Acta Part A: Molecular and Biomolecular Spectroscopy **137**.

[28] T. Echigo, M. Kimata, A. Kyono, M. Shimizu and T. Hatta, Mineralogical Magazine, 2005, **69** (2005) 77-88.

[29] Frausto-Reyes C1, Loza-Cornejo S, Terrazas T, Miranda-Beltr-n Mde L, Aparicio-Fern-ndez X, L-pez-Mac-as BM, Morales-Mart-nez SE, Ortiz-Morales M.; Appl Spectrosc. **68** (2014) 1260-5.

[30] H. G. M. Edwards, D. W. Farwell, R. Jenkins, M. R. D. Seaward; Journal of Raman spectroscopy, **23** (1992) 185-189.

[31] Edwards, H Seaward, Mark J Attwood, Stacey Little, Samantha De Oliveira, Luiz Mauro, Tretiach. The Analyst. **128** (2003) 1218-21.

[32] D.DollimoreG.R.HealJ.Mason; Thermochemica Acta, **24** (1978) 307-313.

[33] Bahloul-Hourlier, Djamila. Journal of Thermal Analysis and Calorimetry. **136** (2018).

[34] F. A. Al-NewaiserS. A. Al-ThabaitiA. O. Al-YoubiA. Y. ObaidM. A. Gabal; Chemical Papers- Slovak Academy of Sciences, **61** (2007)370-375.

[35] A.H.VerdonkA.Broersma; Thermochemica cta, **6** (1973) 95-110.

[36] Y. Yamazaki and M. Satou, Jpn. J. Appl. Phys. **12** 998 (1973).

Chapter 7

Summary and Future Scopes

7.1 Summary of results

In this thesis we have focused on the crystallization and characterization of the 12 hybrid crystals including four metallic adipates (calcium, cobalt, copper and zinc), three metallic citrates (calcium, copper and cadmium), copper ascorbate, four alkaline earth metal oxalates (magnesium, calcium, strontium and barium). The main aim of the research work conducted in this study was growth of single crystals of the above mentioned biologically important crystals and detailed characterization of the as grown crystals with the help of advanced experimental techniques. The important results and conclusions arrived from the research work carried out are summarized below.

7.1.1 Metal adipates:

Four metal adipate crystals, calcium adipate monohydrate, cobalt adipate tetrahydrate, copper adipate monohydrate and zinc adipate dihydrate, have been grown by single diffusion gel technique. Single crystals have been obtained for calcium and cobalt adipates, whereas crystallization of the copper and zinc adipates resulted in the growth of polycrystalline aggregates, even after repeated trials. The grown crystals were characterized structurally and spectroscopically by different

Table 7.1: Optimum conditions for the growth of adipate crystals

Paramaeters	CaAMH	CoATH	CuAMH	ZnADH
Gel density	1.05	1.06	1.05	1.05
pH	6	6	6	6
Gel set time	1 day	1 day	1 day	1 day
Growth period	35 days	28 days	35 days	35 days
Concentration of ascorbic acid	1M	1M	1M	1M
Concentration of upper reactant	1M	1M	1M	1M

techniques such as single crystal XRD, powder XRD, FTIR, micro Raman and diffuse reflectance spectroscopic studies. The thermal decomposition behavior of the grown crystals was investigated by TG-DTG, DTA and DSC studies, dielectric property studies also have been performed. The major results of these crystals are given below.

- It was found that experimental conditions, such as pH, density of gel, concentration of reactants and gel aging, have strong influence on the nucleation kinetics and growth of the crystals. The optimum growth conditions attained by the authors for the growth of good-quality crystals of adipates are depicted in Table 7.1.

- The structure of cobalt adipate is analysed by single crystal X-ray diffraction and in which, Co^{2+} ion is situated in a six coordinate environment, defined by six O atoms from six different adipate anion $(C_6H_8O_4)^{2-}$. The Co-O bond distances vary between 2.027 and 2.210 Åand O-Co-O bond angles vary in a very wide range from 85.14 to 180.0 Å. The four water molecules present in the crystal involve the extensive network of hydrogen bond among themselves and are responsible for the stability of the structure. The structure of calcium adipate monohydrate, copper adipate monohydrate and zinc adipate dihydrate is analysed by powder X-ray diffraction. The cell parameters, space group and volume of different crystals obtained are presented in Table 7.2.

Table 7.2: Crystal data and structure parameters for adipate crystals

Parameter	CaAMH	CoATH	CuAMH	ZnADH
Crystal system	Triclinic	Monoclinic	Monoclinic	Monoclinic
Space Group	P-1(2)	P21/n	P21/c(14)	C2/c(15)
Unit cell dimension	a = 6.807 Å	a = 7.9805 Å	a = 7.980 Å	a = 18.31 Å
	b = 10.838 Å	c = 14.972 Å	b = 14.972 Å	b = 11.23 Å
	c = 5.040 Å	b = 9.5815 Å	c = 9.58 Å	c = 9.76 Å
	$\alpha = 98.24^0$	$\alpha = \gamma = 90^0$	$\alpha = \gamma = 90^0$	$\alpha = \gamma = 90^0$
	$\beta = 96.99^0$	$\beta = 90.689^0$	$\beta = 90.689^0$	$\beta = 109.35^0$
	$\gamma = 79.08^0$			
Volume	421.253 $Å^3$	1144.75 $Å^3$	1893.5 $Å^3$	851.815 $Å^3$

- The FTIR and micro Raman spectral studies, reported the modes of vibration of different functional groups such as -CH_2, O-H and COO- present in the crystal. The adipate phase formation associated with water of hydration is also identified. The diffuse reflectance spectra of all the four crystals were recorded in the wavelength range 200 - 900 nm, band gap of the materials were estimated, based on Kubelka Munk function. The calculated band gaps are 5.3, 2.18, 3.45 and 5.66 eV for calcium, cobalt, copper and zinc adipates respectively.

- To study the thermal decomposition behavior of these crystals, TG, DTA and DSC studies have been carried out. It is revealed that a three stage degradation of calcium adipate monohydrate, giving the final product $CaCO_3$. The intermediate compounds are anhydrous calcium adipate and calcium oxalate respectively. Two stage decomposition is observed in cobalt adipate tetrahydrate and cobalt carbonate as final product. The intermediate compound is anhydrous cobalt adipate. Both copper and zinc adipate undergo one stage decomposition and copper oxalate and zinc oxide as final product. The exact stochiometric composition of the grown calcium, cobalt, copper and zinc adipate crystals are $Ca(C_6H_8O_4)$ H_2O, $Co(C_6H_8O_4)$ $4H_2O$, $Cu(C_6H_8O_4)$ H_2O and $Zn(C_6H_8O_4)$ respectively.

- The dielectric behavior of the grown crystals with respect to variation in the applied frequency have also been studied. It is observed that all metal adi-

pate crystals exhibit a normal dielectric behavior that the dielectric constant decreases with increase of frequency and becoming a constant at higher frequencies and also dielectric loss decreases with increase of frequency whereas ac conductivity increases with frequency. The space charge effect and orientational polarization have responsible for the variation of dielectric constant, dielectric loss and ac conductivity. The value of dielectric constant at high frequency are 55.66, 2.16, 3.39 and 2.62 for calcium, cobalt, copper and zinc adipate respectively.

7.1.2 Metal citrates:

Single diffusion gel technique were used for the growth of three metal citrate crystals, calcium citrate pentahydrate, copper citrate dihydrate and cadmium citrate hexahydrate. Single crystal has been obtained for cadmium citrate hexahydrate and crystallization of the calcium and copper citrates are also been studied. The grown crystals were characterized structurally and spectroscopically by different techniques such as single crystal XRD, powder XRD, FTIR, micro Raman and diffuse reflectance spectroscopic studies. The thermal decomposition behavior of the grown crystals was investigated by TG-DTG, DTA and DSC studies, dielectric property studies also have been performed. The major results of these crystals are abridged below.

- It was found that experimental conditions, such as pH, density of gel, concentration of reactants and gel aging, have strong influence on the nucleation kinetics and growth of the crystals. The optimum growth conditions for the growth of good-quality crystals of citrates are summarized in Table 7.3.

- The structure of cadmium citrate is analysed by single crystal X-ray diffraction and a unit cell consisting of two crystallographically independent citrate ions, three Cd^{2+} ions and six water molecules. Each cadmium ion exists an octahedral geometry through short contacts with the citrate ions, the six apices

Table 7.3: Optimum conditions for the growth of citrate crystals

Paramaeters	CaCPH	CuCDH	CdCHH
Gel density	1.05	1.03	1.03
pH	6	6	6
Gel set time	1 day	1 day	1 day
Growth period	35 days	40 days	21 days
Concentration of citric acid	1M	1M	1M
Concentration of upper reactant	1M	1M	1M

Table 7.4: Crystal data and structure parameters for citrate crystals

Parameter	CaCPH	CuCDH	CdCHH
Crystal system	Triclinic	Monoclinic	Monoclinic
Space Group	P-1	I4/m(87)	P21/n
Unit cell dimension	a = 5.463 Å	a = 16.176 Å	a = 12.552 Å
	b = 6.505 Å	b = 9.732 Å	b = 10.266 Å
	c = 11.157 Å	c = 6.921 Å	c = 18.006 Å
	$\alpha = 101.121^0$	$\alpha = \gamma = 90^0$	$\alpha = \gamma = 90^0$
	$\beta = 88.855^0$	$\beta = 116.57^0$	$\beta = 109.015^0$
	$\gamma = 81.382^0$		
Volume	384.21	974.46 $Å^3$	2193.75 $Å^3$

of the oxygen co-ordination octahedron are occupied as three co-ordination positions are occupied by one citrate ligand, which employs both the central alcoholic and carboxylate oxygen atoms as well as one of its terminal carboxylate oxygens to bind Cd(1). The other two co-ordination positions are occupied by two additional citrate ligands from two adjacently located octahedral Cd(2) and Cd(3) ions are reaching out and co-ordinate to Cd(1) through the oxygen atoms of their respective central carboxylate groups. The remaining co-ordination site is occupied by a water molecule. The second terminal carboxylate group of the citrate ligand is protonated so did not participate in any co-ordination. It remains free, moving away from the Cd sites. The structure of calcium citrate pentahydrate and copper citrate dihydrate is analysed by powder X-ray diffraction. The cell parameters, space group and volume of different crystals obtained are presented in Table 7.4.

- The FTIR and micro Raman spectral studies, reported the modes of vibration of different functional groups such as -CH_2, O-H and COO- present in the

crystal. The citrate phase formation associated with water of hydration is also identified. The diffuse reflectance spectra of all the three crystals were recorded in the wavelength range 200 - 900 nm, band gap of the materials were estimated, based on Kubelka Munk function. The calculated band gaps are 5.6, 2.78 and 5.15 eV for calcium, copper and cadmium citrates respectively.

- To study the thermal decomposition behavior of these crystals, TG, DTA and DSC studies have been carried out. It is revealed that the three citrate crystals show two stage degradation giving the final product as CaC_2O_4 for calcium and, carbonate for copper and cadmium. The intermediate compounds are anhydrous form of respective crystals. The exact stochiometric composition of the grown calcium, copper and cadmium citrate crystals are $Ca_3(C_5H_6O_7)_2$ $5H_2O$, $Cu_3(C_6H_5O_7)_2.2H_2O$ and $Cd_3(C_6H_5O_7)_2$ $6H_2O$ respectively.

- The dielectric behavior of the grown crystals with respect to variation in the applied frequency have also been studied. It is observed that all metal citrate crystals exhibit a normal dielectric behavior as observed for adipate crystals. The value of dielectric constant at high frequency are 1.35, 7.73 and 9.62 for calcium, copper and cadmium citrate respectively.

7.1.3 Copper ascorbate dihydrate:

Copper ascorbate dihydrate single crystals have been grown by copper ion diffusion through hydro silica gel medium impregnated with ascorbic acid anion. Single crystal X-ray diffraction reveals that the structure of the grown crystal as cubic copper. It is very rarely observed that the X-rays may dissociates copper ascorbate dihydrate crystals into copper crystals, so the obtained data resembles with that of metallic copper. It is also noticed that the initial simulated powder pattern well matched with the powder XRD pattern obtained that of ascorbate. The FTIR spectra show all the representative peaks expected for ascorbate compounds associated with hydration. The material undergoes four-stage decomposition process and the end product is copper oxide. The stoichiometric composition of the grown crystals

is confirmed to be $Cu(C_6H_6O_6)$ $2H_2O$. The estimated optical band gap of the crystal is found to be 2.76 eV. . It is observed that copper ascorbate crystals exhibit a normal dielectric behavior as observed for adipate crystals. The value of dielectric constant at high frequency is 17.47 for the crystal. The results of spectroscopic, thermal, optical and dielectric studies confirms that the grown crystal is copper ascorbate dihydrate.

7.1.4 Metal oxalates:

Alkaline earth metal oxalate single crystals were grown by the decomposition of L-ascorbic acid in silica gel medium. We conducted experiments to grow alkaline earth metal ascorbate crystals by using ascorbic acid as one of the reactants. Instead of ascorbates we have found the oxalate crystals of respective alkaline earth metals. The grown oxalates have different features than the oxalate grown by the oxalic acid as one of the reactant as found in literature [1-4]. Oxalates grown by ascorbic acid are not found in literature. During the growth of AEMO crystals it was found that experimental conditions, such as pH, density of gel, concentration of reactants and gel aging, have strong influence on the nucleation kinetics and growth of the crystals. The optimum growth conditions for the growth of good-quality crystals of oxalates are encapsulated in Table 7.5. The results obtained from powder XRD are summarized in Table 7.6. The oxalate phase formation was identified using recorded FTIR spectra and the band assignments were interpreted. The TG-DTA analysis depicted that the crystals are completely anhydrous below 300 ^{0}C. The optical band gap of the grown crystals are found to be 4.72, 2.71, 4.62 and 2.58 eV. The stoichiometric composition of the crystals are established to be $X(C_2O_4)$ nH_2O (where X = Mg, Ca, Sr and Ba; n = 2 for Mg, Ca and Sr; n = 1 for Ba). The dielectric constant of metal oxalate crystals, decreases gradually with increasing frequency of the applied ac field. The value of dielectric constant at high frequency are 1.03, 1.55, 11.19 and 3.42 for magnesium, calcium, strontium and barium oxalate respectively.

Table 7.5: Optimum conditions for the growth of oxalate crystals

Parameters	Mg	Ca	Sr	Ba
Gel density	1.03	1.03	1.03	1.03
pH	6	6	7	7
Gel set time	1 day	1 day	1 day	1 day
Growth period	45 days	40 days	28 days	28 days
Concentration of ascorbic acid	1M	1M	1M	1M
Concentration of upper reactant	1M	1M	1M	1M

Table 7.6: Crystal data and structure parameters for oxalate crystals

Parameter	Mg Oxalate	Ca oxalate	Sr Oxalate	Ba Oxalate
Crystal system	Monoclinic	Tetragonal	Tetragonal	Monoclinic
Space Group	C2/c(15)	I4/m(87)	I4/m(87)	C2/c
Unit cell dimension	a = 12.675 Å	a = b = 12.371 Å	a = b = 12.819Å	a = 8.703Å
	b = 5.4060 Å	c = 7.3570 Å	c = 7.533Å	b = 7.970 Å
	c = 9.9840 Å	$\alpha = \beta = \gamma = 90^0$	$\alpha = \beta = \gamma = 90^0$	c = 6.868 Å
	$\alpha = \gamma = 90^0$			$\alpha = \gamma = 90^0$
	$\beta = 129.45^0$			$\beta = 100.10^0$
Volume	528.259 $Å^3$	1125.927 $Å^3$	1237.874 $Å^3$	469.002 $Å^3$

7.2 Future scopes

Biologically important crystals play an important role in human body, animals, plants and micro organisms hence biomineral formation under controlled conditions inspires researchers to develop designed single crystals. In this work we have tried to grow single crystals of metal adipate, metal citrate and metal ascorbate crystals by single diffusion gel growth technique. Eventhough this growth technique could not yield single crystals of metal ascorbates (except for copper ascorbate),conditions other than standard single diffusion method can be tried to get single crystals of metal ascorbates. The scope for future study based on this thesis can be listed as follows.

- Propose to grow metal ascorbate crystals by other growth techniques and by varying reagents.
- Studies on the biological applications of the prepared citrates may have to be explored.

- Dielectric characterization on these crystals can be done at different temperature to get more insight into behaviour of these crystals in human and animal calculi.
- These crystals are showing paramagnetic as well as ferromagnetic in nature, the exact magnetic behaviour at body temperature has to be explored.
- The study can be explored to rare earth metal adipates, citrates and ascorbates.
- Many of the grain size of the crystal can be modified to nano and its features have to be found and explained.
- Most of the organic molecules show non-linear optical properties which is to be observed for all the grown crystals.

References

[1] P. V Dalal, K.B. Saraf, Bull. Mater. Sci., **34** (2011) 377-381.

[2] Chen et al. Acta Cryst. **64** (2008) 863.

[3] R. Neder, M. Burghammer, H. Schulz, Zeitschrift fr Kristallographie **211** (1997) 305-309.

[4] D Valarmathi, Leela Abraham S Gunasekaran, Indian Journal of Pure Applied Physics **48** (2010) 36-38.